

INFORMATION TO USERS

This manuscript has been reproduced from the microfilm master. UMI films the text directly from the original or copy submitted. Thus, some thesis and dissertation copies are in typewriter face, while others may be from any type of computer printer.

The quality of this reproduction is dependent upon the quality of the copy submitted. Broken or indistinct print, colored or poor quality illustrations and photographs, print bleedthrough, substandard margins, and improper alignment can adversely affect reproduction.

In the unlikely event that the author did not send UMI a complete manuscript and there are missing pages, these will be noted. Also, if unauthorized copyright material had to be removed, a note will indicate the deletion.

Oversize materials (e.g., maps, drawings, charts) are reproduced by sectioning the original, beginning at the upper left-hand corner and continuing from left to right in equal sections with small overlaps.

Photographs included in the original manuscript have been reproduced xerographically in this copy. Higher quality 6" x 9" black and white photographic prints are available for any photographs or illustrations appearing in this copy for an additional charge. Contact UMI directly to order.

ProQuest Information and Learning
300 North Zeeb Road, Ann Arbor, MI 48106-1346 USA
800-521-0600

UMI[®]

University of Alberta

**Micro Total Analysis Systems, μ TAS:
New Instrumental Developments and Applications**

by

Gregor Ocvirk



A thesis submitted to the Faculty of Graduate Studies and Research in partial fulfillment of the requirements for the degree of doctor of philosophy

Department of Chemistry

Edmonton, Alberta

Spring 2000



**National Library
of Canada**

**Acquisitions and
Bibliographic Services**

**395 Wellington Street
Ottawa ON K1A 0N4
Canada**

**Bibliothèque nationale
du Canada**

**Acquisitions et
services bibliographiques**

**395, rue Wellington
Ottawa ON K1A 0N4
Canada**

Your file Votre référence

Our file Notre référence

The author has granted a non-exclusive licence allowing the National Library of Canada to reproduce, loan, distribute or sell copies of this thesis in microform, paper or electronic formats.

The author retains ownership of the copyright in this thesis. Neither the thesis nor substantial extracts from it may be printed or otherwise reproduced without the author's permission.

L'auteur a accordé une licence non exclusive permettant à la Bibliothèque nationale du Canada de reproduire, prêter, distribuer ou vendre des copies de cette thèse sous la forme de microfiche/film, de reproduction sur papier ou sur format électronique.

L'auteur conserve la propriété du droit d'auteur qui protège cette thèse. Ni la thèse ni des extraits substantiels de celle-ci ne doivent être imprimés ou autrement reproduits sans son autorisation.

0-612-60008-4

Canada

University of Alberta

Library Release Form

Name of Author: Gregor Ocvirk

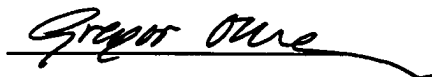
Title of Thesis: Micro Total Analysis Systems, μ TAS:
New Instrumental Developments and Applications

Degree: Doctor of Philosophy

Year this Degree Granted: 1999

Permission is hereby granted to the University of Alberta Library to reproduce single copies of this thesis and to lend or sell such copies for private, scholarly or scientific research purposes only.

The author reserves all other publication and other rights in association with the copyright in the thesis, and except as herein before provided, neither the thesis nor any substantial portion thereof may be printed or otherwise reproduced in any material form whatever without the author's prior written permission.

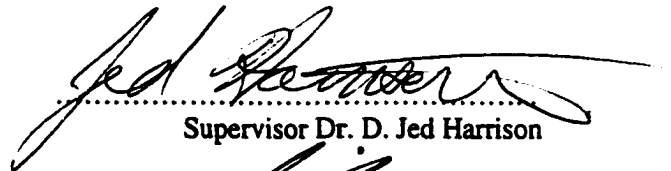


Cottagestrasse 1/13
1140 Wien
Austria

Date: October *21*, 1999

University of Alberta
Faculty of Graduate Studies and Research

The undersigned certify that they have read, and recommend to the Faculty of Graduate Studies and Research for acceptance, a thesis entitled Micro Total Analysis Systems, μ TAS: New Instrumental Developments and Applications, submitted by Gregor Ocvirk in partial fulfillment of the requirements for the degree of Doctor of Philosophy.



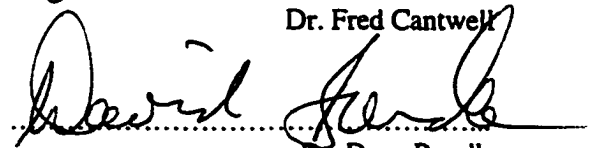
Supervisor Dr. D. Jed Harrison



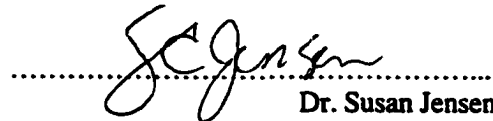
Dr. Norman Dovichi



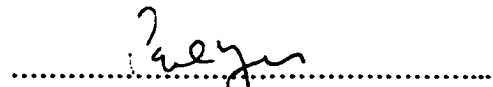
Dr. Fred Cantwell



Dr. Dave Bundle



Dr. Susan Jensen



External Examiner Dr. Paul Yager

Date: October 4, 1999

LESS IS MORE
M. VAN DER ROHE

Thesis Abstract

A wide range of bioanalytical demonstrations on Micro Total Analysis Systems, μ TAS, has established the advantageous features of planar microfluidic devices. However, practical problems, such as the difficulty of chip interfacing could limit the use of μ TAS. We describe a novel, reversible and simple chip-to-capillary interface, which withstood working pressures of up to at least 20 atm and allowed for the coupling of capillaries to glass chips with moderate dead volume.

The construction of a confocal epifluorescence microscope for on-channel detection is described, wherein a 40 x, 0.6 numerical aperture (N.A.) lens is used to focus a laser beam to an excitation spot of 12 μ m diameter. A 400 μ m pinhole showed optimum signal to noise, S/N, ratios for 30 μ m deep, isotropically etched, glass channels. Continuously pumped fluorescein solutions, 300 fM in concentration, were detected with an average S/N, of 6.1. The lowest detectable concentration of electrokinetically injected fluorescein plugs was 1 pM (average S/N = 5.8), corresponding to 570 detected molecules on average.

A β -Galactosidase assay of single cell lysates on a microchip is illustrated for the first time. A non-denaturing 400 μ M FDG and 0.1 % Triton[®]X-100 solution is mixed with a single cell stream at a mixing ratio of ~ 1:1 and a flow velocity of ~40 μ m/s, followed by lysis for 30-60 s, incubation of single cell lysates for ~ 80-110 s and on-chip fluorescence detection. Inherent drawbacks of conventional single cell analysis tools, such as flow cytometry, can be circumvented by integrating single cells analysis steps as demonstrated in this study.

Unmodified Polydimethylsiloxane, PDMS, an inexpensive and hence disposable device material, was investigated for chip-based capillary electrophoresis. The devices exhibited cathodic electroosmotic flow when in contact with phosphate buffers (pH 3-10.5) and stable retention times (\pm 8.6% RSD) over a period of 5 days when filled with water. Contact angles were unchanged (\pm 1.9% RSD) over a period of 16 weeks of dry storage. Tight definition of fluorescein plugs was obtained by continuous voltage control of all fluidic ports, yielding 64200 theoretical plates ($E=1340$ V/cm). The charge origin on PDMS surfaces was investigated and self-adhesive, microfluidic 3D PDMS manifolds were constructed.

Acknowledgements

I find myself indebted to a great many of people who helped me during my time in Edmonton, i.e. the time I was pursuing my Ph.D. at the University of Alberta. First of all I would like to thank my good friends Udo Verkerk, Thompson Tang and Nora Chan for shortening the adjustment period during my first year in Edmonton. Cultural, social and ethic differences are not to be underestimated. In terms of my professional life I would like to thank following people:

First and uppermost, my boss and advisor, Professor D. Jed Harrison for giving me a lot of room and funding to explore ideas; for crucial advise at the right time, for all the conferences he sent me to and his more recent tolerance of "Euro Trash".

My sincere thanks go to some members in Professor Harrison's research group. I, indeed, enjoyed the uniquely multicultural environment, which, I believe to be a distinctive feature of the Canadian system. Over the years I have enjoyed the professional and private advice of Udo Verkerk, Thompson Tang, Per Andersson, Christa Colyer, Hossein Salimi Moosavi, Rick Oleschuk, Karl Fluri, Markus Rothmair and Nicolas Bings in our group. I would also like to thank my friends Nora Chan, Edgar Arriaga, Costas Stathakis and Wojciech Gabryelski, all former or present members of the Department of Chemistry, for professional and private support.

I wish to express my gratitude to Norman Dovichi, Fred Cantwell, Dave Bundle, Susan Jensen and Paul Yager for being my examining committee.

I extend my thanks to all my Euro buddies, Roman Lipiecki, Stan Luxa, Erich Schartner, Dieter Starke and Hubert Hofmann, in the Machine Shop for the high quality of the machined items. Thanks also to Ed Feschuk and Kim Do in the Electronic shop. I am grateful to Glen Fitzpatrick and Lianne Lester at the Alberta Microelectronic Corporation (AMC) for the micromachining training I received. Thanks to Graham McKinnon and Yuebin Ning (AMC) for their cooperation in various projects. Ken Westra for his machining of silicon devices.

In case I forgot someone: You know me well. I didn't mean to.

I am greatly indebted to my parents for their constant moral and financial support. Without them I would not have finished this endeavor successfully. I sincerely acknowledge the Republic of Austria for giving me an excellent and complimentary post secondary education prior to this program. Finally, the National Science and Engineering Research Council of Canada is acknowledged for financial support of the studies presented in this thesis.

Table of Contents

Chapter 1: Introduction

1.1	Miniaturized Total Analysis Systems.....	1
1.1.1	Total Analysis Systems.....	1
1.1.2	Micro Total Analysis Systems, μ TAS.....	1
1.2	Motivations for this Study.....	4
1.3	The Microfluidic Chip to World Interface.....	5
1.4	Detection Methods for μ TAS.....	11
1.4.1	Confocal Microscopy.....	12
1.5	Single Cell Analysis.....	14
1.5.1	Single Cell Analysis: Relevance and Methods.....	14
1.5.2.	Microchip-based Single Cell Analysis.....	17
1.6	Capillary Electrophoresis in Polymeric Microfluidic Devices.....	19
1.6.1.	Capillary Electrophoresis.....	19
1.6.2	Origin of Electroosmotic Flow in Microfluidic Channels.....	22
1.6.2.1	Electroosmosis.....	22
1.6.2.2	Origin of Surface Charge on Channel Walls.....	23
1.6.3	Fundamentals and Resolution of CE Separations.....	24
1.6.3.1	Migration of Ions in CE.....	24
1.6.3.2.	CE Separation Efficiency.....	25
1.7.	Scope of this Thesis.....	27
1.8	References.....	29

Chapter 2: Confocal Epifluorescence Microscopy for Miniaturized Total Analysis Systems

2.1	Abstract.....	39
2.2	Introduction.....	39
2.3	Experimental Section.....	41
2.3.1	Materials and Reagents.....	41
2.3.2	Device Design and Fabrication.....	42
2.3.3	Instrumentation.....	44
2.3.4	Procedures.....	45
2.4	Results and Discussion.....	46
2.4.1	Fluidic Interface.....	46
2.4.2	Optical Characteristics.....	47
2.4.3	Detection Performance.....	51
2.5	Acknowledgements.....	55
2.6	References.....	55

**Chapter 3:
 β -Galactosidase Assays of Single Cell Lysates on a Microchip:
A Complementary Method for Enzymatic Analysis
of Single Cells**

3.1	Abstract.....	58
3.2	Introduction.....	59
3.3	Experimental Section.....	61
3.3.1	Reagents & Media.....	61
3.3.2	Cell Culture.....	61
3.3.3	Devices & Equipment.....	62
3.3.3.1	Microdevices.....	62
3.3.3.2	Chip Instrumentation.....	62
3.3.4	Procedures.....	63
3.3.4.1	Flow cytometry.....	63
3.3.4.2	Well Plate Assay.....	64
3.3.4.3	Capillary Electrophoresis.....	64
3.3.4.4	Chip based Assay.....	65
3.3.4.4.1	Off-chip Incubation and On-chip Lysis.....	65
3.3.4.4.2	On-chip Incubation and On-chip Lysis.....	65
3.4	Results and Discussion.....	65
3.4.1	Optimization of The Intra Cellular β -Gal Assay of HL-60 Cells....	66
3.4.1.1	Lysis and β -Gal Extraction.....	66
3.4.1.2	Reaction Rate and Reaction Products.....	68
3.4.1.3	Substrate Concentration.....	70
3.4.2	Cell Manipulation On-Chip.....	73
3.4.3	Lysing and Detection of β -Gal Activity of Preincubated Cells On-Chip.....	74
3.4.4.	On-Chip Lysing, On-Chip Incubation and Detection of β -Gal Activity.....	75
3.5	Acknowledgements.....	78
3.6	References.....	79

Chapter 4:
Electrokinetic Control of Fluid Flow in Native
Poly(dimethylsiloxane) Capillary Electrophoresis Devices

4.1	Abstract.....	82
4.2	Introduction.....	82
4.3	Experimental Section.....	87
4.3.1	Master Fabrication.....	87
4.3.2	Device Molding.....	89
4.3.3	Materials & Reagents.....	89
4.3.4	Instrumental Setup.....	90
4.3.5	Device Conditioning.....	91
4.3.6	EOF Measurement.....	91
4.3.7	Contact Angle Measurement	92
4.4	Results and Discussion.....	92
4.4.1	EOF in PDMS Devices.....	93
4.4.2	CE Performance.....	97
4.4.3	Device Stacking.....	99
4.5	Conclusion.....	100
4.6	Acknowledgements.....	101
4.7	References.....	101

Chapter 5	106
Conclusions and Suggestions for Future Experiments.....	

List of Tables and Figures

Tables:

Table 4.1:	Polymer Micromachining by Photoablation.....	84
Table 4.2:	Templates for Embossing and Molding: Materials and Machining Methods.....	85
Table 4.3:	Injection Molded Microfluidic Devices.....	86
Table 4.4:	Device Dimensions and Impedances.....	93
Table 4.5:	Effect of Tetrabutylammonium ion (TBA ⁺) on Electroosmotic mobility.....	95

Figures:

Figure 1.1:	Chip holder for capillary to chip coupling.....	7
Figure 1.2:	Capillary to chip coupling with a photopatterned prealignment platform.....	8
Figure 1.3:	Capillary to chip coupling with coaxial insertion holes matching the o.d and i.d of the fused silica capillary.....	8
Figure 1.4:	Capillary to chip coupling with a coaxial insertion hole and a circular channel matching the i.d. and o.d of the capillary, respectively.....	8
Figure 1.5:	Capillary to chip coupling with a plastic press fitting.....	8
Figure 1.6:	End-on capillary to chip coupling without insertion hole.....	9
Figure 1.7:	End-on capillary to chip coupling with drilled insertion hole.....	9
Figure 1.8:	End-on capillary to chip coupling with approximately circular, etched insertion hole... 10	
Figure 1.9:	A, trans-illumination confocal microscope; B, Epi-illumination confocal microscope... 12	
Figure 1.10:	Effect of microscope N.A. on optical sectioning strength.....	13
Figure 1.11:	Schematic view of electroosmotic flow (EOF) and electrophoretic migration in a negatively charged glass microchannel.....	21
Figure 2.1:	Micromachining sequence of microfluidic glass devices.....	42
Figure 2.2:	Geometric layout of device AMC 27, patterned onto 0211 glass.....	43
Figure 2.3:	Confocal epifluorescence apparatus for detection on a CE chip.....	44
Figure 2.4:	Chip connectors and chip holder.....	46
Figure 2.5:	Measurement of flow velocity in AMC 27 device.....	47
Figure 2.6:	On-chip laser induced epifluorescence detection illustrating the laser beam spot size... 48	
Figure 2.7:	Signal to noise ratio (S-B)/N, versus vertical displacement of chip (Δz) for various pinhole diameters.....	49
Figure 2.8:	Background corrected fluorescence signals versus vertical displacement of chip (Δz) for various pinhole diameters.....	49
Figure 2.9:	Excitation, detection and probe volumes for confocal epifluorescence detection on-chip.....	50
Figure 2.10:	Signal levels for vacuum driven continuous flow of pH 9 buffer, 300 fM and 10 pM fluorescein solutions in the same running buffer.....	52
Figure 2.11:	Log-log plot of fluorescence intensity from continuous flow, corrected for background fluorescence, as a function of fluorescein concentration.....	52
Figure 2.12:	Four separate electrophoregrams of 1 pM fluorescein solutions.....	54

Figure 3.1:	Geometric layout of PCRD 2 device.....	62
Figure 3.2:	Optical setup comprising an inverted confocal epifluorescence microscope	63
Figure 3.3:	Fluorescence signal after incubation of a HL-60 cell suspension and a lysate of the same solution with various 200 μ M FDG detergent solutions for 10 minutes.....	66
Figure 3.4:	Time of lysis after addition of various detergent solution to a suspension of HL-60 cells.....	67
Figure 3.5:	β -Galactosidase catalyzed turnover of fluorescein-di- β -D-galactopyranoside, FDG.....	69
Figure 3.6:	Capillary electrophoresis of a reaction mixture of a HL-60 cell suspension, incubated with a 200 μ M FDG 0.1 % Triton X-100 solution for 110 min.....	70
Figure 3.7:	Enzymatically generated fluorescence response in dependence of FDG concentration.....	70
Figure 3.8:	A: Fluorescence response during incubation of a viable HL-60 cell suspension and a cell lysate in 100 μ L of a 200 μ M FDG solution, containing 0.1% Triton X-100; B: Background corrected fluorescence response of a supernatant solution and the separated cell pellet after incubation with a 200 μ M FDG solution.....	71
Figure 3.9:	Flow cytometric fluorescence analysis of HL-60 cells.....	72
Figure 3.10:	Sequence of transport and lysis of one single HL-60 cell on a microchip.....	73
Figure 3.11:	On-chip lysis of off-chip incubated and unincubated cells.....	74
Figure 3.12:	On-chip lysis of on-chip incubated and unincubated cells.....	76
Figure 4.1:	Transmittance [%] of a Sylgard 184 slab for wavelengths in the UV/VIS range.....	86
Figure 4.2:	Micromachining of a silicon master for PDMS molding.....	88
Figure 4.3:	SEM images of a double T injection detail, molded into PDMS.....	89
Figure 4.4:	Optical setup for on-channel LIF detection in Sylgard [®] 184 PDMS devices.....	90
Figure 4.5:	Voltage control sequence for sample injection and separation on PDMS devices.....	91
Figure 4.6:	EOF measurement by current monitoring.....	91
Figure 4.7:	Geometric layouts of devices ABS 10, ABS 18 and PCCD 25, molded into PDMS.....	93
Figure 4.8:	Effect of SDS addition to the running buffer on the electroosmotic mobility in Sylgard [®] 184 PDMS devices at pH 3 and 9 buffer.....	95
Figure 4.9:	Effect of pH on EOF in Sylgard [®] 184 PDMS devices.....	96
Figure 4.10:	A,B: Electropherograms of fluorescein in an ABS 10 device with and without application of pushbackvoltages into the side channel; C: Current-voltage curves in ABS-10 and PCCD 25 devices.....	98
Figure 4.11:	Series of on-chip electropherograms of fluorescein on an ABS-10 device.....	99
Figure 4.12:	Device stack consisting of two PCCD 25 devices	100

Chapter 1: Introduction

1.1 Miniaturized Total Analysis Systems

1.1.1 Total Analysis Systems, TAS

The need for portable and automated analytical systems in ecological and industrial process control was the main driving force for the development of the Total Analysis System, TAS, concept, as envisioned and realised by the late Michael Widmer and coworkers at the Central research laboratories of Ciba Geigy in Basel, Switzerland. The integration of all necessary steps of an analytical investigation into one single automated instrumental system was suggested to result in a significant reduction of human transfer steps. Therefore a reduction in total analysis time and cost per single analysis was anticipated. The steps of every chemical analysis were identified to consist of sampling steps, followed by transport, separation of individual components, detection or identification of these components and data collection for quantitation [1]. The conceived advantages were first demonstrated with a sample enrichment module, consisting of a specific adsorbent, coupled to a gas chromatograph for the analysis of air samples [2]. This approach was consequently extended to the analysis of volatile sample components in waste water effluents [3]. The power and complexity of these gas phase-based TAS was further increased by adding a gas extraction system to the enrichment step and a fourier-transform infrared detector to the GC separation. However, the limitations of GC monitoring for the analysis of polar and non-volatile compounds made the development of liquid phase TAS a necessity. The first demonstrated liquid flowing system was the flow injection based monitoring of glucose in a fermentation process [4]-[7]. Hereby, the glucose concentration could be monitored in two minute intervals allowing for accurate prediction of the endpoint of glucose consumption. Nonetheless the realized fluidic setup was fairly large and hence stationary, while the reagent and sample volumes were in the mL range. The desired reduction of reagent cost, waste generation and analysis time, as well as the need for portability thus led to miniaturization efforts, i.e. a Micro Total Analysis System, μ TAS.

1.1.2 Micro Total Analysis System, μ TAS

The improvements in analytical performance of separation systems, to be gained from miniaturization, have been known for quite some time [8]. The development of microbore HPLC, open tubular LC, capillary electrophoresis and capillary gas chromatography are all attributable to

the gain in separation efficiency, which is achievable by miniaturization. The decreased characteristic diameter, d , i.e. the capillary diameter and/or the diameter of chromatographic packing material results in a significant reduction in overall on-column bandbroadening. Terry et al. first recognized the usefulness of microfabrication technologies for the miniaturization of chemical separation devices [9],[10]. The integration of a split injector, a GC column and a thermal conductivity detector (TCD) on a silicon wafer stack (5 cm in diameter) was demonstrated. The conventional GC column was replaced with a 1.5 m long, 200 μm wide and 30 μm deep microchannel, etched isotropically into silicon, coated with OV-101 oil and covered with a pyrex wafer. The TCD detector was batch fabricated by deposition of nickel onto a separate silicon wafer and mounted on the GC wafer by mechanical clamping. The scope of this pioneering approach remained unrecognized until the advantages of performing liquid chromatography separations on micromachined planar fluidic devices were highlighted by Manz et al. [11],[12]. A detailed discussion of scaling laws followed [13],[14], demonstrating the feasibility and usefulness of integrating various liquid phase based chemical analysis systems onto micromachined planar devices. Briefly, the achievable resolution of a separation per unit time, the reduction of fluid volumes, the possibility of hyphenating several techniques on one device, with zero dead volume, the facility of performing multiple parallel analyses on one device as well as the possibility of inexpensive mass production of devices with high replication fidelity were pointed out as inherent advantages of μTAS . Indeed, all these advantages have been realized by several chip-based analysis techniques, which shall be discussed shortly.

The flow injection analysis setup mentioned above (see 1.1.1) was miniaturized by generating fluidic channels in planar plexiglass modules, whereupon several distinct modules of varying functionality were stacked to yield a fluidic network [15]. Different reagents were hereby introduced, split and mixed in different modules, followed by detection on an attached detection module. Further miniaturization of the modules and hence of the sample and reagent volumina to the nL range was achieved by replacing the plexiglass modules with micromachined silicon discs. A glucose and lactate monitor for mammalian cell cultivation [16] was demonstrated. External syringe pumps were utilized to pump the sample and the reagents through the fluidic manifold. In an attempt to miniaturize the system, microfabricated pumps were used for fluid handling and for demonstration of a phosphate analyzer for bioprocess surveillance [17]. The advantage of portability and reduced fluid volumes exhibited by these pumps had nonetheless to be contrasted with the low pressure ratings and the sensitivity to contaminants they suffered from.

Electrokinetic fluid handling offers an alternative to fluid control with microfabricated pumps in microchannels. A detailed description of the phenomenon of electroosmotic pumping

will be given in section 1.6. In short, the direction and speed of electrolyte solutions in microchannels can be controlled by applying a voltage across a filled channel due to the existence of a thin double layer of mobile ions at the channel wall. A flat flow profile is generated, resulting in a reduction of the bandbroadening term associated with the resistance to mass transfer in the mobile phase. Further, no mechanical valves are required for fluidic switching at channel intersections, while the application of potentials to the liquid reservoirs can easily be automated. This principle of electrokinetic fluid control has since been utilized extensively in chip-based capillary zone electrophoresis, CZE, introduced by Harrison et al. [18]-[21], cyclic CZE [22]-[24], capillary gel electrophoresis, CGE [25]-[27], micellar electrokinetic chromatography, MECC [28]-[30] and electrokinetically driven chromatography [31]-[33]. Excellent CE separation efficiencies – up to 32 theoretical plates/V - were attainable in separation times of less than 14 seconds [34]. More recently on-chip CE separations in milliseconds [35] have impressively illustrated the separation performance of these devices.

Capillary based separation techniques such as CE and open tubular chromatography, OTLC, have set new standards regarding the consumption of samples, reagents and eluent volumes. These advantages are a straightforward consequence of the small cross sectional area of the capillaries employed. However, the connection of capillaries with each other to form fluidic manifolds for mixing and reacting of sample components with reagents, represents a major problem due to the dead volume invariably introduced. Microfluidic monolithic devices represent an elegant alternative since complex branched channels can be easily patterned into these planar devices with standard photolithographic techniques. Processing, precolumn reactions, injections, separations, post-separation reactions and detection steps can therefore be integrated onto one device. The stringent demands on the mass and concentration detection limits have resulted in the frequent use of laser induced fluorescence detection schemes (see section 1.4) and consequently sample derivatization with fluorescent reagents. Derivatizations have been demonstrated on-chip in the precolumn mode, either with a continuous flow [36] or a stopped flow system [37], as well as in the postcolumn mode [38],[39]. Various other examples such as on-chip digestion of plasmid DNA with a restriction enzyme [40] and polymerase chain reaction, PCR, prior to CGE separation of the amplified fragments, have been reported [41].

The ability to pattern multiple channels on one device allows for the scale up of sample throughput as well as reduction of the fabrication cost per single fluidic network. This approach, capillary array electrophoresis, CAE, was first illustrated by Mathies et al. with a 12 channel device [42], wherein 12 samples can be injected and separated independently on 12 separation channels. Meanwhile several groups have constructed array chips of varying complexity

[43],[44]. So far, a maximum number of 96 parallel electrophoretic separations has been demonstrated on one device [45]. Since the density of the sample wells per unit area for high throughput screening is increasing constantly, it is likely that a higher channel density per device will be implemented in the near future. Thus the total cost per separation will decrease correspondingly.

As a conclusion of this section the interested reader shall be referred to more recently published reviews in this area [46]-[51] as well as the μ -TAS proceedings, published biannually since 1994 [52]-[54].

1.2 Motivations for this Study

The demonstrated advantages of exemplary μ TAS for bioanalytical analyses have resulted in a strong drive to extend the applicability of these systems. Practical problems of the use of μ TAS, such as the difficulty of the fluidic coupling of external devices to microfluidic devices, could significantly limit the use of μ TAS. Several different approaches, discussed briefly in this chapter, have been realized recently to minimize the dead volume introduced by capillary to chip connections. One main criterion in the development of connectors has been the reversibility of the connection. So far, no specific world-to-chip connectors are available commercially, which triggered our interest in utilizing available fittings for the construction of a new chip interface.

The detection of minute sample amounts in nanoliter volumes represents a significant challenge in bioanalytical chemistry. Detection concepts, which were introduced previously for capillary-based assays and separations, are applicable to μ TAS in many cases. One of these concepts, confocal epifluorescence microscopy, has also been demonstrated prior to this study for detection in microchannels. Our interest in this detection approach originated from the previously illustrated detection performance and the simplicity of the optical setup. Therefore we constructed a confocal epifluorescence microscope and then characterized the instrument for capillary electrophoresis and continuous flow analysis in microchannels. The basic concepts of confocal microscopy are introduced in this chapter.

The analysis of complex biological samples requires the separation of cells from tissue, followed by sorting and analysis of single cells. The relevance of single cell analysis in the biological sciences, reviewed briefly in this chapter, has been recognized for some time. Consequently several single cell analysis techniques have been developed over the last decades. More recently the use of μ TAS has been suggested and used for single cell analyses. A wide range of different single cell analyses have been performed on-chip, leading to better insight into

the advantages and challenges of microchip-based analysis of real biological samples. The drawbacks of conventional analysis tools for enzymatic assays of single cells were recognized by Edgar Arriaga and Per Andersson, former research associates in Norman Dovichi's and Jed Harrison's group, respectively. Consequently a β -Galactosidase assay of single cell lysates on a microchip was envisioned and first feasibility studies were performed with Edgar's and Per's participation. The integration of cell introduction, manipulation, lysis and analysis onto one planar device, presented in this thesis, represents one important step towards the enzymatic screening of large cell populations with high throughput.

The high cost of micromachining microfluidic manifolds in glass has led to the search for an alternative plastic device material. Poly(dimethylsiloxane), PDMS was suggested as a substitute substrate material, offering favorable bulk and surface properties for miniaturized CE and FIA devices and very low machining and material cost. Previous studies of electrophoretic separations performed with these devices, which were molded from micromachined templates, did not include a characterization of electrokinetic fluid handling and electroosmotic flow. Therefore we tested native PDMS devices, which were determined to be preferable to surface oxidized PDMS devices in terms of EOF constancy and shelf life in this study, for the use in capillary zone electrophoresis, CZE. Due to the study, described in this thesis, we have acquired insight into the potential range of samples, which can be analysed in these devices. The possibility of integrating several parallel channels onto one planar device allows multiple analyses to be performed at the same time. The simultaneous monitoring of several sample zones, however, represents a significant detection challenge. The stacking of several devices therefore opens up the possibility of vertical instead of lateral scanning of the device or detector. A vertical scan of thin stacked devices potentially reduces the scan distance and thus increases the possible data acquisition rate. We utilized the self adhesive properties of PDMS to create a device stack which consisted of two identical fluidic layers. The ease of assembly and the possibility to extend this concept to > 2 layers makes this study an interesting proof of the proposed concept.

1.3 The Microfluidic Chip to World Interface

The technology for fabricating microfluidic devices out of silicon, glass and a variety of polymeric substrates is advancing rapidly (see chapter 4). However, the connection to external liquid reservoirs, pumps and detectors, i.e. the coupling of conventional tubing to microfluidic devices remains one of the main challenges of the application of μ TAS [55]. The challenge of the coupling lies in the mismatch of on-chip analyte plug volumes, typically several 100 picoliters, and the typical μ L volume of conventional fluid delivery systems. The introduction of large

mixing and dead volumes in capillary-to-chip interconnections results in increased minimum sample introduction volumes and the danger of sample carry over effects when capillaries are used as connectors to sample reservoirs. Further, excessive bandbroadening is introduced in post-chip on-capillary detection schemes. Small interconnection volumes can only be realized if a tight seal between an aligned capillary and a microchannel of matching geometries can be realized with high accuracy and reproducibility. In addition, the facility of device handling and the reversibility of the connection are of great importance. Several different approaches have addressed this problem and shall be discussed briefly.

The most obvious approach of capillary to chip interconnects involves the orthogonal connection of the tubing to an access hole defined in the coverglass or the device itself. The shortcoming of this approach is clearly the high dead volume of the interconnect, which is given by the thickness of the coverglass or device and the minimum diameter of the access hole which can be realized by etching or drilling. The bonding of the capillary to the chip is realized either by mechanical fastening, i.e. the use of compression fittings with flanges [56], O rings [57], or ferrules [58] (see also chapter 2), or by gluing with a chemically inert adhesive. Figure 1.1 depicts the first approach. The fabrication of chip holders with incorporated threads for accomodation of the fittings allows for facile alignment of the capillary to the chip. If adhesive bonding is employed, micromanipulation tools and microscopic observation are required for proper alignment. Clearly, the latter approach represents a labor intensive step, introducing unwanted variability of the introduced dead volume. In addition, seeping of adhesive into the microchannel is a danger of this method, which can be circumvented by bonding of microcouplers to the chip top surface, as described recently [59]. This technique further facilitates the connection to flexible tubing and eliminates the need for alignment and bonding of a rigid sleeve for mechanical strength as with adhesive capillary-to-chip bonding.

Alternatively, orthogonal insertion channels can be etched iso- or anisotropically into the substrate allowing for tight and prealigned insertion of capillaries. This approach has been utilized in several studies [60]-[64]. The most impressive results shall be highlighted. A silicon device with 75 μm wide and 75 μm deep microchannels, defined by dry etching and isolated with thermally grown SiO_2 , was coupled with a 75 μm i.d. fused silica capillary with virtually no dead volume [60],[61] (see figure 1.2). Access holes were anisotropically etched through the device, resulting in a photo patternable alignment platform for the capillary end. The capillary ends were polished, butt coupled and glued on the outside. However, the device was used exclusively as an injector for conventional CE with fused silica capillaries and therefore no functional assessment of the introduced dead volume was given. The realized structure reportedly sustained pressures up to 120 bar. A functionally similar silicon device was realized by dry etching of circular insertion holes, matching the outside and inside diameter of the

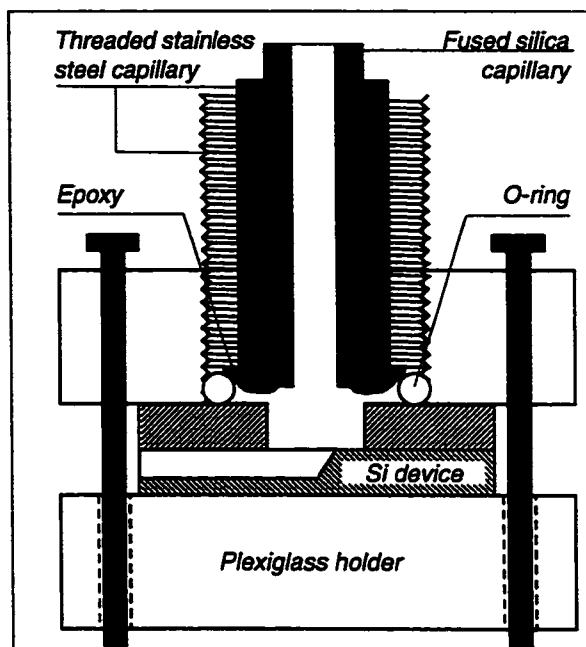


Figure 1.1.

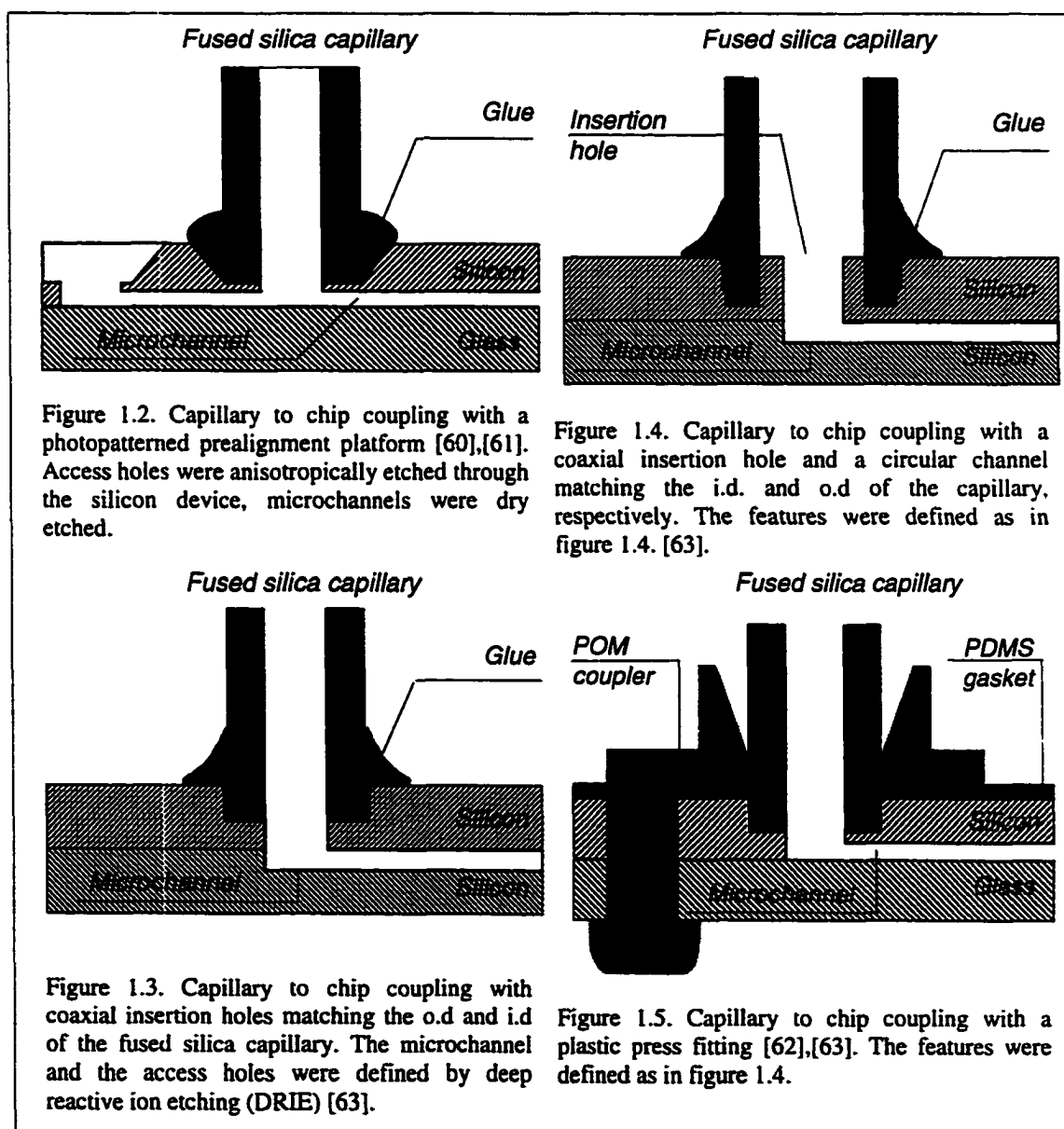
Chip holder for capillary to chip coupling.

Ocvirk et al. [57] mounted a 350 μm thick silicon device between 1.5 cm thick steel blocks with access threads. Hereby O-rings were compressed by threaded steel capillaries (1.6 mm O.D., 0.3 mm I.D., screwed into the bottom block) against the silicon chip, allowing a tight seal at pressure at up to 140 bar pressure. Fused silica capillaries (255 mm I.D., 25 μm I.D.) were inserted into the steel capillaries, glued on the outside and connected to the etched through holes (180 x 180 μm at the hole edge) on the bottom of the device. Flanged teflon tubing (O.D. 1.6 mm) was used instead of O-rings for low pressure connections by Raymond et al. [56]. Alternatively, deformable ferrules were used in combination with a plexiglass holder in this thesis. The flange-free connection with ferrules allows for the connection of sheathed fused silica capillaries to the chip and sustains pressures of up

capillary for elimination of dead volume, as depicted in figure 1.3 [62]. The drawback of this method is the lack of an adhesive barrier, thus allowing for seeping of adhesive into the microchannel. The addition of a concentric sleeve, as depicted in figure 1.4, circumvented this shortcoming [63]. However, some dead volume was introduced by this coupling. Figure 1.5 depicts the use of a reusable microfluidic coupler with incorporated alignment posts. The coupler is fabricated by injection molding of polyoxymethylene (POM) plastic. The posts are inserted into alignment holes, fabricated into glass by ultrasonic drilling, and melted at temperatures up to 250°C to form a monolithic structure. A 250 μm thick PDMS gasket, fabricated with an etched

silicon mold, is placed at the glass/plastic interface and fused silica capillaries are press fit into the access hole. The demonstrated assembly proved to be leak tight at pressures as high as 250 psi. Low pressure connections to flexible tubing were achieved by stretching the tubing around the input port of the coupler.

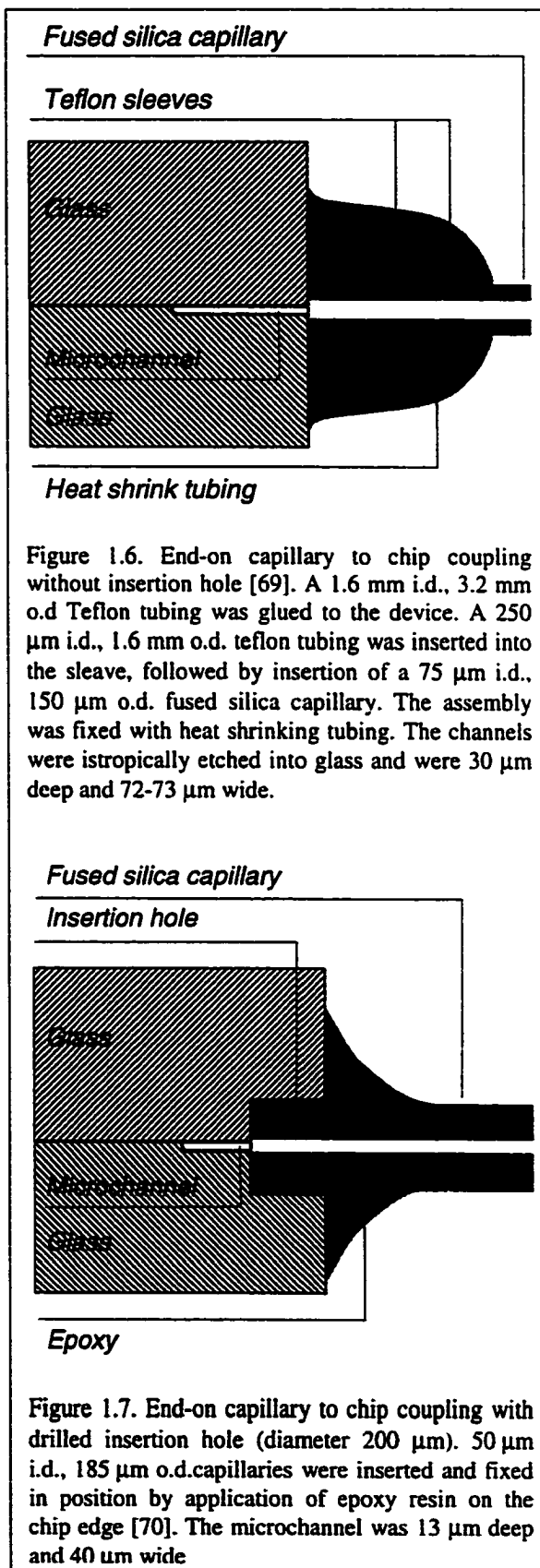
All above mentioned approaches are based on silicon devices which allow for the definition of flat structures and holes. Unfortunately, silicon devices are not capable of sustaining the high electric fields that glass devices exploit for efficient CE separations [65]. The required etch depths for the definition of similar features in glass, are not achievable by available etching



techniques and therefore other techniques have to be employed for glass-chip to capillary couplings.

Several groups have drilled insertion holes, with diameters slightly larger than the capillary o.d., into glass cover plates, followed by insertion of the capillary into the bonded device and gluing on the outside [66],[67]. The disadvantages lie in the difficulty of reproducible alignment, the lack of an adhesive barrier, and, as for all glued connections, the lack of reversibility of the connection. In light of these limitations, two alternative solutions for this challenging problem can be identified.

The first approach is applicable for polymeric devices and simply utilizes the described potential of silicon micromachining. All above mentioned approaches of silicon-chip to capillary couplings should be transferable to polymer devices when negatives of the described silicon devices are used for replication. Secondly, the interest in chip to detector couplings and the need for short transfer capillaries has led to the development of end-on capillary-to-glass chip connectors [68]-[71]. The first attempt, depicted in figure 1.6, was based on gluing of an assembly of sheathed tubing to a microchip, which was cut perpendicularly to the microchannel [69]. The approach suffered from high dead volumes due to poor alignment, and thus the targeted microchip



based CE-MS coupling was not attainable. Bings et al. [70] recently demonstrated an end-on connector with minimal dead volume by drilling a capillary joint into the microchannel. The use of a flat bottom drill (200 μm diameter) allowed for accurate definition of an insertion hole and positioning of a fused silica capillary, as depicted in figure 1.7. Plugging of microchannels while drilling and gluing was prevented by filling the channel with a removable adhesive. Zhang et al. [71] realized an end-on capillary insertion channel of approximately circular cross section (400 μm in diameter) by bonding of two devices with identical 200 μm deep channels. A 380 μm o.d., 75 μm i.d. fused silica capillary was then glued into the channel opening with the edge of the capillary being tapered to match the shape of the channel (see figure 1.8). Efficient electrophoretic separations with hyphenated MS detection were realized by both approaches [71],[72].

The challenge of a chip-to world interface with low dead volume has clearly been met, as described in this section. The described arsenal of interconnections is expected to grow until the introduction of commercially available, miniaturized, disposable and reversible connectors. However, considering the multitude of conventional capillary connection formats, the standardization of chip/capillary interfaces appears to be rather unlikely.

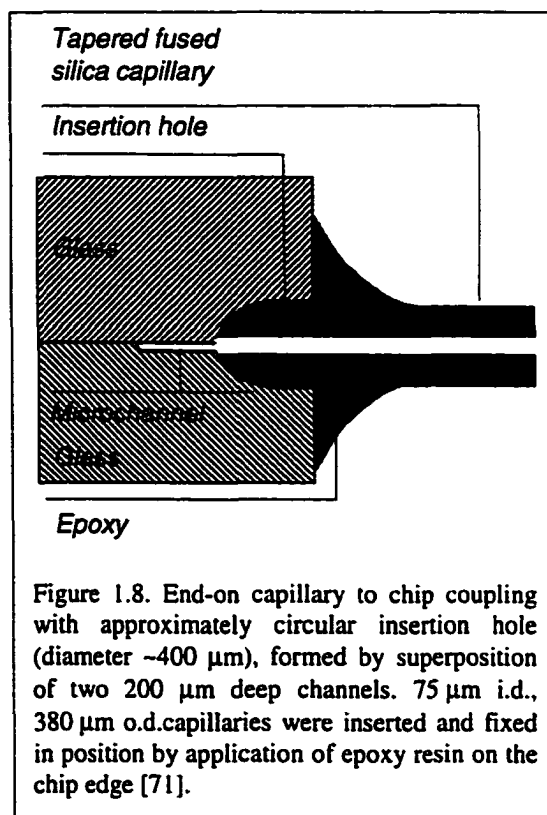


Figure 1.8. End-on capillary to chip coupling with approximately circular insertion hole (diameter $\sim 400 \mu\text{m}$), formed by superposition of two 200 μm deep channels. 75 μm i.d., 380 μm o.d. capillaries were inserted and fixed in position by application of epoxy resin on the chip edge [71].

1.4 Detection Methods for μ TAS

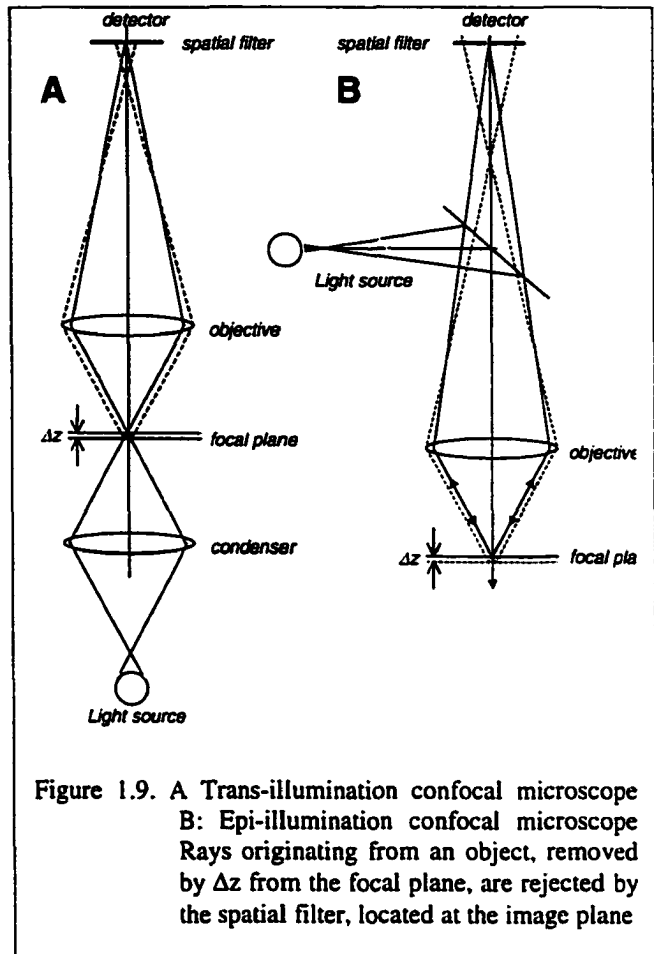
Microchip based analytical methods frequently require the measurement of subnanomolar sample concentrations in subnanoliter sample volumes. Hence laser induced fluorescence (LIF) detection has frequently been used due to its inherent sensitivity [34],[73],[74], which was demonstrated before in on-column [75] and post-column LIF detection schemes [76]-[90]. Due to the non fluorescent nature of most analytes of interest in the visible spectrum there has been a vital interest in alternative, sufficiently sensitive detection methods. Chip based approaches have mostly used on-channel detection due to the difficulties of zero dead volume couplings to commercially available on-capillary detectors. However, the demonstration and availability of LC and CE-ESI-MS couplings has recently triggered a strong research effort in microchip-ESI-MS hyphenation and hence chip to capillary couplings [69]-[72],[91],[92], that may alleviate the hyphenation to external detectors.

On-channel detection schemes can be classified into optical and electrochemical methods (see for example [93],[94]) with most reports employing optical detection schemes. Except for fluorescence, optical schemes have utilized absorbance, refractive index (RI), Raman spectroscopy, chemiluminescence and most recently thermo-optical detection [95]. While RI detection is inherently insensitive [96],[97], absorbance detection is, particularly when employing path length extension [98]-[101], a very attractive, universal optical method for detection of low μ M sample concentrations on-chip. In addition, an upright Raman microscope was used for on-channel detection of isotachophoretic zones in the μ M concentration range [102]. Chemiluminescence detection of luminol with hydrogen peroxide was demonstrated in the low nM concentration range in detection volumes of \sim 3.9 nL [103], employing a post-separation chemiluminescence reaction. Ruthenium based electrochemiluminescence detection has been employed by several groups [104]-[106] with mass detection limits as low as 30000 molecules [105].

LIF detection has, however, due to its sensitivity, maintained its original importance in μ TAS approaches. Several groups have focused on the development of off-chip LIF optical instrumentation [31],[107]-[110] and the application of previously employed approaches for gel scanning [111] and capillary array electrophoresis [112],[113], since the integration of optical elements onto microfluidic devices does not offer significant advantages in handling, instrumentation cost or device performance at the current stage of miniaturization. The interested reader may be referred to recent publications, describing the latest developments in the integration of micro optics onto planar devices [100],[114]-[120].

1.4.1 Confocal Microscopy

Two lenses with one common focal point represent a confocal system [121]. This definition therefore includes a conventional microscope, where the focal points of condenser and imaging lens coincide. More commonly however, a confocal imaging system is understood to be a system in which both a diffraction limited illumination point and a detector point are focused on the same object point [122], as depicted in figure 1.9. A confocal aperture, in most implementations a pinhole or a slit, is positioned on the microscope axis at the image plane. thereby restricting the field of view. The result is that the resolution perpendicular to the optical axis is slightly improved over a comparable conventional microscope [123]. More importantly however,



resolution along the optical axis, i.e. axial resolution, is introduced into the system [123], as evident from ray tracing in figure 1.9. Layers removed from the focal plane by a distance Δz are defocused and are not detected. Two confocal setups can be differentiated. A trans-illuminating setup consists of a condenser and a collection objective (see figure 1.9A), whereas in the epi-illuminating mode one single objective lens serves both as the condenser for illumination and as objective lens for light collection (see figure 1.9B). In the latter approach a dichroic beam splitter is used for separation of excitation and emission wavelengths. In confocal fluorescence microscopy a laser source is most often used for excitation and is focused at the object plane of the microscope. A converging illumination cone passes through the sample to reach the plane of focus, excites a section of fluorescent material and passes out through a diverging cone. The lowest detectable fluorescence light level of a fluorescent section, embedded in a medium of high background fluorescence and scattering, depends on the degree of background rejection and the ratio of detected over generated fluorescence light.

The sectioning power of a confocal fluorescence microscope, i.e the ability to reject out of focus background fluorescence and scattering, depends on the numerical aperture of the condenser and the objective, the employed wavelength and the size of the spatial filter. For an epifluorescence microscope with an infinitesimal pinhole, the sectioning power can be expressed as full width half maximum, FWHM, of the depth of field function of confocal microscopy, given in equation 1.1. [123],

$$I(u) = \left[\frac{\sin(u/4)}{u/4} \right]^4 \quad (1.1)$$

$$u = \frac{8\pi}{\lambda} n z \sin^2 \left(\frac{\alpha}{2} \right) \quad (1.2)$$

where u is a normalized axial coordinate z , as given by equation 1.2 [124]. λ is the wavelength of detected radiation [μm], n the refractive index of the immersing medium, z the axial coordinate [μm] and α the cone angle. Figure 1.10, depicting the theoretical axial response of a confocal microscope, when a fluorescent point object is scanned axially through the focal plane ($z=0$), illustrates the effect of the microscope numerical aperture, N.A., on the optical sectioning strength. In contrast to this response, a conventional microscope, i.e. a system with no pinhole at the image plane, as well as a confocal system with very large pinholes, show no signal variation when a fluorescent object is scanned axially [124]. As evident from Figure 1.10, high N.A. objectives are preferable for narrow sectioning and thus good background rejection. For a given microscope setup the axial resolution will further improve with decreasing Stoke shifts, as pointed out by Wilson [125].

There is a trade-off of light collection efficiency for depth of field in confocal microscopy. The knowledge of the effect of pinhole size on signal to background, S/B, and signal to noise ratios, S/N, is thus crucial for optimum performance. A discussion of this correlation is given in references [126] for a shot noise limited system. Briefly, measurements of the signal from a fluorescent point source and a large uniform scattering volume with finite pinhole diameters, indicated a quadratic increase of S and B with pinhole diameter in the small aperture limit, i.e. $v <$

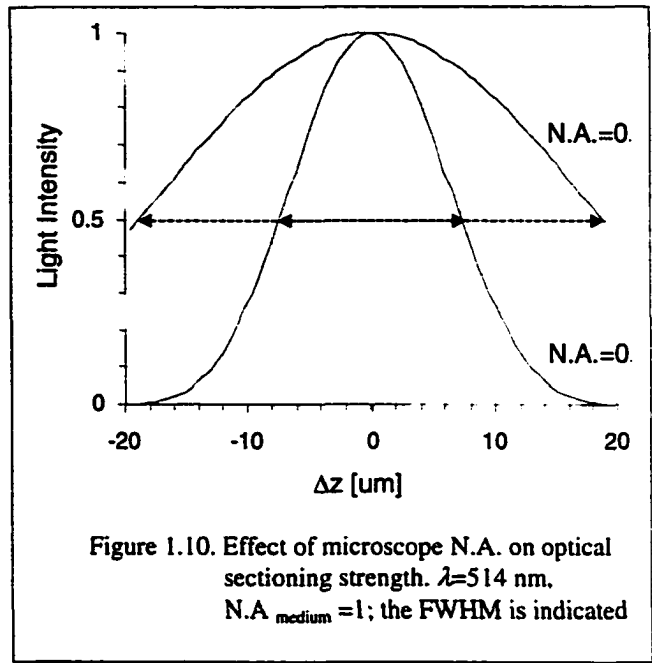


Figure 1.10. Effect of microscope N.A. on optical sectioning strength. $\lambda=514 \text{ nm}$, $N.A._{\text{medium}} = 1$; the FWHM is indicated

2.5, where ν represents the pinhole radius, r , in dimensionless optical units, as given by equation 1.3. [127]

$$\nu = \frac{2\pi}{\lambda} r \sin \alpha \quad (1.3)$$

At infinitely small pinhole radii and maximum background rejection, a unity S/B ratio was obtained. At $\nu > 7$ signal levels show a plateau, while the background signal increases parabolically, hence resulting in a decreased S/B ratio at $\nu > 7$. Since the shot noise N rises as the square root of the total detected signal ($S+B$), S/N shows a linear increase with ν at $\nu < 2.5$ and decays with increasing ν as B increases. Apart from the size of the spatial filter, care must be taken that the losses of optical transfer efficiency, OTE, i.e. the fraction of fluorescent light emitted by fluorophores within the focal volume at the object plane that is detected [126], are minimized. Therefore the transfer efficiency of all optical elements, i.e. the objective, dichroic filter, tube lens, band pass filters and the detector, frequently a photomultiplier tube, have to be maximized. All derived equations apply for an ideally corrected optical lens system. In reality however, spherical and chromatic aberrations as well as curvature of field can affect the sectioning power of the instrument [123],[128],[129]. Thus it is advisable to evaluate the optical setup experimentally prior to routine use, as performed in this study (see chapter 2).

1.5 Single Cell Analysis

1.5.1 Single Cell Analysis: Relevance and Methods

The chemical analysis of single cells is of great interest in the biological and medical sciences. Insight into the chemical makeup and dynamics of single cells should result in mechanistic understanding of cell function in complicated cellular environments. More specifically, it is necessary to identify and sort specific cell populations out of a heterogeneous cell population in order to correlate patterns of gene expression with the particular function of the cell type. Furthermore, multiple measurements are necessary per single cell in order to determine the concentrations of several intracellular components, to correlate the component concentrations to the volume of the cell, to gain insight into the mechanism of intracellular reactions and to obtain chemical information on the subcellular level. This knowledge should lead to structural and functional mapping of the investigated viable cell type and ultimately to understanding of cellular differentiation.

Analytical instrumentation for single cell analysis should meet a number of criteria, as pointed out previously [130]. The analysis should be non-destructive, with in vivo capabilities;

the obtainable concentration detection limits should allow for analysis of minor intracellular components; the response time should allow for monitoring of chemical dynamics on a time scale similar to that of cellular processes; spatial differentiation within one cell should be possible and high throughput is required to allow for examination of large cell populations. Currently, no analytical technique satisfies all criteria. However, several complementary techniques are in use, which shall be discussed briefly prior to the discussion of chip based single cell analysis.

Digitized fluorescence microscopy of stained single cells provides a way to dynamically probe the chemical identity of single viable cells at high resolution in space and time. A small number of isolated cells or biological tissues are stained with highly sensitive and specific fluorescent or fluorogenic probes. An extensive arsenal of probes for measurement of intracellular ions, enzymes, pH, membrane potentials et altera is in widespread use in cell biology (see for example [131],[132]). The kinetics of intracellular reactions as well as intercellular interactions can thus be monitored with subcellular resolution when image acquisition software is used. The use of laser scanning confocal microscopes allows for three dimensional imaging of cells at low light levels. However, every static microscopic technique suffers from the inherently low rate of analysis which results from the small number of cells contained in the field of view.

Flow cytometry is the logical extension of the above described approach and represents the principal technique of cytoanalysis. Briefly, a fluidic system is coupled to a fluorescence microscope allowing for colour discriminated fluorescence analysis of single cells with high throughput. Cells are suspended in a conductive, isotonic liquid, pumped hydraulically at a constant flow rate through a sheath flow assembly for hydrodynamic focusing and are exposed to a laser beam one cell at a time [133]. The uptake of fluorescent labels, i.e. fluorochrome labeled antibodies, fluorescent membrane, nuclear and cytoplasmic stains as well as fluorogenic enzyme substrates, into viable cells and subsequent incubation allows for the determination of a cell specific chemical profile. In addition to fluorescence, relative light scattering is recorded by separate detectors and permits cells to be differentiated on the basis of size and granularity. Forward light scattering, i.e. scattering at small angles ($0.5-2^\circ$) from the incident laser beam, yields information about the cell volume after calibration of the cytometer [134], while side scattering or right angle scattering, i.e. scattering detected 90° to the incident beam, permits distinction of cell type based on granularity. Since flow cytometers are multiparameter instruments, subpopulations of a heterogeneous cell populations can be identified by means of their scattering and fluorescent intensities. A fundamental advantage of flow cytometry is the ability to sort viable subpopulations which have been identified by the preceding analysis. In most commercial instruments this sorting is achieved by vibrating the flow chamber at high

frequency. Consequently the sheath flow is segmented into uniform droplets, containing one cell at a time. By application of charge to the sample stream at the exit of the flow cell, each droplet which carries one sorted cell, can be deflected into a predefined cell vessel. This sorting ability, combined with light scattering and fluorescence properties to identify a response, and time to evaluate the kinetics of this response, has made flow cytometry a widely used technique in cell biology. One obvious disadvantage of flow cytometry is the necessary disintegration of biological tissues resulting in loss of substantial information on intercellular communication [135]. In addition, most commercial instruments suffer from an undesirably long time gap between incubation of the cell suspension with reagents and the actual fluorescence measurement in the sheath flow cuvette. This limitation can be eliminated when a coaxial flow assembly, allowing for rapid mixing of reagents with the cell stream, is inserted prior to analysis in the cuvette, as described previously [136].

Numerous monographs have been published on the subject of flow cytometry. The interested reader shall be referred to a representative selection for an overview of techniques and applications [137]-[143].

The separation of multiple intracellular components and reaction products is frequently a *sine qua non* for quantitative chemical analysis of single cells. Capillary based separation techniques, such as open tubular LC [144]-[146] and capillary electrophoresis (CE) [149]-[155] offer the required separation efficiency, while laser induced fluorescence (LIF) detection permits the quantitation of yoctomoles (10^{-24} moles) of multiple intracellular analytes in one single cell [155]. In order to avoid undesired dilution of cell content, cell lysis and turnover with reagents have frequently been performed on-column, i.e. after introduction of one single cell into the separation capillary [155]. The chemical profile obtained of one cell can then be inter-correlated, yielding important mechanistic information. However, this method suffers from significant drawbacks. Due to the difficulty of cell introduction and the resulting serial nature of this approach, only low sample throughputs are obtainable. Further, the minimum response time for dynamic monitoring of cellular events is given by the separation time and is hence frequently unsuitable for monitoring of rapid kinetic events. The correlation to cell size has to be established prior to separation by alternative methods, clearly demonstrating the complementary nature of this CE approach.

The limitations of the above described approaches explain the desire for a method which provides rapid mixing of single cells with reagents, the detection of rapid kinetic events, the ability to separate and detect the reaction products with high throughput and which utilizes disposable devices. Microchip based approaches shall be discussed in this context.

1.5.2 Microchip-based Single Cell Analysis

Accurate manipulation, transport and incubation of single cells require fluidic channels on near the same scale as the cell themselves. Such fluidic features can be defined with high complexity and reproducibility in a variety of planar substrates when micromachining methods are employed. The flatness of the microchip cover offers the advantage of undistorted microscopic observation of all on-chip processes. Reactions of single cells can thus be monitored at predefined locations in the fluidic network. This concept was first introduced by Li and Harrison [156], demonstrating the transport, mixing and lysis of *Escherichia coli* and *Saccharomyces cerevisiae* with sodium dodecyl sulphate. Electrokinetic fluid handling was employed to drive the cells and the reagents within a microfluidic network, patterned onto a planar glass device.

Electrokinetic fluid handling of cell suspensions suffers from severe drawbacks with regard to accurate fluidic control of single cells. The electrophoretic mobility of a single cell is directly proportional to its surface charge density and hence results in a velocity distribution of cells according to the cell type. In order to avoid cell size-based fractionation within the same cell type, the ionic strength of the suspension medium has to exceed a size dependent concentration threshold, as reported previously [157]. An additional restriction arises when the channel surface is modified with fetal calf serum (FCS) [158] to prevent cell to wall adhesion. The resulting reduction of electroosmotic flow then results in insufficiently low pumping action at applicable voltages, i.e. at field strengths that do not lead to cell lysis. Due to these limitations, pressure-driven systems have mostly been utilized for on-chip cell manipulation. Syringe pumps [159] (see also chapter 3), HPLC pumps [160] or simply siphoning across the fluidic network [161] have been used to apply positive or negative pressure to the fluidic network. Prior to introduction into the microchannels, cell suspensions are contained in the employed syringes, injected into a flow circuit via an injection valve or inserted into on-chip reservoirs in these approaches.

Dielectrophoresis represents an alternative mechanism for manipulation of single cells in microstructures [162]. Cells are polarised by application of strong AC fields on the order of several kV/ μm . A non uniform field of low frequency results then in a force on the induced dipole in the cell, driving the cell towards regions of high field strength, whereas higher AC frequencies result in a force towards regions of low field strength. An electrode pattern, defined on the device and energized with a high frequency traveling wave allows for the movement and sorting of cells along predefined trajectories [163]-[167]. Cells are attracted to or levitated above the electrode pattern according to their dielectric properties while the traveling wave exerts a

torque to levitated cells along the defined pattern. When a circular or rectangular microelectrode pattern is deposited onto a microfluidic device, cells can be trapped in a field cage for further studies of intracellular reactions [168],[169].

Alternatively, hydrodynamic pumping was utilized recently to transport, incubate and react compounds with single cells on a microfluidic device [158]. The use of an on-chip stopped flow method, highly sensitive fluorogenic stains and microscopic fluorescence imaging allowed for monitoring of the kinetic event of cellular calcium influx in human lymphocytes. Further, oxidative burst kinetics was monitored in human neutrophils after on-chip activation. The advantage of this approach over conventional microscopic techniques lies in the ability of controlled mixing and the possibility of high throughput of cells through the system, thus allowing for screening of large cell populations.

The feasibility of pumping a wide range of biological fluids and cell suspensions in microchannels has been demonstrated in various studies. Studies of flow dynamics in channels of different cross sections [161],[170]-[176] have yielded valuable insight into the physical properties of various cell types. More recently, microchips have been utilized for counting [159] and sorting [160] of viable cells. Several microfabricated flow cytometer flow channels have been reported [177]-[180]. On-chip cell sorting of rare cells reportedly exhibits several advantages [160]-lower dilution factor, higher recovery rate of sorted cell populations and avoidance of contamination-over sorting in conventional sheath flow cuvettes, contained in commercial flow cytometers [181]. An inherent advantageous feature of microdevice-based single cell analysis is the reduction of reagent consumption to a few μL or less per experiment [182]. Therefore the reagent costs for expensive reagents and/or a large number of tests can be reduced significantly. In combination with the possible reduction of sample volume and above mentioned advantages, microfluidic devices create a tool for single cell analysis that is more flexible than, and complementary to flow cytometry (see section 1.5.1).

The objective of chapter 3 is to demonstrate an extension of the previous on-chip single cell analysis schemes. The manipulation and lysis of single cells, followed by incubation with an enzyme substrate and detection of enzyme reaction products were performed. This demonstration meets all outlined criteria of a desirable single cell analysis system (see 1.5.1) except the implementation of a post reaction separation step. The additional integration of post reaction CE of single cell lysates represents, however, a significant challenge which is beyond the scope of this thesis.

1.6 Capillary electrophoresis in Polymeric Microfluidic Devices

1.6.1 Capillary Electrophoresis

Capillary electrophoresis (CE), a contemporary, automated and rapid adaption of electrophoresis to small volumes, has established a previously unknown efficiency of analyte separation. Electrophoresis, introduced in 1897 [183], is a technique for the separation of charged molecules based on their migration under an applied field. Slab gels, cellulose acetate and paper have been used as support media prior to the introduction of free flow electrophoresis in tubes. In case of slab gel electrophoresis, a viscous gel acts as support for the background electrolyte, as separation matrix and as anticonvective medium. Several disadvantages of electrophoresis were successfully eliminated by miniaturization. The use of cooled narrow quartz tubes (3 mm I.D.), first demonstrated by Hjerten [184], allowed for charge based separations in free solution, since the tube walls replaced the gel as support medium. As a consequence of smaller dimensions, higher field strengths could be applied without heat induced convection, resulting in a significant improvement in separation efficiency. The serial nature of the separation technique opened up the possibility of automation, eliminating the necessity of labor-intensive assays carried out in electrophoretic gels. The application of hydrodynamic sample injection into the capillary and on-column fluorescence detection by Jorgenson and Lukasz [185],[186] finally permitted the use of capillaries (75 μm I.D) for zone electrophoresis in free solution, and hence the application of high field strengths across the capillary. Subsequently high separation efficiencies were demonstrated for a diverse spectrum of analytes in analysis times of one hour or less, justifying the term high performance capillary electrophoresis (HPCE) [187]. Due to the aforementioned potential of the technique and the complementary nature to HPLC, the utilization of the technique has exploded in academic research (see [188]-[190] for reviews). Consequently a variety of commercial CE instruments have become available [191]-[194].

CE separations are performed in buffer filled capillaries, whereas the sample is injected as a narrow plug either hydrodynamically or electrokinetically, i.e. by application of pressure or voltage to one end of the capillary, respectively. A fluidic and conductive path through the capillary is established by insertion of both ends of the capillary and of two electrodes, connected to a high voltage power supply and ground, respectively, into two buffer vials. Application of an electric field across the buffer vials results in two ion transport phenomena. Electroosmotic bulk flow, EOF, and electrophoretic migration. EOF of the background electrolyte is generated as a result of an immobilized charge on the capillary wall. The direction of EOF is dependent on the sign of immobilized charge and is frequently cathodic, due to negative charges on the capillary

wall. Possible sources of the immobilized charge on the capillary wall will be discussed in section 1.6.2.2. Figure 1.11 illustrates an exemplary electrophoretic separation with cathodic EOF. The flow vector of uncharged analytes and the EOF is identical, while ions are separated electrophoretically according to their charge, shape and size. The addition of electrophoretic and electroosmotic flow vectors of anions and cations results in sequential elution of cations, neutrals and anions. The flow of anions however, may be reversed if the electrophoretic mobility of anions exceeds the electroosmotic mobility.

The origin of electroosmotic flow including a definition of electroosmotic and electrophoretic mobilities shall now be discussed in section 1.6.2. The effect of experimental parameters on CE separation efficiency will be given in section 1.6.3 as an introduction for the discussion in chapter 4.

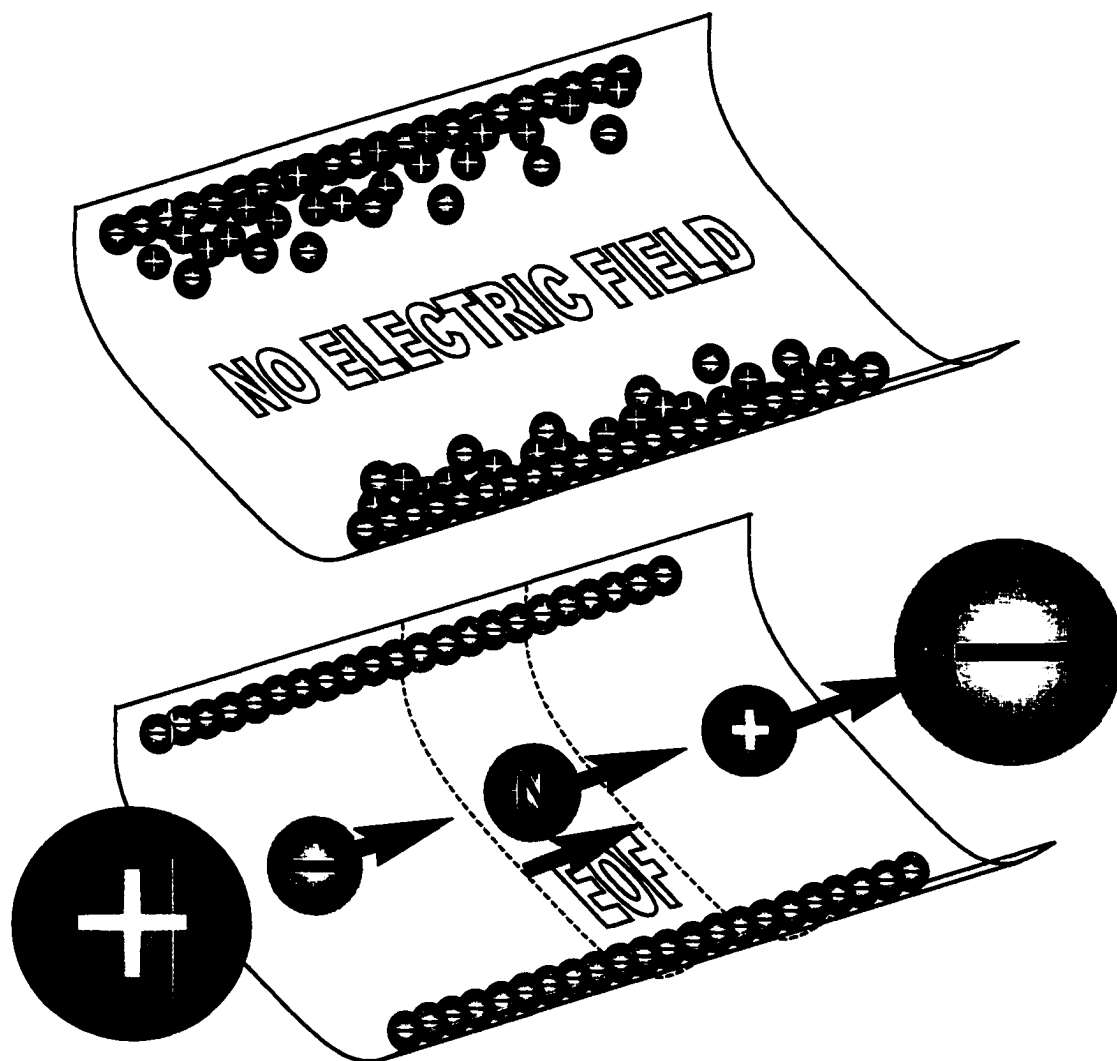


Figure 1.11: Schematic view of electroosmotic flow (EOF) and electrophoretic migration in a negatively charged glass microchannel. The top and bottom images illustrate the formation of the electrical double layer without applied voltage and the differential migration of cations, neutrals and anions in an applied field, respectively

1.6.2 Origin of Electroosmotic Flow in Microfluidic Channels

1.6.2.1 Electroosmosis

The application of an electric field across an electrolyte filled microchannel frequently results in electroosmosis, i.e the movement of liquid relative to a stationary surface charge at the channel wall. The immobilized charge layer at the wall results in a potential between the wall and the bulk solution ϕ [V] and an electrical double layer at the wall. The insight into the nature of the electrical double layer and its dependence on surface and solution parameters has led to a qualitative understanding of electroosmosis. The first double-layer model, presented by von Helmholtz [195], assumed that each immobilized charge would be neutralized by an adjacent counter charge, resulting in a fixed double layer. Gouy and Chapman [196],[197] refined this model by taking into account the thermal motion of solvent molecules, and thus suggested the existence of a diffuse double layer. Stern [198] unified these two models by postulation of a compact double layer, immediately adjacent to the wall, and a diffuse layer which extends into the bulk solution. The thickness of the diffuse layer is given by the reciprocal of the Debye Hückel constant κ , as evident from eq 1.4,

$$\frac{1}{\kappa} = \sqrt{\frac{\epsilon k T}{2000 e^2 N_{AV} I}} \quad (1.4)$$

where e is the electron charge [1.60×10^{-19} C], N_{AV} the Avogadro constant, I the ionic strength [M], ϵ the permittivity of the electrolyte [C/Vm], k the Boltzmann constant [1.38×10^{-23} J/K] and T the absolute temperature [K]. The potential at the plane of shear between the compact and diffuse parts of the double layer at a plane surface is known as the zeta potential ζ_{EOF} [V] which is given by eq. 1.5,

$$\zeta_{EOF} = \frac{\rho}{\epsilon \kappa} \quad (1.5)$$

where ρ is the surface charge density [C/m^2]. The linear electroosmotically flow velocity, v_{EOF} [m/s], can then be calculated from the von Smoluchowski equation [199],

$$v_{EOF} = \frac{\rho \epsilon E}{\eta / 10} \quad (1.6)$$

where η is the dynamic viscosity of the electrolyte [poise] and E the applied field strength [V/m]. The electroosmotic mobility μ_{EOF} [m^2/Vs] is v_{EOF}/E . Thus the electroosmotic pumping action can be calculated if the surface charge density of the channel wall is known under the employed electrolyte conditions. More commonly however, the given equations are being used after experimental measurement of v_{EOF} to determine ζ and ρ .

1.6.2.2 Origin of Surface Charge on Channel Walls

Glass and most polymers exhibit a zeta potential, ζ , when in contact with electrolyte solutions [200],[201]. The charge on the capillary or channel wall can be attributed to various origins. If dissociative groups, such as silanol, carboxy, hydroxy and amino functionalities are incorporated in the wall material, a pH dependent surface charge is generated on the wall. These functionalities are either due to a bulk property of the used substrate, as in glass, or are introduced by the addition of fillers for property modification, as e.g. in poly(dimethylsiloxane), PDMS (see chapter 4). Charged and/or chargeable functionalities can further be introduced in the polymerization process by catalysts and initiators. In addition, hydrolysis of the surface is a possible mechanism for charge generation, as described recently for PDMS [202]. Preferential sorption of potential determining electrolyte ions to the surface can be another charge origin [201],[203],[204]. Electrostatic, chemical and dispersive interactions between the wall and the ions can be differentiated [204].

The majority of CE separations have been performed in fused silica capillaries, due to the excellent electrical and optical properties of the wall material. However, the high charge density of fused silica, resulting from silanol groups on the capillary wall, frequently leads to unwanted sorption of analytes and a strongly pH dependent electroosmotic flow velocity [205]. In addition to the wide range of published fused silica surface modification procedures [206],[207], alternative polymeric capillary materials have been suggested and used to circumvent these drawbacks. So far, Teflon (PTFE) [205]-[211], poly(fluoroethylenepropylene) (FEP) [203], polyethylene (PE) [203], polypropylene (PP) [212]-[214], polyvinylchloride (PVC) [203], polymethyl methacrylate (PMMA) [215], poly(butylene terephthalate) (PBTP) [216], ethylene/vinyl acetate [216], and nylon [216] capillaries have been characterized for CE. The surface charge density of all listed capillary materials was found to be lower than fused silica under the employed conditions. However, a direct comparison of surface charge densities of all capillary materials cannot be made at this point due to the manifold of employed buffer conditions. All materials exhibited negative and pH dependent zeta potentials in the pH 4-10 range. This may point to acidic sites on the capillary wall.

The possibility of preferential ion adsorption onto uncharged substrates was demonstrated recently by Jacobasch et al [204]. Poly(ether ether ketone), PEEK, characterized as an uncharged surface by X-ray photoelectron spectroscopy, was exposed to multiple electrolyte solutions. Negative surface potentials were determined by atomic force microscopy under all employed

conditions (electrolytes: KOH, KCl, KBr, Na₃PO₄, $c_{\text{electrolyte}} = 10^{-5}$ - 10^{-2} M), leading to the hypothesis of van der Waals force induced specific ion adsorption onto the uncharged surface.

Unlike the motivation for the use of polymeric capillary materials, the search for suitable polymeric device materials for on-chip CE, has been driven by the desire to decrease device manufacturing costs. An overview of materials and machining techniques will be given in chapter 4. To the best of our knowledge, only one study on EOF in polymer substrates has been published as yet [217]. The magnitude of cathodic electroosmotic flow in various photoablated substrates was found to follow the series: Polycarbonate (PC) < polystyrene (PS) < cellulose acetate (CA) < poly(ethylterephthalate) (PET). The absolute zeta potentials of all substrates were found to be significantly lower than in fused silica under identical conditions. The surface charge was assumed to originate from the photoablation process. Amino, hydroxyl and carboxylic functionalities are assumed to be generated on the polymer surface due to the incorporation of oxygen or nitrogen into the structure. However, the determined differences in surface potentials between the different polymers may be attributable to differences in surface roughness and hence surface charge densities created during the photoablation process.

As a conclusion of the discussion of possible charge contributions, the impact of prewetting agents on EOF in polymeric substrates, as described by Nielen [212], and the importance of sufficient and consistent equilibration for EOF constancy (see for example [203],[211]) is crucial for reproducible electroosmotic pumping.

1.6.3 Fundamentals and Resolution of CE Separations:

1.6.3.1 Migration of Ions in CE

Electrophoretic separations of charged species result from distinct electrophoretic mobilities of ions. While neutral analytes elute at a linear velocity v_{EOF} , charged species experience an additional force which results in acceleration or retardation according to the sign of charge in an applied field. The exhibited electric force, F_E [N], on the ion is given by eq. 1.7.

$$F_E = q E \quad (1.7)$$

where q and E are the effective charge of the ion [C] and the applied electric field strength [V/m], respectively. For small ions ($\kappa r \ll 1$) $q = \zeta_{EP} 4\pi\epsilon r$ and eq. 1.7 can be rearranged to give eq. 1.8.

$$F_E = \zeta_{EP} 4\pi\epsilon r E \quad (1.8)$$

A frictional drag force, F_F , opposes the electric force and is given by eq. 1.9

$$F_F = v_{EP} 6\pi \frac{\eta}{10} r \quad (1.9)$$

where v_{ep} and r are the electrophoretic velocity [m/s] and the hydrodynamic radius [m] of the ion, respectively. At steady state, the electrophoretic velocity v_{EP} can thus be written as

$$v_{EP} = \frac{\zeta_{EP} \varepsilon E}{1.5 \eta / 10} \quad (1.10)$$

relating the relaxation or acceleration velocity vector of an ion to the zeta potential ζ_{EP} of the ion, the permittivity, ε , and viscosity of the medium, η , and the applied field strength E . When an electric field is applied to an ion in an electrolyte, electrophoretic and electroosmotic forces act simultaneously on the ion. The observed velocity of an ion is hence an addition of the electroosmotic and electrophoretic vector, as given by eq. 1.11

$$v_{OBS} = \mu_{OBS} E = (\mu_{EP} + \mu_{EOF}) E \quad (1.11)$$

The migration time of an ion can then be expressed by eq. 1.12

$$t_m = \frac{L}{(\mu_{EP} + \mu_{EOF}) E} = \frac{L^2}{(\mu_{EP} + \mu_{EOF}) V} \quad (1.12)$$

where L is the length of the separation channel, μ_{EOF} the electroosmotic and μ_{EP} the electrophoretic mobility.

1.6.3.2 CE Separation Efficiency

The efficiency of any electrophoretic separation can be measured by calculation of the resolution, R , of the separation, as defined by eq. 1.13.

$$R = \frac{t_2 - t_1}{\frac{1}{2}(w_1 + w_2)} \quad (1.13)$$

where t_1 and t_2 are the elution times and w_1 and w_2 are the baseline bandwidths of two analyte peaks. Clearly, a large difference of migration rates of two analytes and the minimization of the peak and thus zone width leads to a high R value, i.e. high resolution of the separation.

Equation 1.13 can be expressed as eq. 1.14 [218]

$$R = \frac{\sqrt{N}}{4} \times \frac{\Delta v}{v_{av}} \quad (1.14)$$

where Δv is the difference in component flow velocity, v_{av} the average component velocity and N the number of theoretical plates. Evidently, a large difference in electrophoretic mobilities and a

low electroosmotic velocity will favor good resolution. A high number of plates, N , defined by eq. 1.15, is further desirable for an efficient separation.

$$N = \frac{L^2}{\sigma_i^2} \quad (1.15)$$

where σ_i is the peak variance of a Gaussian peak and L the capillary length. The use of long separation channels is hence favorable for achievement of high plate numbers and thus high R values. σ_i contains all dispersive effects, i.e. bandbroadening terms, that are detrimental to an efficient separation. Bandbroadening in on-chip CE can arise from longitudinal diffusion, excessive injection and detection volumes, an inappropriately long detection time constant, interaction of the analyte with the capillary walls, and insufficient heat dissipation of Joule heating leading to thermal velocity gradients. The overall variance σ_i^2 can therefore be expressed as

$$\sigma_i^2 = \sigma_{LD}^2 + \sigma_{INJ}^2 + \sigma_{DET}^2 + \sigma_{WALL}^2 + \sigma_J^2 \quad (1.16)$$

where σ_{LD}^2 denominates bandbroadening induced by longitudinal diffusion, σ_{INJ}^2 by the sample injection, σ_{DET}^2 by the on-channel detector, σ_{WALL}^2 by analyte to wall interactions and σ_J^2 by Joule heating. σ_{LD}^2 is given by the Einstein equation

$$\sigma_{LD}^2 = 2Dt_m = \frac{2DL^2}{\mu_{obs}V} \quad (1.17)$$

where D [cm²/s] is the diffusion coefficient of the analyte in the electrophoretic medium, t_m [s] the observed migration time, L [cm] the channel length, μ_{obs} [cm²/Vs] the observed mobility of the analyte and V [V] the applied voltage. The diffusion related variance can thus be reduced by an increased applied field strength for a given electrophoretic medium and a particular analyte. The injection related bandbroadening term, σ_{INJ}^2 , has turned out to be of great significance in microchip-based separations and can be expressed by eq. 18 if a rectangular injection profile is assumed [74].

$$\sigma_{INJ}^2 = \frac{w_{inj}^2}{12} \quad (1.18)$$

where w_{inj} is the plug width. σ_{WALL}^2 can be minimized by an appropriate choice of buffer conditions and surface modification procedures (see for example [207]). The σ_J^2 term is highly dependent on the channel cross section, the ionic strength of the medium and the applied field strength. Operation within the linear region of an Ohm's law plot, i.e. a plot of current versus applied voltage, guarantees sufficient heat dissipation and insignificance of σ_J^2 .

1.7 Scope of this Thesis

The demonstrated advantages of exemplary μ TAS for bioanalytical analyses have resulted in a strong drive to extend the applicability of these systems. Practical problems of the use of μ TAS, such as the difficulty of the fluidic coupling of external devices to microfluidic devices, could significantly limit the use of μ TAS.

In Chapter 2, the construction of a simple, yet novel capillary-to-chip connector will be presented. The connector was tested up to 20 atm pressure and provided a reversible world-to-chip interface. Capillaries of different inner diameters have been connected to the access hole of microfluidic chips within the scope of this study. The quick-connect fitting itself could also be used as sample and buffer reservoir. The insertion of electrodes into the fitting, followed by application of high voltage, allowed for electroosmotic fluid handling on-chip, thus avoiding frequent problems encountered with adhesively bonded liquid reservoirs. A syringe pump or simply house vacuum could be connected to the same fitting after removal of the electrode for hydrodynamic pumping. This interface, in connection with a novel chip holder design, eliminated the need for optical realignment after introduction of liquids into the chip and after application of vacuum to the device. The development, the characterization of a confocal epifluorescence microscope and the results obtained for on-channel detection are reported. The affect of essential parameters such as pinhole size, channel depth, excitation intensity and laser spot size on the performance of the detector are discussed.

In Chapter 3, the use of glass chips, featuring a 20 μ m deep fluidic network, for a continuous β -Gal assay of single cell lysates is presented. The monitoring of β -gal activity of HL-60 cells by off-chip and on-chip incubation with fluorescein-di- β -D-galactopyranoside, FDG, followed by on-chip lysis and on-detection of the enzymatic product is described. The report demonstrates the first-time integration of lysis and incubation of single cells onto a microfluidic chip. The results given demonstrate the feasibility of performing enzymatic assays of single cell lysates on-chip with moderate to high throughput. Enzymatic analyses of cell lysates are contrasted with *in-cella* analyses. The advantage of analysing single cell lysates for their enzymatic activity is substantiated by performing β -Gal assays of a large population of viable cells and cell lysates. Results obtained by flow cytometric β -Gal analysis of viable cells are compared with results obtained from analysing chemically lysed cells. Error sources of the analysis of viable cells, which can be circumvented by the analysis of lysates, are highlighted in this context.

In Chapter 4 we describe the electrokinetic handling of fluids on poly(dimethylsiloxane) (PDMS) CE microchips. Continuous voltage control of all intersecting channels in the fluidic

network, was found to be a *sine qua non* for adequate definition of injection plugs. In contrast, catastrophic leakage at channel intersections was observed, when the side channels were left floating. This contrasts with the behaviour of similar flow channel designs fabricated in glass substrates. The formation of reproducible and tightly defined injection plugs, as monitored by detection of fluorescent plugs in a separation channel, is described. Native PDMS devices exhibited stable retention times over several days as well as good device to device reproducibility. The observation of cathodic electroosmotic flow under all conditions employed led to an investigation of the charge origin on Sylgard 184 PDMS devices. The affect of ions of differing hydrophobicity, added to the background electrolyte, was determined, in this context. Therefore important insight into the range of possible analytes, which can be separated on such devices in free solution, was gained. A method to stack multiple channel layers in PDMS, yielding a 3D fluidic network, is also reported.

Finally, Chapter 5 provides a brief summary of the preceding chapters. The future outlook is briefly discussed.

1.8 References

- 1 Widmer, H.M. *Trends Anal. Chem.* 1983, 2, VIII
- 2 Widmer, H. M., Grass, G. in: Ahuja, S. (Ed.), *ACS Symposium Series 250*, 1984, pp. 13
- 3 Widmer, H.M., Erard, J.F., Grass, G. *Intern. J. Environ. Anal. Chem.* 1984, 18, 1-10
- 4 Garn, M. B., Gisin, M., Thommen, C., Cervey, P. *Biotechnol. Bioeng.* 1989, 34, 423-428
- 5 Fillipini, C., Sonnleitner, B., Fiechter, A., Bradley, J., Schmind, R. *J. Biotechnol.* 1991, 18, 153-160
- 6 Haemmerli, S., Schaeffler, A., Manz, A., Widmer, H. M. *Sens. Actuators B* 1992, 7, 404-407
- 7 Blom, N., Fettinger, J.C., Koch, J., Lüdi, H., Manz, A., Widmer, H.M. *Sens. Actuators B* 1991, 5, 75-78
- 8 *Microcolumn Separations: Columns, Instrumentation and Ancillary Techniques* (J. Chromatogr. Lib. Vol. 30), Novotny, M.V., Ishii, D. (Eds.); Elsevier Amsterdam, 1985
- 9 Terry, S. C. *Ph.D. Dissertation*, Stanford University, 1975
- 10 Terry, S.C., Jerman, J.H., Angell, J.B. *IEEE Trans. Electron Devices* 1979, ED-26, 1880-1886
- 11 Manz, A., Miyahara, Y., Miura, J., Watanabe, Y., Miyagi, K., Tsukada, K. *Sens. Actuators B*, 1990, 1, 249-255
- 12 Miura, J., Manz, A., Watanabe, Y., Miyahara, Y., Miyagi, K., Tsukada, K. *US patent* 5,132,012, 1992
- 13 Manz, A., Graber, N., Widmer, H. M. *Sens. Actuators B*, 1990, 1, 244-248
- 14 Manz, A., Fettinger, J.C., Verpoorte, E., Lüdi, H., Widmer, H.M., Harrison, D.J. *Trends Anal. Chem.* 1991, 10, 144-149
- 15 Fettinger, J.C., Manz, A., Lüdi, H., Widmer, H.M. *Sens. Actuators B*, 1993, 17, 19-25
- 16 Dempsey, E., Diamond, D., Smyth, M.R., Urban, G., Jobst, G., Moser, I., Verpoorte, E.M.J., Manz, A., Widmer, H.M. *Anal. Chim. Acta* 1997, 346, 341-349
- 17 Verpoorte, E.M.J., van der Schoot, B.H., Jeanneret, S., Manz, A., Widmer, H.M., de Rooij, N.F. *J. Micromech. Microeng.* 1994, 4, 246-256
- 18 Harrison, D.J., Manz, A., Fan, Z., Lüdi, H., Widmer, H.M. *Anal. Chem.* 1992, 64, 1926-1932
- 19 Manz, A., Harrison, D.J., Verpoorte, E., Fettinger, J.C., Paulus, A., Lüdi, H., Widmer, H.M. *J. Chromatogr.* 1992, 593, 253-258
- 20 Seiler, K., Harrison, D.J., Manz, A. *Anal. Chem.* 1993, 65, 1481-1488
- 21 Harrison, D.J., Fan, Z., Seiler, K., Manz, A., Widmer, H.M. *Anal. Chim. Acta* 1993, 283, 361-366
- 22 Burggraf, N., Manz, A., Effenhauser, C.S., Verpoorte, E., de Rooij, N.F., Widmer, H.M. *J.High Resolut. Chromatogr.* 1993, 16, 594-596
- 23 Burggraf, N., Manz, A., de Rooij, N.F., Widmer, H.M. *Anal. Methods. Instrum.* 1993, 1, 55-59

- 24 Burggraf, N., Manz, A., Verpoorte, E., Effenhauser, C.S., Widmer, H.M., de Rooij, N.F. *Sens. Actuators B*, 1994, 20, 103-110
- 25 Effenhauser, C.S., Paulus, A., Manz, A., Widmer, H.M. *Anal. Chem.* 1994, 66, 2949-2953
- 26 Woolley, A.T., Mathies, R.A. *Proc. Natl. Acad. Sci USA* 1994, 91, 11348-11352
- 27 Woolley, A.T., Mathies, R.A. *Anal. Chem.* 1995, 67, 3676-3680
- 28 von Heeren, F., Verpoorte, E., Manz, A., Thormann, W. *Anal. Chem.* 1996, 68, 2044-2053
- 29 Kutter, J.P., Jacobson, S.C., Ramsey, J.M. *Anal. Chem.* 1997, 69, 5165-5171
- 30 von Heeren, F., Verpoorte, E., Manz, A., Thormann, W. *J. Microcol. Sep.* 1996, 8, 373-381
- 31 Jacobson, S.C., Hergenroeder, R., Koutny, L.B., Ramsey, J.M. *Anal. Chem.*, 1994, 66, 2369-2373
- 32 Kutter, J.P., Jacobson, S.C., Matsubara, N., Ramsey, J.M. *Anal. Chem.*, 1998, 70, 3291-3297
- 33 He, B., Tait, N., Regnier, F. *Anal. Chem.* 1998, 70, 3790-3797
- 34 Harrison, D.J., Fluri, K., Seiler, K., Fan, Z., Effenhauser, C.S., Manz, A. *Science* 1993, 261, 895-897
- 35 Jacobson, S.C., Culbertson, C.T., Daler, J.E., Ramsey, J.M. *Anal. Chem.*, 1998, 70, 3476-3480
- 36 Jacobson, S.C., Hergenroeder, R., Moore, A.W., Ramsey, J.M. *Anal. Chem.* 1994, 66, 4127-4132
- 37 Harrison, D.J., Fluri, K., Chiem, N., Tang, T., Fan, Z. *Technical Digest, Transducers 95, Eurosensors IX*, Stockholm 1995, pp. 752
- 38 Fluri, K., Fitzpatrick, G., Chiem, N., Harrison, D.J. *Anal. Chem.* 1996, 68, 4285-4290
- 39 Jacobson, S.C., Koutny, L.B., Hergenroeder, R., Moore, A.W., Ramsey, J.M. *Anal. Chem.* 1994, 66, 3472-3476
- 40 Jacobson, S.C., Ramsey, J.M., *Anal. Chem.* 1996, 68, 720-723
- 41 Woolley, A.T., Hadley, D., Landre, P., deMello, A.J., Mathies, R.A., Northrup, M.A. *Anal. Chem.* 1996, 68, 4081-4086
- 42 Woolley, A.T., Sensabaugh, G.F., Mathies, R.A. *Anal. Chem.* 1997, 69, 2181-2186
- 43 Manz, A., Becker, H. *Technical Digest, Transducers 97, 9th Intl. Conf. Solid-State Sensors Actuat.*, Chicago 1997, pp. 915-918
- 44 Harrison, D.J., Skinner, C., Cheng, S.B., Ocvirk, G., Attiya, S., Bings, N., Wang, C., Li, J., Thibault, P., Lee, W. *Technical Digest, Transducers 99, 10th Intl. Conf. Solid-State Sensors Actuat.*, Sendai 1999, pp. 12-15
- 45 Simpson, P.C., Roach, D., Woolley, A.T., Thorsen, T., Johnson, R., Sensabaugh, G.F., Mathies, R.A. *Proc. Natl. Acad. Sci. USA* 1998, 95, 2256-2261
- 46 Manz, A., Harrison, D.J., Verpoorte, E., Widmer, H.M. in: *Adv. Chromatogr. Vol. 33*, Brown, P.R., Grushka, E. (Eds.), Marcel Decker, 1993, pp. 1-66
- 47 Kricka, L.J., Wilding, P. in: *Handbook of Clinical automation, Robotics, and Optimization*, John Wiley & Sons, New York 1996, pp. 45-77
- 48 Colyer, C.L., Tang, T., Chiem, N.H., Harrison, D.J. *Electrophoresis* 1997, 18, 1733-1741

- 49 Effenhauser, C.S, Bruin, G.J.M., Paulus, A. *Electrophoresis* 1997, 18, 2203-2213
- 50 *Microsystem Technology in Chemistry and Life Science*, Manz, A., Becker, H. (Eds.); Springer, Berlin 1998
- 51 Regnier, F.E., He, B., Lin S., Busse, J. *Trends Biotechnol.* 1999, 17, 101-106
- 52 *Proc. μ TAS '94 Workshop*, Van den Berg, A., Bergveld, P. (Eds.), Kluwer Academic Pub., Dordrecht 1995
- 53 *Proc. μ TAS '96 Anal. Methods. Instrum. 1996, Spec. Ed.*, Widmer, H.M., Verpoorte, E., Barnard, S. (Eds.)
- 54 *Proc. μ TAS '98 Workshop*, Harrison, D.J., Van den Berg, A. (Eds.), Kluwer Academic Pub., Dordrecht 1998
- 55 Bergveld, P. in: *Proc. μ TAS '94*, Kluwer Academic Publishers, Dordrecht 1995, Van den Berg, A., Bergveld, P. (Eds.); pp. 1-4
- 56 Raymond, D.E., Manz, A., Widmer, H.M. *Anal. Chem.* 1994, 66, 2858-2865
- 57 Ocvirk, G., Verpoorte, E., Manz, A., Grasserbauer, M., Widmer, H.M. *Anal. Methods Instrum.* 1995, 2, 74-82
- 58 Ocvirk, G., Tang, T., Harrison, D. J. *Analyst* 1998, 123, 1429-1434
- 59 Lee, W.E., Jemere, A.B., Attiya, S., Chiem, N.H., Paulson, M., Ahrend, J., Burchett, G., Bader, D.E., Ning, Y., Harrison, D.J. submitted to *J. Cap. Electrophoresis, June 1999*
- 60 Spiering, V.L., van der Moolen, J.N., Burger, G.J., van den Berg, A. *Technical Digest, Transducers 97, 9th Intl. Conf. Solid-State Sensors Actuat.*, Chicago 1997, pp. 511-514
- 61 van der Moolen, J. N., Poppe, H., Smit, H.C. *Anal. Chem.* 1997, 69, 4220-4225
- 62 Mourlas, N.J., Jaeggi, D., Maluf, N.I., Kovacs, G.T.A. *Technical Digest, Transducers 99, 10th Intl. Conf. Solid-State Sensors Actuat.*, Sendai 1999, pp. 1888-1889
- 63 Jaeggi, D., Gray, B.L., Mourlas, N.J., van Drieënhuizen, B.P., Williams, K.R., Maluf, N.I., Kovacs, G.T.A. *Proc. of the Solid State Sensor and Actuator Workshop '98*, Hilton Head, SC, 1998, pp. 112-115
- 64 Hannoe, S., Sugimoto, I., Yanagisawa, K., Kuwano, H. *Technical Digest, Transducers 97, 9th Intl. Conf. Solid-State Sensors Actuat.*, Chicago 1997, pp. 515-518
- 65 Harrison, D.J., Glavina, P.G., Manz, A. *Sens. Actuators B* 1993, 10, 107-116
- 66 Manz, A., de Mello, A.J. *Science* 1998, 280, 1046-1048
- 67 Norlin, P., Öhman, O., Ekström, B., Forssén, L. *Technical Digest, Transducers 97, 9th Intl. Conf. Solid-State Sensors Actuat.*, Chicago 1997, pp. 507-510
- 68 Reay, R.J., Daddo, R., Storment, C.W., Zare, R.N., Kovacs, G.T.A. *Proc. Of The Solid State Sensor and Actuator Workshop, Hilton Head, SC, 1994*, pp. 61-64

- 69 Figeys, D., Ning, Y., Aebersold, R. *Anal. Chem.* 1997, 69, 3153–3160
- 70 Bings, N. H., Wang, C., Skinner, C.D., Colyer, C.L., Thibault, P., Harrison, D.J. *Anal. Chem.* 1999, 71, 3292-3296
- 71 Zhang, B., Liu, H., Karger, B.L., Foret, F. *Anal. Chem.* 1999, 71, 3258-3264
- 72 Li, J., Thibault, P., Bings, N.H., Skinner, C.D., Wang, C., Colyer, C., Harrison, D.J. *Anal. Chem.* 1999, 71, 3036-3045
- 73 Harrison, D. J., Manz, A., Fan, Z. H., Luedi, H., Widmer, H. M. *Anal. Chem.* 1992, 64, 1926-1932
- 74 Fan, Z., Harrison, D.J. *Anal. Chem.* 1994, 66, 177-184
- 75 Gozel, P., Gassmann, E., Michelsen, H., Zare, R.N. *Anal. Chem.* 1987, 59, 44-49
- 76 Lee, I.H., Pinto, D., Arriaga, E.A., Zhang, Z., Dovichi, N.J. *Anal. Chem.* 1998, 70, 4546-4548
- 77 Pinto, D.M., Arriaga, E.A., Craig, D., Angelova, J., Sharma, N., Ahmadzadeh, H., Dovichi, N.J., Boulet, C.A. *Anal. Chem.* 1997, 69, 3015-3021
- 78 Craig, D.B., Wong, J.C.Y., Dovichi, N.J. *Anal. Chem.* 1996, 68, 697-700
- 79 Chen, D.Y., Adelhelm, K., Cheng, X.L., Dovichi, N.J. *Analyst* 1994, 119, 349-352
- 80 Zhao, J.Y., Diedrich, P., Zhang, Y., Hindsgaul, O., Dovichi, N.J. *J. Chromatogr.* 1994, 657, 307-313
- 81 Lu, H., Arriaga, E., Chen, D.Y., Dovichi, N.J. *J. Chromatogr. A* 1994, 680, 497-501
- 82 Chen, D.Y., Dovichi, N.J. *J. Chromatogr.* 1994, 657, 265-269
- 83 Zhao, J.Y., Chen, D.Y., Dovichi, N.J. *J. Chromatogr.* 1992, 608, 117-120
- 84 Wu, S., Dovichi, N.J. *Talanta* 1992, 39, 173-178
- 85 Zhang, J.Z., Chen, D.Y., Wu, S., Harke, H.R., Dovichi, N.J. *Clin. Chem.* 1991, 37, 1492-1496
- 86 Hoon Hahn, J., Soper, S. A., Nutter, H. L., Martin, J. C., Jett, J. H., Keller, R. A. *Appl. Spectrosc.*, 1991, 45, 743-746
- 87 Chen, D.Y., Swerdlow, H.P., Harke, H.R., Zhang, J.Z., Dovichi, N.J. *J. Chromatogr.* 1991, 559, 237-246
- 88 Wu, S., Dovichi, N.J. *J. Chromatogr.* 1989, 480, 141-155
- 89 Cheng, Y.F., Dovichi, N.J. *Science* 1988, 242, 562-564
- 90 Nguyen, D. C., Keller, R. A., Jett, J. H., Martin, J. C. *Anal. Chem.* 1987, 59, 2158-2161
- 91 Figeys, D., Aebersold, R. *Anal. Chem.* 1998, 70, 3721-3724
- 92 Figeys, D., Gygi, S. P., McKinnon, G., Aebersold, R. *Anal. Chem.* 1998, 70, 3728-3734
- 93 Woolley, A.T., Lao, K., Glazer, A.N., Mathies, R.A. *Anal. Chem.* 1998, 70, 684-688
- 94 Darling, R.B., Yager, P., Weigl, B., Kriebel, J., Mayes, K. *Proc. μ TAS '98 Workshop*, Harrison, D.J., Van den Berg, A. (Eds.), Kluwer Academic Pub., Dordrecht 1998, pp. 105-108
- 95 Kitamori, T., Fujinami, M., Odake, T., Tokeshi, M., Sawada, T. in: *Proc. μ TAS '98 Workshop*, Harrison, D.J., Van den Berg, A. (Eds.); Kluwer Academic Pub., Dordrecht 1998, pp. 295-298
- 96 Burggraf, N., Krattiger, B., de Mello, A.J., de Rooij, N. F., Manz, A. *Analyst*, 1998, 7, 1443-1447

- 97 Pickering, L.W., Baldock, S.J., Fielden, P.R., Goddard, N.J., Snook, R.D., Treves Brown, B.J. in: *Proc. μ TAS '98 Workshop*, Harrison, D.J., Van den Berg, A. (Eds.); Kluwer Academic Pub., Dordrecht 1998, pp. 101-104
- 98 Manz, A., Verpoorte, S. *US Patent 5,599,503*, 1997
- 99 Manz, A., Verpoorte, E., Effenhauser, C.S., Burggraf, N., Raymond, D.E., Harrison, D.J., Widmer, H.M. *HRC* 1993, 16, 433-436
- 100 Liang, Z.H., Chiem, N., Ocvirk, G., Tang, T., Fluri, K., Harrison, D.J., *Anal.Chem.* 1996, 68, 1040-1046
- 101 Harrison, D.J., Chiem, N., Ocvirk, G., Salimi-Moosavi, H., Jiang, Y. *US Patent Appl. 09/016,142*, Jan 30, 1998
- 102 Walker, P.A., Morris, M.D., Burns, M.A., Johnson, B.N. *Anal. Chem.* 1998, 70, 3766-3769
- 103 Mangru, S.D., Harrison, D.J. *Electrophoresis* 1998, 19, 2301-2307
- 104 Hsueh, Y.T., Collins, S.D., Smith, R.L., *Technical Digest, Transducers '97, 9th Intl. Conf. Solid-State Sensors Actuat.*, Chicago 1997, pp. 175-178
- 105 Arora, A., de Mello, A.J., Manz, A. *Anal. Commun.* 1997, 34, 393-395
- 106 Fiaccabrino, G.C., Koudelka-Hep, M., deRoos, N.F. *Anal. Chim. Acta.* 1998, 359, 263-267
- 107 Effenhauser, C.S., Manz, A., Widmer, H.M. *Anal. Chem.* 1993, 65, 2637-2642
- 108 Seiler, K., Fan, Z.F., Fluri, K., Harrison, D.J. *Anal. Chem.* 1994, 66, 3485-3491
- 109 Ocvirk, G., Tang, T., Harrison, D. *J. Analyst* 1998, 123, 1429-1434
- 110 Fister, J.C., Jacobson, S.C., Davis, L.M., Ramsey, J.M. *Anal.Chem.* 1998, 70, 431-437
- 111 Quesada, M.A., Rye, H.S., Gingrich, J.C., Glazer, A.N., Mathies, R.A. *BioTechniques* 1991, 10, 616-625
- 112 Huang, X.C., Quesada, M.A., Mathies, R.A. *Anal. Chem.* 1992, 64, 2149-2154
- 113 Clark, S.M., Mathies, R.A. *Anal. Biochem.* 1993, 215, 163-170
- 114 Roulet, J.C., Fluri, K., Verpoorte, E., Völkel, R., Herzig, H.P., deRoos, N.F., Dändliker, R. *Proc. μ TAS '98 Workshop*, Harrison, D.J., Van den Berg, A. (Eds.); Kluwer Academic Pub., Dordrecht 1998, pp. 287-290
- 115 Roulet, J.C., Fluri, K., Verpoorte, E., Völkel, R., Herzig, H.P., deRoos, N.F., Dändliker, R. *Technical Digest, Transducers 99, 10th Intl. Conf. Solid-State Sensors Actuat.*, Sendai 1999, pp. 120-123
- 116 Leistiko, O., Jensen, P.F. *Proc. μ TAS '98 Workshop*, Harrison, D.J., Van den Berg, A. (Eds.); Kluwer Academic Pub., Dordrecht 1998, pp. 291-294 detection: a cytometer
- 117 Bruno, A.E., Barnard, S., Rouilly, M., Waldner, A., Berger, J., Ehrat, M. *Anal. Chem.* 1997, 69, 507-513

- 118 Budach, W., Abel, A.P., Bruno, A.E., Neuschäfer, D. *Anal. Chem.* ASAP Article 1999
- 119 Bruno, A.E., Bär, E., Voelkel, R., Effenhauser, C.S. *Proc. μ TAS '98 Workshop*, Harrison, D.J., Van den Berg, A. (Eds.); Kluwer Academic Pub., Dordrecht 1998, pp. 281-284
- 120 Ford, S.M., Kar, B., McWhorter, S., Davies, J., Soper, S.A., Klopff, M., Calderon, G., Saile, V. *J. Microcolumn Sep.* 1998, 10, 413-422
- 121 Corle, T.R., Kino, G.S. *Confocal Scanning Optical Microscopy and Related Imaging Techniques*, Academic Press, San Diego 1994, pp. 1-44
- 122 Webb, R.H. *Optics & Photonics* 1991, July, 8-12
- 123 Wilson, T., Sheppard, C. *Theory and practice of scanning optical microscopy*, Academic Press, London 1984, pp. 1-64
- 124 Sheppard, C.J.R. in: *Multidimensional Microscopy*, Cheng, P.C., Lin, T.H., Wu, W.L., Wu, J.L. (Eds.); Springer, New York 1994, pp. 1-18
- 125 Wilson, T. *J. Microsc.* 1989, 154, 143-156
- 126 Webb, W.W., Wells, K.S., Sandison, D.R., Strickler, J. in: *Optical Microscopy for Biology*, Herman, B., Jacobson, K. (Eds.), Wiley-Liss, New York 1990, pp. 73-108
- 127 Born, M., Wolf, E. *Principles of optics: electromagnetic theory of propagation, interference and diffraction of light*, 6th ed., Pergamon Press, Oxford, New York 1980
- 128 Wilson, T. in: *Handbook of Confocal Microscopy*, Pawley, J.P. (Ed.); Plenum Press, New York 1990, pp. 113-126
- 129 Keller, H.E. in: *Handbook of Confocal Microscopy*, Pawley, J.P. (Ed.); Plenum Press, New York 1990, pp. 77-103
- 130 Hogan, B.L. in: *Pharmaceutical and Biomedical Applications of Capillary Electrophoresis*, Lunte, S.M., Radzik, D.M. (Eds.); Pergamon (Elsevier Science), Amsterdam 1996, pp. 467-502
- 131 Kasten, F.H. in: *Cell Structure and Function by Microspectrofluorometry*, Kohen, E., Hirschberg, J.G. (Eds.); Academic Press, San Diego 1989, pp. 3-50
- 132 Slavik, J. *Fluorescent Probes in Cellular and Molecular Biology*, CRC Press, Boca Raton 1994
- 133 Macey, M.G. in: *Flow Cytometry-Clinical Applications*, Macey, M.G. (Ed.); Backwell Scientific Publications, Oxford 1994, pp. 1-44
- 134 Shapiro, H.M. *Practical Flow Cytometry*, 3rd ed., A.R. Liss, New York 1995, pp. 231-232
- 135 O'Connor J.E. in: *Fluorescence Microscopy and Fluorescent Probes*, Slavik, J. (Ed.); Plenum Press, New York 1996, pp. 61-66
- 136 Scampavia, L.D., Blankenstein, G., Ruzicka, J., Christian, G.D. *Anal. Chem.* 1995, 67, 2743-2749
- 137 *Clinical flow cytometry: principles and application*, Bauer, K.D., Duque, R.E., Shankey, V. (Eds.); Williams & Wilkins, Baltimore 1993
- 138 *Flow cytometry applications in cell culture*, Al-Rubeai, M., Emery, A.N. (Eds.);

- Marcel Dekker, New York 1996
- 139 Shapiro, H.M., *Practical flow cytometry*, 3rd ed., A.R. Liss, New York 1995
- 140 *Flow Cytometry-Clinical Applications*, Macey, M.G. (Ed.); Backwell Scientific Publications, Oxford 1994
- 141 *Flow cytometry and clinical diagnosis*, Keren, D.F., Hanson, C.A., Hurtubise, P. (Eds.); ASCP Press, Chicago 1994.
- 142 *Flow cytometry and sorting*, Melamed, M.R., Lindmo, T., Mendelsohn, M.L. (Eds.); Wiley-Liss, New York 1990
- 143 *Handbook of flow cytometry methods*, Robinson, J.P. (Ed.), Darzynkiewicz, Z. (as. Ed.); Wiley-Liss, New York 1993
- 144 Kennedy, R.T., Oates, M.D., Cooper, B.R., Nickerson, B., Jorgenson, J.W. *Science* 1989, 246, 57-63
- 145 Kennedy, Jorgenson, J.W. *Anal. Chem.* 1989, 61, 436-441
- 146 Oates, M.D., Cooper, B.R., Jorgenson, J.W. *Anal. Chem.* 1990, 62, 1573-1577
- 147 Cooper, B.R., Jankowski, J.A., Leszczyszyn, D.L., Wightman, R.M., Jorgenson, J.W. *Anal. Chem.* 1992, 64, 691-694
- 148 Cooper, B.R., Wightman, R.M., Jorgenson, J.W. *J. Chromatogr. B* 1994, 653, 25-34
- 149 Zhu, A., Chen, Y. *J. Chromatogr. A* 1989, 470, 251-260
- 150 Lillard, S.J., Yeung, E.S., Lautamo, M.A., Mao, D.T. *J. Chromatogr. A* 1995, 718, 397-404
- 151 Xue, Q., Yeung, E.S. *Anal. Chem.* 1994, 66, 1175-1178
- 152 Kitagawa, S., Kawaura, C., Hashimoto, O., Takahashi, T., Naoi, M., Tsuda, T. *Electrophoresis* 1995, 16, 1364-1368
- 153 Wallendorf, R.A., Ewing, A.G. *Anal. Chem.* 1988, 60, 1977-1979
- 154 Ewing, A.G., Mesaros, J.M., Gavin, P.F. *Anal. Chem.* 1994, 66, 527A-537A
- 155 Le, X.C., Tan W., Scaman, C.H., Szpacenko, A., Arriaga, E., Zhang, Y., Dovichi, N.J., Hindsgaul, O., Palcic, M.M. *Glycobiology* 1999, 9, 219-225
- 156 Li, P.C.H., Harrison, D.J. *Anal. Chem.* 1997, 69, 1564-1568
- 157 Hanning, K., Wirth, H., Meyer, B-H., Zeiller, K. *Hoppe-Seyler's Z. Physiol. Chem.* 1975, 356, 1209-1223
- 158 Andersson, P. E., Li, P. C. H., Smith, R., Szarka, R. J., Harrison, D. J. in: *Technical Digest, Transducers 97, 9th Intl. Conf. Solid-State Sensors Actuat.*, Chicago 1997, pp. 1311-1314
- 159 Altendorf, E., Zebert, D., Holl, M., Vannelli, A., Wu, C. Schulte, T. in: *Proc. μ -TAS Workshop '98*, Harrison, D. J., van den Berg, A., (Eds); *Kluwer Academic Publishers, Dordrecht 1998*, pp. 73-76
- 160 Wolff, A., Larsen, U.D., Blankenstein, G., Philip, J., Telleman, P. in: *Proc. μ -TAS Workshop '98*, Harrison, D. J., van den Berg, A., (Eds); *Kluwer Academic Publishers, Dordrecht 1998*, pp. 77-80

- 161 Tracey, M.C., Greenaway, R.S., Das, A., Kaye, P.H., Barnes, A.J.
IEEE Trans. Biomed. Eng. 1995, 42, 751-761
- 162 Fuhr, G., Shirley, G. in: *Microsystem Technology in Chemistry and Life Sciences*
Manz, A., Becker, H., (Eds.); Springer, Berlin 1997, pp. 83-116
- 163 Fuhr, G., Hagedorn, R., Müller, T., Benecke, W., Wagner, B., Gimsa, J.
Studia Biophys. 1991, 140, 79-
- 164 Hagedorn, R., Fuhr, G., Müller, T., Gimsa, J. *Electrophoresis* 1992, 13, 49-54
- 165 Cheng, J., Sheldon, E.L., Wu, L., Heller, M.J., O'Connell, J.P. *Anal. Chem.* 1998, 70, 2321-2326
- 166 Yang, J., Huang Y., Wang, X.B., Becker, F.F., Gascoyne, P.R. *Anal. Chem.* 1999, 71, 911-918
- 167 Cheng, J., Sheldon, E. L., Wu, L., Uribe, A., Gerrue, L. O., Carrino, J., Heller, M. J., O'Connell, J. P.
Nature Biotech. 1998, 16, 541-546
- 168 Fuhr, G., Müller, T., Schnelle, Th., Hagedorn, R., Voigt, A., Fiedler, S., Arnold, W.M.,
Zimmermann, U., Wagner, B., Heuberger, A. *Naturwissenschaften* 1994, 81, 528-535
- 169 Schnelle, Th., Hagedorn, R., Fuhr, G., Fiedler, S., Müller, T.
Biochim. Biophys. Acta 1993, 1157, 127-140
- 170 Kikuchi, Y., Sato, K., Ohki, H., Kaneko, T. *Microvasc. Res.* 1992, 4, 226-240
- 171 Cokelet, G.R., Soave, R., Pugh, G., Rathbun, L. *Micorvasc. Res.* 1993, 46, 394-400
- 172 Wilding, P., Pfahler, J., Bau, H.H., Zemel, J.N., Kricka, L.J. *Clin. Chem.* 1994, 40, 43-47
- 173 Brody, J.P., Han, Y., Austin, R.H., Bitensky, M. *Biophys. J.* 1995, 68, 2224-2232
- 174 Sutton, N., Tracey, M.C., Johnston, I.D., Greenaway, R.S., Rampling, M.W.
Microvasc. Res. 1997, 53, 272-281
- 175 Carlson, R.H., Gabel, C.V., Chan, S.S., Austin, R.H., Brody, J.P., Winkelman, J.W.
Phys. Rev. Lett. 1997, 79, 2149-2152
- 176 Kricka, L. J., Faro, I., Heyner, S., Garside, W. T., Fitzpatrick, G., McKinnon, G., Ho, J., Wilding, P.
J. Pharm. Biomed. Anal. 1997, 5, 1443-1447
- 177 Altendorf, E.H., Yager, P., U.S. patent 5,726,75, 1998 and cited references
- 178 Altendorf, E., Iverson, E., Schutte, D., Weigl, B., Osborn, T.D., Sabeti, R., Yager, P.
SPIE Proceedings, 1996, 2678, 267
- 179 Schrum, D.P., Culbertson, C.T., Jacobson, S.C., Ramsey, J.M. *Anal. Chem.* 1999, ASAP article
- 180 Altendorf, E., Zebert, D., Holl, M., Yager, P. In: *Proceedings of the 9th International Conference on Solid-State Sensors and Actuators: Transducers '97*; IEEE Electron Dev. Soc., Chicago, 1997, Vol. 1, pp. 531-534
- 181 Larsen, K. in: *Hematopoietic Stem Cells: The Mulhouse Manual*, Wunder, E., Solvalat, H., Henon, P., Sweke, S. (Eds.), AlphaMed Press, Dayton OH 1994, pp. 133-140

- 182 Salimi-Moosavi, H., Szarka, R., Andersson, P., Smith, R., Harrison, D. J. in:
Proc. μ -TAS Workshop '98, Harrison, D. J., van den Berg, A., (Eds); *Kluwer Academic Publishers, Dordrecht 1998*, pp. 69-72
- 183 Kohlrausch, F. *Ann. Phys. (Leipzig)* 1897, 62, 209
- 184 Hjerten, S. *Chromatogr.Rev.* 1967, 9, 122-124
- 185 Jorgenson, J., Lukacs, K.D. *Anal. Chem.* 1981, 53, 1298-1302
- 186 Jorgenson, J., Lukacs, K.D. *Science* 1983, 222, 266-272
- 187 Gordon, M.J., Huang, X., Pentoney, S. L., Zare, R. N. *Science* 1988, 242, 224-228
- 188 Beale, S.C. *Anal. Chem.* 1998, 70, 279-300
- 189 St. Claire. R. L. *Anal. Chem.* 1996, 68, 569 -586
- 190 Monnig, C. A., Kennedy, R. T. *Anal. Chem.* 1994, 66, 280R-314R
- 191 Kunkel, A., Degenhardt, M., Schirm, B. Wätzig, H. *J.Chromatogr.* 1997, 768, 17-27
- 192 Oda, R.P., Spelsberg, T.C., Landers, J.P. *LC-GC* 1994, 12, 50-51
- 193 Warner, M. *Anal. Chem.* 1994, 66, 1137A-1141A
- 194 Stevenson, R. *Am. Lab.* 1994, 26, 29-33
- 195 von Helmholtz, H.L.F. *Wiss. Abhandl. Physik-tech. Reichsanstalt*, 1879, 1, 925
- 196 Gouy, G. *J. Physique* 1910, 9, 457-467
- 197 Chapman. D.L. *phil.Mag.* 1913, 25, 475
- 198 Stern, O. *Zeitschrift für Elektrochemie* 1924, 30, 508-516
- 199 von Smoluchowski, M. *Bull. Int. Acad. Sci. Cracovie* 1903, 184
- 200 Schurz, J., Erk, G., Schempp, W., Ribitsch, V. *J. Macromol. Sci.-Chem.* 1990, A27, 1673-1692
- 201 Morris, C.J.O.R., Morris, P., *Separation Methods in Biochemistry*, Pittman Publishing, London 1976, pp. 718-724
- 202 Chou, H.P., Spence, C., Scherer, A., Quake, S., *Proc. Natl. Acad. Sci. USA* 1999, 96, 11-13
- 203 Schützner, W., Kenndler, E., *Anal. Chem.* 1992, 64, 1991-1995
- 204 Jacobasch, H.J., Simon, F., Weidenhammer, P. *Colloid. Polym. Sci.* 1998, 276, 434-442
- 205 Lukacs, K.D., Jorgenson, J.W. *J. High Resolut. Chromatogr.* 1985, 8, 407-411
- 206 Weinberger R., *Practical Capillary Electrophoresis*, Academic Press, Boston 1993, pp. 57-58
- 207 Chiari, M., Nesi, M, Righetti, P.G., in *Capillary Electrophoresis in Analytical Biotechnology*, Righetti, P.G. (Ed.); CRC Press, Boca Raton 1996, pp. 1-36
- 208 Reijenga, F.C., Aben, G.V.A., Verheggen, Th. P.E.M. Everaerts, F.M.
J.Chromatogr. 1983, 260, 241-254
- 209 Tsuda, T., Nomura, K., Nakagawa, G. *J.Chromatogr.* 1983, 264, 385-392
- 210 Tsuda, T. *J. High Resolut. Chromatogr.* 1987, 10, 622-624
- 211 Van de Goor, A.A.A.M., Wanders, B.J., Everaerts, F.M. *J.Chromatogr.* 1989, 470, 95-104

- 212 Nielen, M. W. F. *J. High Resolut. Chromatogr.* 1993, 16, 62-64
- 213 Lamb, J., Huxford, T.L., Czirr, K.B. *J. Chromatogr. A*, 1996, 739, 373-378
- 214 Liu, P.Z., Malik, A., Kuchar, M.C.J., Vorking, W.P., Lee, M.L. *J. Microcolumn Sep.* 1993, 5, 245-253
- 215 Chen, S., Lee, M. L. *J. Microcolumn Sep.* 1997, 9, 57-66 check
- 216 Bayer, H., Engelhardt, H. *J. Microcolumn Sep.* 1996, 8, 479-484
- 217 Roberts, M.A., Rossier, J.S., Bercier, P., Girault, H., *Anal. Chem.* 1997, 69, 2035-2042
- 218 Grossman, P. D., Colburn, J.C. *Capillary Electrophoresis: Theory and Practice*, Academic Press, San Diego 1992

Chapter 2

Confocal Epifluorescence Microscopy for Miniaturized Total Analysis Systems[♦]

2.1 Abstract

A confocal epifluorescence detection scheme, optimized to give sub-picomolar detection within planar glass substrates etched to a 30 μm depth is described. A 40x, 0.6 numerical aperture (N.A.) lens with a 3.7 mm working distance was used to create a focused laser spot about 12 μm in diameter, by under filling the lens aperture to give an effective, measured N.A. of 0.12 for the laser beam. The sectioning power (optical axis field of view) of various pinholes and the corresponding detector probe volumes (overlap of the excitation and observation volumes) were: (pinhole diam., sectioning power, probe volume.) 100 μm , 18 μm , 0.1 pL, 200 μm , 20 μm , 0.4 pL, 400 μm , 26 μm , 2.0 pL, 600 μm , 36 μm , 3.4 pL. A log-log plot of fluorescence intensity versus fluorescein concentration, measured in continuous flow mode using the optimal 400 μm pinhole, showed a correlation coefficient of 0.996 and a slope of 0.85. In this mode 300 fM fluorescein gave a signal of 34.6 ± 8.1 mV over background with an S/N of 6.1, representing the lowest measured fluorescein dye concentration reported on-chip. Capillary zone electrophoresis of 1 pM fluorescein resulted in a mean S/N ratio of 5.8. The injection plug, estimated to be about 5470 molecules, corresponds to 570 detected molecules on average. The design and use of quick-fit, flangeless fittings for interfacing tubing, fused silica capillaries or pressurized systems to microfluidic channels etched in planar glass chips is briefly presented.

Keywords: microchip, confocal epifluorescence detection, capillary electrophoresis, microfluidics, fluidic interface

2.2 Introduction

Microchip based analytical methods frequently involve the measurement of subnanomolar sample concentrations in subnanoliter sample volumes. Hence laser induced fluorescence (LIF) detection has originally been used for μ -TAS due to its inherent sensitivity [1]-[3], as demonstrated originally for on-capillary detection (see for example [4]) and for post-capillary detection [5]-[19]. From the very beginning of μ -TAS, on-channel LIF detection schemes were developed

[♦] A version of this chapter has been published:
Ocvirk, G., Tang, T., Harrison, D. J. *Analyst* 1998, 123, 1429-1434

since conventional on-capillary detectors could not be coupled to the chip without introducing significant dead volume into the separation system. However very recently, tremendous progress has been made in the development of zero-dead volume chip connectors due to the interest in microchip CE-ESI-MS hyphenation [20]-[25]. Since the integration of optical elements, such as lenses and waveguides, onto microfluidic devices does not offer significant advantages in terms of handling, instrumentation costs or detection limits in a research environment at the current stage of miniaturization, most efforts have been concentrated on the development of off-chip LIF optical instrumentation.

One particular LIF detection scheme has been used widely due to the simplicity of its construction [26]-[29]. A laser beam is focused onto the separation channel at an incident angle of $\sim 55^\circ$, measured at the chip-plane, and fluorescence emission is collected with a microscope mounted perpendicular to the chip. This approach has allowed for concentration detection limits, LOD's, of ~ 10 pM fluorescein. The LOD is limited by the necessity of an excitation focusing lens with a long focal length ($f > 10$ cm), resulting in large excitation spot diameters, and the requirement of a collection lens of sufficient working distance to accommodate both the lens and the focusing beam near the chip. Due to the physical size of the collection objective, excitation angles of $\sim 55^\circ$ and a typical chip thickness of 0.6-2 mm, the numerical aperture (N.A.) of the objective is less than 0.4 in all cases. In order to reduce the field of view and hence background scatter and fluorescence, a relatively large circular aperture (~ 800 μm) is mounted in the image plane. The measured background levels are nevertheless fairly high since there is limited discrimination against reflections and scattered light from the cover glass and bottom channel wall. Hence a further improvement in concentration LOD's required higher light collection efficiencies and a significant reduction of background levels. One of several approaches towards high sensitivity employs hydrodynamic focusing of the eluent within sheath flow cuvettes for postcolumn detection [5]-[19]. Adapting this method to microchips will require new microchip device designs and novel orthogonal detection schemes. Another approach, which allows for the use of present chip designs, relies on background rejection by an on-channel coaxial confocal system, i.e. confocal epifluorescence detection, and is the subject of this study.

Confocal epifluorescence microscopy involves the use of high N.A. microscope objectives, allowing for small detection volumes and high collection efficiencies and a pinhole at the image plane for vertical discrimination against reflections and scattered light from capillary walls. This technique has the advantage that it can be used with present chip designs. Mathies et al. introduced the use of confocal fluorescence scanners to detection in gels, on capillary arrays and subsequently on microfabricated capillary array electrophoresis chips [30],[31]. They

demonstrated the high sensitivity of this approach by detecting a 5×10^{-12} M fluorescein derivative in microtiter plates [32]. Several authors have also used epifluorescence detection schemes for on-column detection in fused silica capillaries, showing detection limits in the 1-10 pM range [33],[34]. Single molecule detection has been shown for dyes in the 10 pM range or higher in the fused silica capillary format [35]-[37] and more recently on planar devices [38], [39]. However, the probe volume for single molecule detection has typically been decreased to the fL range in order to reduce the magnitude of the background [40], resulting in 10-100 pM concentration detection limits.

Concentration detection limits can be improved by detecting a larger number of injected molecules through an increase in the probe volume. The detected spot size to channel width ratio should be maximized, while fluorescence generated over the total depth of the separation channel should be collected. Hence the excitation laser spot size at the focal plane should be large for a given channel width. This can be achieved by reducing the excitation aperture i.e. under filling of the back aperture of the microscope objective, while fluorescence is still collected with the full N.A. of the lens [41]. In order to evaluate this approach in our chip, the affect of essential parameters such as pinhole size, channel depth, excitation intensity and laser spot size were measured. The aim of this work is to provide the concentration detection sensitivity that is necessary for a variety of biological assays on chip.

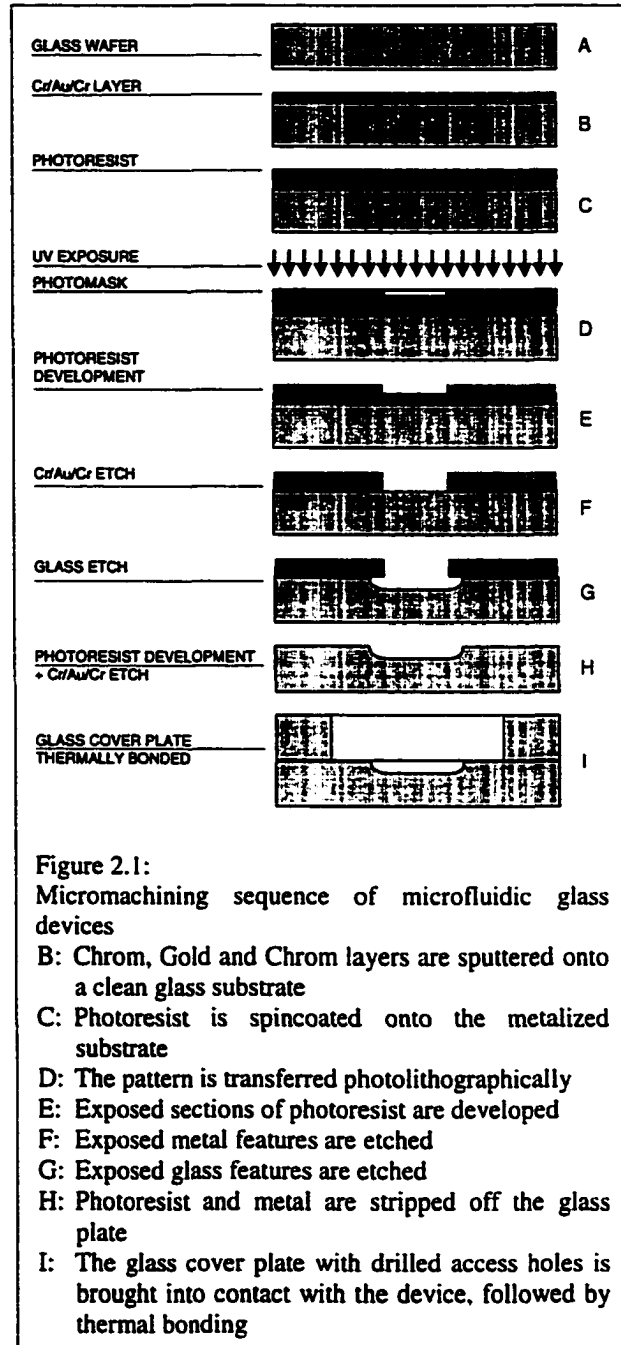
2.3 Experimental Section

2.3.1 Materials And Reagents

A 1 mM stock solution of fluorescein di-sodium salt (Sigma) was prepared in a 1.9 mM borate (Baker, Phillipsburg, NJ, USA)/ 6.3 mM Tris (tris(hydroxymethylamino)methane, Sigma) pH 9 buffer. All buffers were prepared in double distilled and deionized water. Further solutions were prepared by serial dilution of the 1 mM fluorescein stock solution with the same running buffer. Sets of 100 mL volumetric flasks were used for all dilutions. All glass flasks and vials were cleaned with a mixture of $\text{H}_2\text{SO}_4/\text{H}_2\text{O}_2$ (3:1), followed by thorough rinsing with double distilled and deionized water. Using this cleaning method, reproducible fluorescence signals were obtained from replicate solutions prepared in different sets of flasks. Solutions were filtered (Millipore 0.22 μm filters) before introduction into the chip.

2.3.2 Device Design and Fabrication

Devices were fabricated in 3 x 3", 540 μm thick cover slip glass (Corning 0211, Corning Glass Works, Parkridge, IL, USA) at the Alberta Microelectronic Corporation (Edmonton, Canada). Chips were produced by thermal bonding of patterned devices and cover glasses with mechanically drilled access holes. The lithographic pattern transfer and etching steps, described previously [44], are depicted in Figure 2.1. Briefly, the device glass was cleaned in a cold piranha mixture (H₂SO₄/H₂O₂=3/1) for 10 minutes. After thorough aqueous rinsing and drying, Cr/Au/Cr layers were sputtered onto the glass substrates. A solution of photoresist (Waycoat HPR 504, Olin Hunt) in methanol was then spin coated onto the substrates (1., 70 s at 500 rpm; 2., 65 s at 2000 rpm) with a photoresist coater/developer (Solitec Wafer Processing, San Jose, CA, USA), followed by soft baking at 110°C for 30 minutes. A 5 x 5" chrome photomask was designed with L-Edit software (Tanner Research, Pasadena, CA, USA) and fabricated by Adtek (Adtek Photomask,



Montreal, Canada). A contact mask aligner (Karl Süss, Garching, Germany) was used to align the substrates with the mask and for UV exposure. The exposed photoresist was removed with Microdeposit 354 developer (Shipley, Newton, MA, USA). Developed substrates were hard baked for 30 minutes at 110°C, the chrom and gold layers were etched with a commercial Cr etch (KTI Chemicals, Sunnyside, CA) and an aqueous potassium iodide/iodine solution (Alberta Microelectronic Corporation), respectively. Glass substrates were then etched using a mixture of

concentrated HF:HNO₃:H₂O (20:14:66). The etch rate and the final channel depth were measured with an alpha-step profilometer (Alphastep 200, Tencor Instruments, KLA-Tencor Corp., San Jose, CA). The photoresist was removed with acetone, followed by immersion of the device in a warm piranha solution for removal of acetone residues. The metal layers were subsequently stripped off as described above.

Access holes were drilled into cover plates by the following procedure. Glass slides were heated to ≈150°C and a thin layer of acetone soluble adhesive (Crystalbond™ 509, Aremco, Ossining, NY, USA) was spread onto the top of the slide. A second slide was thereupon bonded to the coated first slide. This process was repeated for a device stack of up to 4 slides. Sacrificial microscope slides were glued to the top and bottom of the slide stack in the same manner. A stainless steel drill template (hole diameter: 0.077") was attached to the top of the plate stack with 3M vinyl electrical tape. Holes, 0.076" in diameter, were drilled with a Lunzer SL-1 drill with a diamond core drill bit (0.076"OD x 1/4"DL, Lunzer, Saddle Brook, NJ, USA).

After removal of the sacrificial slides, the drilled cover plates were cleaned with acetone in an ultrasonic bath for 15 minutes, followed by aqueous rinsing. Devices and cover plates were immersed in a hot piranha solution for 15 minutes. The devices and cover plates were then stored in water overnight prior to washing with a high pressure cleaning station (Model 2066, MicroAutomation, Fremont, CA, USA). The devices and cover plates were first mounted onto a 4 x 4" wafer frame with a Medium tack blue plastic film (1807465, Semiconductor Equipment Corporation, Moor Park, CA, USA), heated for 10 minutes on a wafer/film frame tape mounter (MicroAutomation) and then scrubbed rigorously with a clean sponge and a dilute detergent solution under a class 100 clean hood. Then the devices and plates were spun under a high pressure water jet (2000 PSI) for 100 s, followed by manual washing as described above. This cleaning sequence was repeated twice, followed by a final drying step for one minute under the built-in IR lamp. The frame mounted devices were then sprayed with a nitrogen

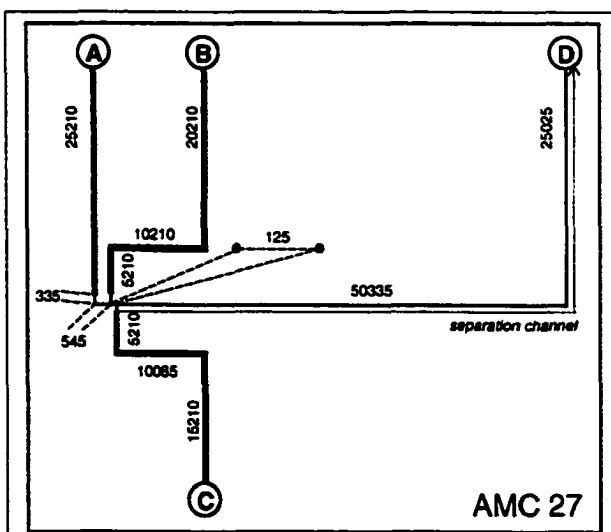


Figure 2.2 Geometric layout of device AMC 27, patterned onto 0211 glass. Channel depths are 30 μm. The separation and the wide introduction channels are 102 and 287 μm wide at the channel top edge, respectively. Letters mark reservoir labels. Channel lengths are given in micrometers.

gun (Dryden Engineering Co, Fremont, CA, USA) to remove remaining particles from the surface and aligned visually. Frame mounted devices and cover plates were brought into contact by applying pressure to the center of the device. After removal from the frame, the devices were bonded thermally in a programmable furnace (Model 6-525, J. M. Ney Co., Yucaipa, CA, USA). A previously described [26], [29], [45] temperature profile (dT/dt, final temperature, duration of heating at final temperature) was used for bonding of all 0211 glass and Photomaskglass devices: 1.) 40 °C/min, 440 °C, 0.5h; 2.) 2 °C/min, 473 °C, 0.5h; 3.) 2°C, 595°C, 3h; 4.) -4.0 °C/min, 473 °C, 0.5h; 5.) natural cooling to room temperature;

A previously employed manifold of injection and separation channels [46], depicted in Figure 2.2, was used in this study. All channels were 30 µm deep, 102 µm wide at the top and 50 µm wide at the bottom. The separation channel was 75.3 mm long, and the injector to detector distance used was 45 mm. The injector design used the double-T format to geometrically define the sample plug volume [27], [46], [47].

2.3.3 Instrumentation

The high voltage control system for the chips has been described previously [26]. High voltage (HV) supplies used in the system were from Gamma High Voltage Research (RMC15/0.12P, Ormond Beach, FL). The diagram in Figure 2.3 illustrates the optical setup. In order to rigidly mount the device, the CE chip was clamped in a 1/2" thick plexiglass holder, allowing for connection of flangeless fittings (P202&P200 Upchurch Scientific, Oak Harbour, WA) to the chip as illustrated in Figure 2.4. This provides a reservoir of up to 180 µL volume. The chip connector was then placed on a plexiglass block that was mounted parallel to the optical table, providing simple connection of the electrodes to HV power supplies. Three translation stages (Newport 423, Irvine, CA) were used for xyz translation of the device, employing microactuators (Newport AJS-1) for horizontal (i.e.

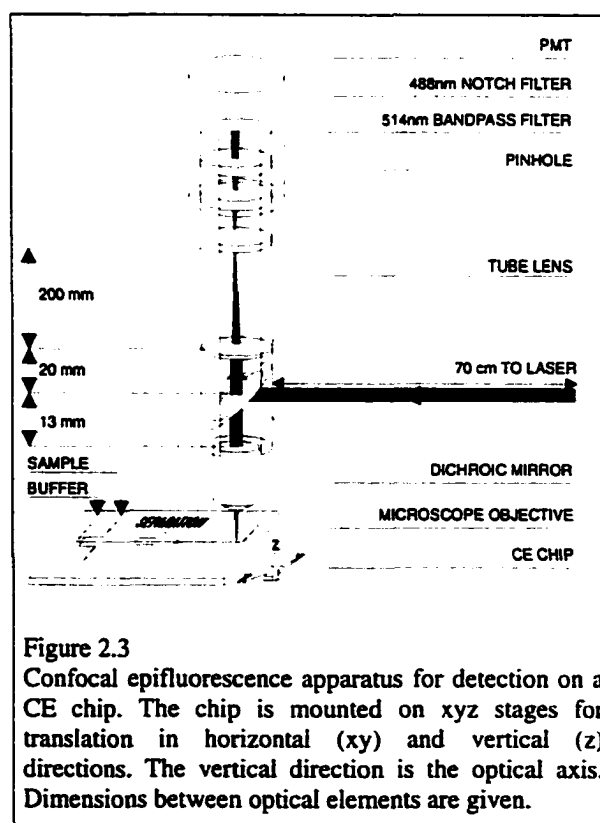


Figure 2.3
Confocal epifluorescence apparatus for detection on a CE chip. The chip is mounted on xyz stages for translation in horizontal (xy) and vertical (z) directions. The vertical direction is the optical axis. Dimensions between optical elements are given.

xy, orthogonal to the optical axis) and a differential micrometer (Newport DM13) for vertical (i.e. z, along the optical axis) translation. Excitation light from an air cooled argon ion laser (488 nm, Uniphase 2014, San Jose, CA) was passed through a 485 nm bandpass filter (485DF22, Omega, Battleboro VT), reflected by a dichroic mirror (505DRLP02, Omega) and focused onto a glass device to a $\approx 12 \mu\text{m}$ spot. We used a 0.6 N.A., 40x long working distance, infinite conjugate, microscope objective (Planachromat LDN 1.2-A, Carl Zeiss Jena) with a cover slip correction collar (0.5-1.6 mm). The fluorescence emission was collected by the same objective, passed through the dichroic mirror and focused with a tube lens (achromat, Newport PAC064, $f=200$ mm) onto a pinhole located at the focal point. Pinholes of 100-600 μm aperture (Melles Griot, Irvine, CA) were aligned with an xyz translation stage (Newport LP-1-XYZ). A photomultiplier tube (PMT, Hamamatsu R1477, bias: 800-1000V), was mounted on top of the microscope tube, with a 514.5 nm bandpass filter (9 nm bandpass, Melles Griot) and a 488 nm rejection band pass filter (Beckman Instruments, Fullerton, CA) used for spectral filtering. The analog signal was filtered with a Butterworth 15 Hz cutoff filter (Krohn-Hite 3442), giving a 150 ms rise time. Electropherograms were recorded on a PowerMac 7100/66 with an NB-MIO16 A/D board and a program written in Labview (National Instruments, Austin, TX) at a sampling rate of 50 Hz. All data was smoothed using a 7 point box smooth algorithm, included in Igor Pro (Wavemetrics, Lake Oswego, OR).

2.3.4 Procedures

In order to align the detection setup the microscope objective was first removed from the microscope tube and a mirror was placed on the chip. The reflected beam was superimposed with the incoming beam by adjustment of the beam steering mirrors. The microscope objective was then mounted, the beam was focused on the mirror by vertically translating the chip holder, and a pinhole was aligned with the transmitted laser beam. Subsequently the mirror was removed, the pinhole was replaced by a 10x Huygens eyepiece (Melles Griot) and the dry separation channel was brought into focus. A 1 nM fluorescein solution was then flushed through the separation channel by application of vacuum at the buffer waste port D, the eyepiece was replaced with the filter and PMT housing, and the position of the pinhole was re-optimized.

The corrected fluorescence signal was obtained by correcting for background, i.e. subtraction of the blank signal. The blank signal was measured by flushing the dilution buffer through the separation channel at the same flow velocity as the sample. The maximum background corrected fluorescence signal at a given fluorescein concentration was found by monitoring the response for both fluorescein and buffer solutions while vertically translating the chip in 1 μm steps.

For continuous flow experiments the flow velocity in the separation channel was determined to be 3.5 mm s^{-1} , by measuring the time required for the dye front to travel from the injector to the detector, as depicted in Figure 2.5. For calibration curves, sample and buffer solutions were alternated, in the order of increasing fluorescein concentration, to ensure the background level correction was accurate and to validate the sample signals. Solutions were introduced by rinsing the reservoirs three times, and flushing the channels under vacuum for several minutes. Data were obtained for 25 s, and averaged to give the mean signal, background and corrected signal. The noise was taken as the standard deviation (s.d.) estimated from the overall variance of the corrected fluorescence signal, obtained by adding the variances of the sample and the buffer background signals.

Capillary zone electrophoresis was performed with 10 s double-T style injections at 2 kV (as discussed previously [27], [46], [47]), followed by separation at 7.5 kV (935 V/cm). The injector to detector distance d_{id} , was 4.5 cm. The S/N for each electropherogram was calculated by dividing the average peak height by the s.d. in the background, determined from the portion of the electropherogram before the peak. The 7 point smooth did not broaden or alter the shape of the peaks, which are defined by about 30 points.

2.4 Results and Discussion

2.4.1 Fluidic Interface

Contacts to the introduction channels on the chip have most often been made with pipet tips glued

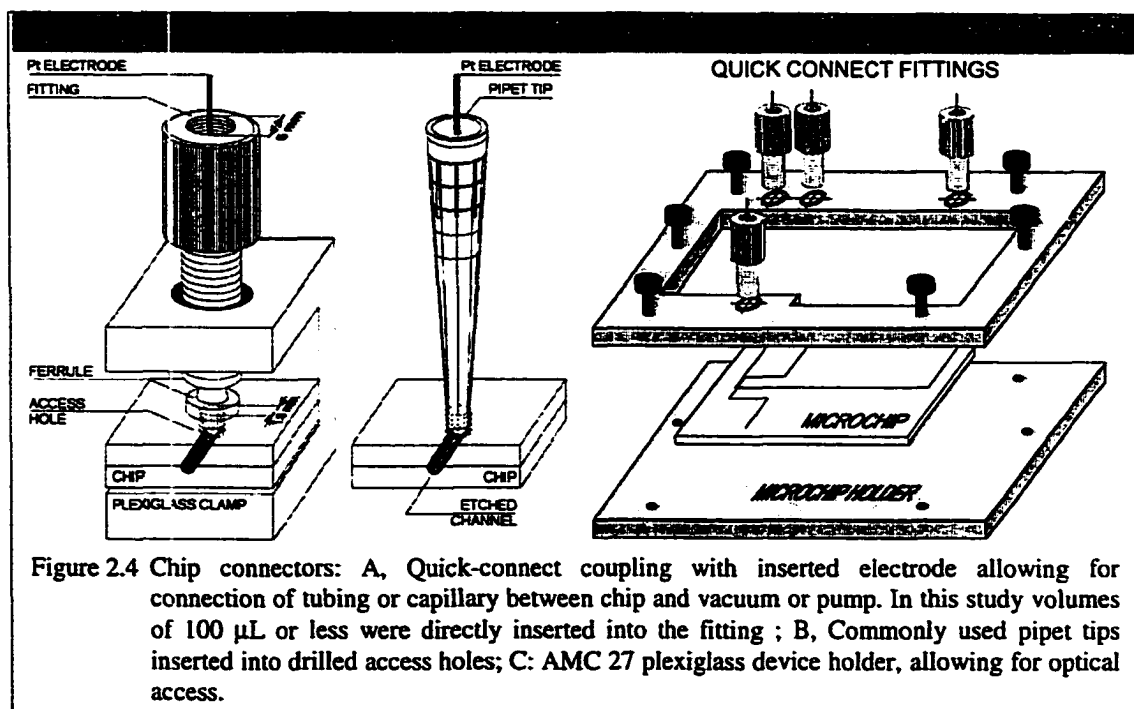


Figure 2.4 Chip connectors: A, Quick-connect coupling with inserted electrode allowing for connection of tubing or capillary between chip and vacuum or pump. In this study volumes of $100 \mu\text{L}$ or less were directly inserted into the fitting ; B, Commonly used pipet tips inserted into drilled access holes; C: AMC 27 plexiglass device holder, allowing for optical access.

in place, as depicted in Figure 2.4 [28]-[27],[30],[48],[49]. In order to overcome the limitations of this initial approach, we developed a chip connector consisting of quick-connect fittings and a plexiglass chip holder as shown in Figure 2.4. Buffers and samples were injected into the through hole of the fitting, and Pt electrodes were inserted into the fittings to apply high voltages. Ferrules provide a seal to the top of the chip. These fittings allow for tubing connections to negative or positive pressure sources (vacuum or pumps). The glass-to-ferrule seal withstood working pressures of up to at least 20 atm when coupled to an HPLC pump with PEEK tubing (O.D.=1.6 mm, I.D.=0.8 mm) for rinsing purposes. Fused silica capillaries can be connected to the chip using flangeless fittings and capillary sleeves, to allow for electrokinetic transfer from off-chip and for 1-2 μl dead volume inter-chip connections.

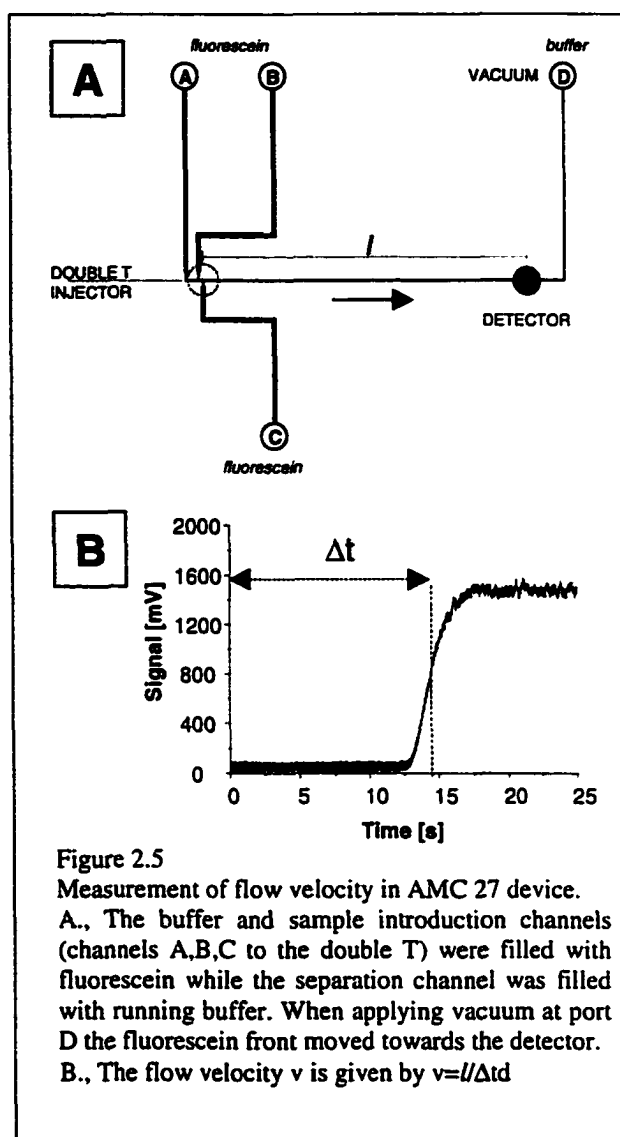


Figure 2.5
 Measurement of flow velocity in AMC 27 device.
 A., The buffer and sample introduction channels (channels A,B,C to the double T) were filled with fluorescein while the separation channel was filled with running buffer. When applying vacuum at port D the fluorescein front moved towards the detector.
 B., The flow velocity v is given by $v=l/\Delta t$

2.4.2 Optical Characteristics

The choice of microscope objective is of crucial importance, as has been shown by Hernandez [50]. The thickness of the two glass plates of the devices limits the minimum working distance, and hence the N.A. of the lens. Given that the glass used [2], [26], [29], [46] is as thick as 2 mm, we chose an objective with a working distance of up to 3.7 mm and an N.A. of 0.6. While the collection efficiency scales with $N.A.^2$, the spot size is inversely proportional to the N.A., which reduces the excitation volume. However, by under filling the back aperture of the microscope objective with the laser beam the numerical aperture used for excitation can be made smaller than the nominal N.A., giving a larger laser probe volume. In order to measure the actual numerical aperture of excitation we scanned a mirror vertically through focus and determined the laser spot

size at various out-of-focus planes. From a plot of laser spot radii versus vertical displacement, Δz , we obtained the angular semi-aperture α . The sine of α ($n_{air}=1$) gives an N.A. of 0.12 for the excitation beam. Assuming a Gaussian beam, the laser beam waist ($1/e^2$) can be calculated from:

$$w^2(z) = w^2_{(z=0)} \left[1 + \left(\frac{\lambda z}{\pi w^2_{(z=0)}} \right)^2 \right] \quad (3.1)$$

where z is the distance from the focal plane, w the beam radius and λ the wavelength. For 488 nm excitation light and a focal length of 4.9 mm for the objective, the calculated $1/e^2$ waist is 4.55 μm in diameter at the focal plane. This value can be compared with an observed spot diameter of $\approx 12 \mu\text{m}$ seen in Figure 2.6. It is possible the glass coversheet contributes to the discrepancy between experiment and theory.

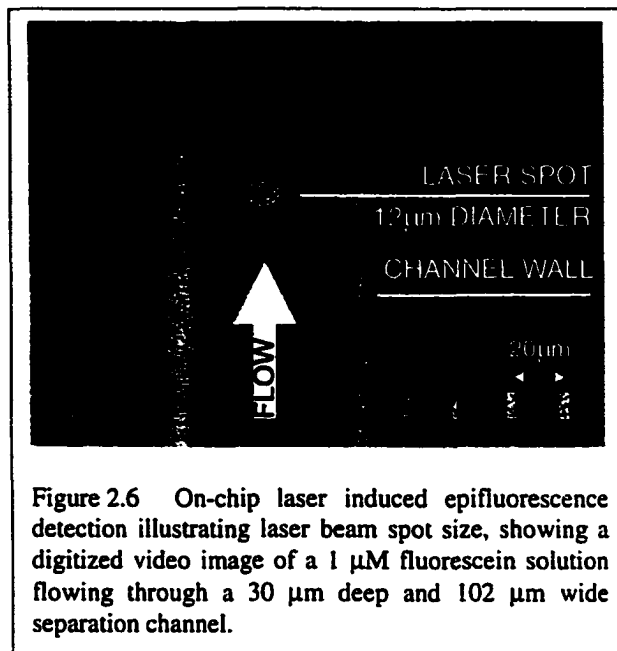


Figure 2.6 On-chip laser induced epifluorescence detection illustrating laser beam spot size, showing a digitized video image of a 1 μM fluorescein solution flowing through a 30 μm deep and 102 μm wide separation channel.

The strength of the optical sectioning is the rate at which the fluorescence intensity decreases with vertical distance between objective and object, and is known as the axial response of a

confocal microscope. Analogous to Wilson [51], we define the vertical displacement given by the full-width-at-half maximum (FWHM) of the axial response as a measure of a microscope's sectioning power. To evaluate our design, a CE chip was scanned vertically through focus in steps of 1 μm . Solutions of 1 nM fluorescein or buffer were alternately flushed through the 30 μm deep flow channel in the chip using vacuum. In Figure 2.7, the corrected fluorescence signals were ratioed to the estimated noise, as described in the Experimental section, then plotted versus the vertical displacement, Δz . The 400 μm pinhole was clearly the optimal choice. A plot of corrected fluorescence signal versus Δz was similar, as evident from Figure 2.8, except that the signals increased monotonically with pinhole size and the curves showed less scatter. The confocal sectioning power and its uncertainty were estimated graphically from the FWHM displacements, using the plots in Figure 2.8 of corrected fluorescence versus Δz . For the 100, 200, 400 and 600 μm sized pinholes, the FWHM displacements were 18 ± 0.7 , 20 ± 0.7 , 26 ± 0.7 and $36 \pm 0.7 \mu\text{m}$, respectively. Estimates from Wilson's model [52] for a $\lambda_{\text{emit}}/\lambda_{\text{excit}}$ ratio of 1 and 100,

200, 400 and 600 μm pinholes are 8, 14, 28, 41 μm FWHM (40x magnification, 0.6 N.A.). These estimates have to be convolved with a slit function model of the channel depth. The observed sectioning power should then be equal to the calculated value when it is equal or larger than the channel depth, and equal to the channel depth when the calculated value is smaller. The measured values for the 400 and 600 μm pinhole agree well with the estimates. For 100 and 200 μm pinholes FWHM values are smaller than the channel depth. We note that all of the pinholes tested were outside the range of calculations presented by Wilson, so we have used a linear extrapolation of his data from the largest pinholes he analyzed, which may account for some of the discrepancy.

In order to determine the number of detected fluorescein molecules over a given acquisition time, the probe volume has to be known. The probe volume is given by the overlap of the detection volume and the excitation volume. From equation 3.1, the $1/e^2$ Gaussian beam diameter at the focal plane is 4.55 μm and at the bottom of the channel is 4.58 μm in diameter. While the actual beam size is larger, given the measured laser spot size of 12 μm , the calculation shows the excitation volume can be

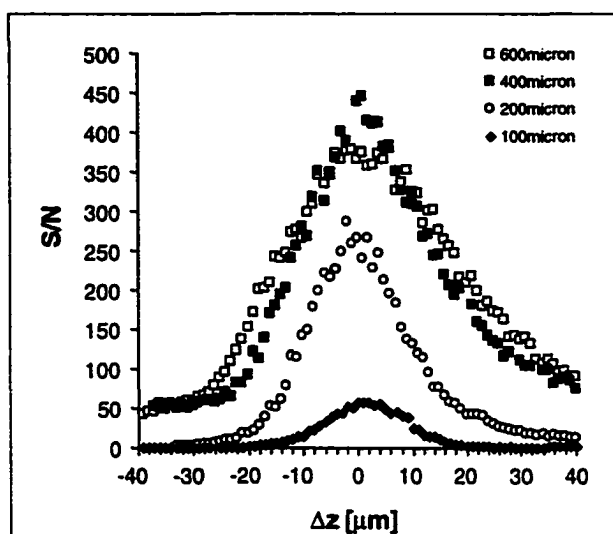


Figure 2.7: Signal to noise ratio (signal corrected for background fluorescence, $(S-B)/N$) versus vertical displacement of chip (Δz) for various pinhole diameters. A 1 nM fluorescein solution in pH 9 buffer was continuously flushed through the separation channel by vacuum (flow velocity: 3.5 mm s^{-1}); Excitation: 488 nm, 3.75 mW; PMT Voltage: 850 V.

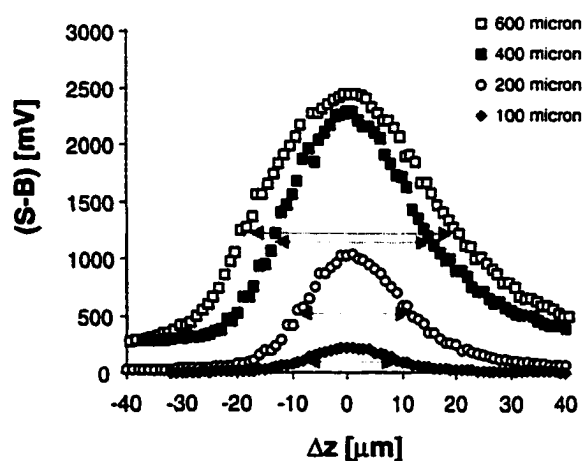


Figure 2.8: Background corrected fluorescence signals versus vertical displacement of chip (Δz) for various pinhole diameters. The full width at half maximum is indicated. A 1 nM fluorescein solution in pH 9 buffer was continuously flushed through the separation channel by vacuum (flow velocity: 3.5 mm/ s); Excitation: 488 nm, 3.75 mW; PMT Voltage: 850 V

approximated as a cylinder, with a 30 μm height resulting from the channel depth. Using the experimentally determined 6 μm beam waist gives an excitation volume of 3.4 pL. The detection volume can be estimated from the pinhole diameter, the magnification and the known sectioning strength. Pinholes of 100, 200, 400 and 600 μm were used with a 40x objective, corresponding to observation spot diameters of 2.5, 5, 10 and 15 μm . For the 400 μm pinhole the axial sectioning was ~ 30 μm . Approximating the shape of the detection zone as a cylinder gives a detection volume of ≈ 2.4 pL for this pinhole. These two volumes lead to a probe cylinder for the 400 μm pinhole that is 10 μm in diameter and 30 μm in height,

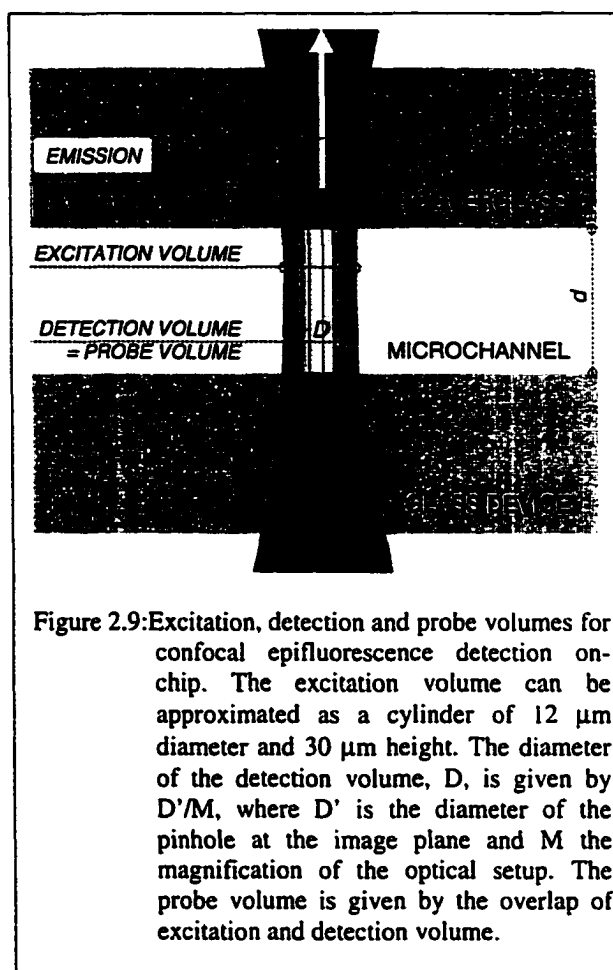


Figure 2.9: Excitation, detection and probe volumes for confocal epifluorescence detection on-chip. The excitation volume can be approximated as a cylinder of 12 μm diameter and 30 μm height. The diameter of the detection volume, D , is given by D'/M , where D' is the diameter of the pinhole at the image plane and M the magnification of the optical setup. The probe volume is given by the overlap of excitation and detection volume.

resulting in an approximate volume of 2.0 pL and a cross sectional area for the probe of 260 μm^2 . The probe volumes for the 100, 200 and 600 μm pinholes are estimated to correspond to 0.1, 0.6 and 3.4 pL. The 30 μm deep channel was 102 μm at the top and 50 μm wide at the bottom, giving a cross sectional area of 2280 μm^2 . Hence the probing efficiency is 11.4 % with a 400 μm pinhole and 0.12 N.A. for the excitation beam.

Figure 2.7 shows that an increase in pinhole diameter from 100 to 400 μm results in an improvement in S/N by a factor of 10. This improvement is consistent with the increased probe volume discussed above, although the fact it is smaller than the 17-fold volume increase may indicate the 400 μm pinhole does not completely discriminate the background arising from the channel walls. For the 600- μm pinhole the depth of field exceeds the channel depth and the observed spot size is larger than the excitation diameter, so that significant background from the channel walls will be measured, causing a decreased S/N ratio, consistent with the data in Figure 2.7. Hence 400- μm diameter pinholes were used for detection in 30- μm deep channels.

Confocal epifluorescence detection schemes for use with channel arrays on microdevices have been demonstrated [30]. A major practical concern is the positioning tolerance required when scanning the chip horizontally: displacement of the focal point from the channel center can result in collection of scattered light from the channel walls and increased background and noise levels. Since the 30 μm deep channels are 50 μm wide at the bottom, a horizontal displacement of more than 25 μm from the channel center will result in decreased S/N. Experimentally, vertical displacement of the chip by 5 μm results in a decrease of $\approx 18\%$ in S/N for a 400- μm pinhole size with a 30- μm channel depth. It should be noted that the decreased sensitivity of the 600- μm pinhole to Δz translation (i.e. focusing) might be convenient in many applications.

2.4.3 Detection Performance

Mathies et al. [53] emphasized the importance of illumination time and incident laser power for high sensitivity fluorescence detection. Due to ground state depletion and photobleaching, the S/N will decrease when exceeding the optimum incident laser power for a given flow rate. We made measurements of the optimum power with both pressure driven (0-7.5 mm s^{-1}) and electrokinetically driven flow (3.5-4.4 mm s^{-1} at 7.5 kV). In electrokinetic flow the flow rate of fluorescein is the vector sum of the electrophoretic and electroosmotic flow rates. The overall linear flow rates of fluorescein were matched in this work, rather than the linear solvent flow rate, in order to ensure equivalent fluorescein flux for pressure and electrokinetically pumped studies. The fluorescein velocity used was the highest attainable within these devices, as arcing became a problem above 7.5-8 kV. In our case the optimum laser output power for the linear flow velocities of 3.5-4.4 mm s^{-1} was measured to be 4.5 mW, with a range of ± 1 mW because the maximum was very broad. This results in $\approx 2.8 \pm 0.6 \times 10^4 \text{ W/cm}^2$ at the estimated $1/e^2$ diameter at the focal plane. The fluorescence signal was studied as a function of electroosmotically driven flow rate at 4.5 mW, and found to vary by no more than 15% between 3.5 and 4.4 mm s^{-1} . Consequently, excluding dispersion effects, the data obtained with pressure driven flow can be readily compared to that for electroosmotically driven flow.

The observed background depended on both the buffer and the buffer concentration used. Photobleaching of fluorescent contaminants in the buffer was evaluated by measuring the background intensity with the flow on and then off. Stopping the electroosmotic or vacuum driven flow typically reduced the background by 4% or less. Decreasing the concentration of the tris/borate buffer by a factor of 4 resulted in a decrease of 2% in background signal on average. Due to adsorption of fluorescein on channel walls, background levels tended to increase after

frequent use. However, rinsing with 0.1 M NaOH for one hour, then running buffer solution, was successful in reducing the background signal to the initial levels in most cases.

In order to determine the instrument response to concentration, various fluorescein solutions were continuously flushed through the separation channel under vacuum. The average blank signal from the buffer for a typical data set was 369.8 ± 5.7 mV, using a laser power of 3.75 mW, 850 V PMT bias, a 25 s collection time and a 7 point box smoothing. Figure 2.10 shows fluorescence signals for buffer, 300 fM and 10 pM fluorescein solutions, 300 fM fluorescein gave a signal 34.6 ± 8.1 mV over background, corresponding to a S/N of 6.1 for this data set. At the linear fluorescein migration velocity of 3.5 mm s^{-1} and hence a volumetric flow rate of 8 nL s^{-1} , 24 molecules were detected on average over the detector response time of 150 ms, given a probing efficiency of 11.4 %.

This data corresponds to detection of 4019 molecules over 25 s, or 241 molecules over 1.5 s, a typical peak width for the electropherograms discussed below. This is, to the best of our knowledge, the lowest detectable fluorescein concentration ever reported on-chip. A log-log plot of background corrected fluorescence signals of 300 fM to 3 nM fluorescein is shown in Figure 2.11 for data obtained with continuous vacuum driven flow. The signal for 300 fM fluorescein remains well above the

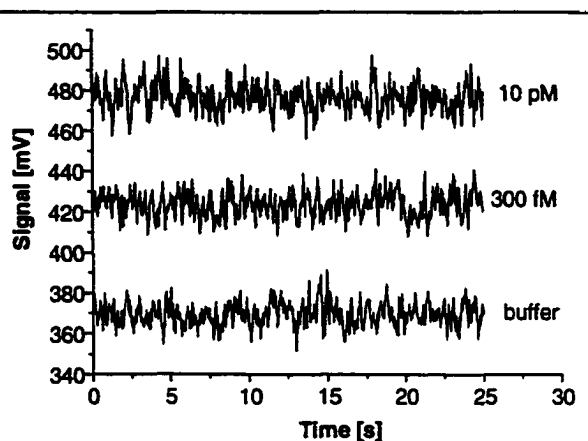


Figure 2.10 Signal levels for vacuum driven continuous flow of pH 9 buffer, 300 fM and 10 pM fluorescein solutions in the same running buffer. Flow velocity: 3.5 mm s^{-1} , pinhole: $400 \mu\text{m}$, Excitation: 488 nm, 3.75 mW; PMT Voltage: 850V

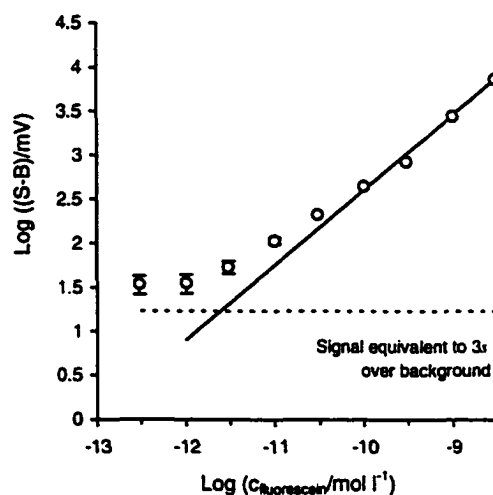


Figure 2.11 Log-log plot of fluorescence intensity from continuous flow, corrected for background fluorescence, as a function of fluorescein concentration. Solutions were hydrodynamically flushed at 3.5 mm s^{-1} . Pinhole: $400 \mu\text{m}$; excitation: 488 nm, 3.75 mW; PMT: 850 V. Error bars are ± 1 s.d., calculated as indicated in the Experimental section, and are smaller than the points where not shown. A line 3 s.d. above the background signal (estimated from the s.d. for 300 fM) is shown to illustrate the signal detection limit floor.

signal detection limit illustrated in the Figure. A weighted linear fit of all data points gives a slope of 0.85 and a regression coefficient of 0.996 for many replicate calibration curves. The weighting factor w_i for a datapoint is given by the reciprocal of the variance. Deviations from unity slope have been reported for fluorescence detection at low concentrations by Hahn [15], Mathies [32] and by Ingle and Wilson [54]. The effects were ascribed to adsorption on glass, either in the detection system or the preparation flasks, to impurities in solution, or to statistical fluctuations in the numbers of molecules at the very lowest concentrations.

On-chip detection of samples under continuous flow conditions is a realistic application of microchip reactor devices, as was recently illustrated by Hadd et al [55], who performed enzyme assays on chip by diluting and mixing reagents in nanoliter volumes with subsequent detection of the enzymatic products in continuous flow mode. However, CE-based separations are also an important application area for the detector. By performing studies of both methods at similar flow rates ($3.5 - 4.4 \text{ mm s}^{-1}$), under conditions that are nearly flow rate independent, the results of both types of experiments are readily comparable after accounting for dispersion [29]. Because of dispersion of the injected sample plugs the peak sample concentration will be decreased 3-fold or more by the time it reaches the detector [29], making the demands on a detector more stringent in CE than in continuous flow measurements.

Figure 2.12 depicts several electrokinetic injections and capillary zone electrophoretic separations of 1 pM fluorescein solutions, utilizing the previously described double T injection system [46]. Signal to noise ratios of 6.5 ± 0.2 , 5.3 ± 0.2 , 5.6 ± 0.2 , 5.7 ± 0.2 (± 1 s.d. of each individual electropherogram, mean 5.8), were obtained. Subsequent injections of buffer solution alone did not show peaks above the noise level, excluding the possibility of false positives due to fluorescent impurities or dust scattering. The same running buffer solution was used as had been used to dilute the fluorescein stock solution, in order to avoid any sample stacking effects. No peaks above background were obtained after double-T injection of 300 fM fluorescein into uncoated channels. We attribute this increased detection limit relative to the continuous flow study to peak dispersion during the separation [29].

In order to determine the mass detected, the injection volume and the probe volume has to be known. In principle, the injection volume is confined by the geometry of the device layout. The double T injector is 202 μm in length (channel edge-to-edge distance) and has a cross sectional area of 2280 μm^2 , resulting in a 461 pL volume. In typical applications of the double-T at higher concentrations we have found leakage effects can on occasion significantly increase the length of the plug formed [2],[56],[57]. Since we are unable to visually monitor the plug shape at these low concentration levels, we have made an upper limit estimate of the injection volume V_{inj} from the

bandbroadening of the peaks. Assuming no non-ideal effects, the bandbroadening contributed by the injector V_{inj} can be calculated from:

$$V_{inj} = \sqrt{12\sigma_{inj}^2}A \quad (2.2)$$

where σ_{inj}^2 is the injector variance and A the cross sectional area of the channel. The value of σ_{inj}^2 can be estimated from equation 1.16, as discussed previously [2]. The important parameters required are the detector size of 12 μm , the average migration time of 10.1 s, and a diffusion coefficient of $3.3 \times 10^{-6} \text{ cm}^2\text{s}^{-1}$ [29]. With equation 1.17, σ_{diff}^2 can then be calculated to be $6.68 \times 10^{-5} \text{ cm}^2$. The variance arising from the detector, σ_{det}^2 , can be neglected for a laser spot size of 12 μm . Under the assumption of no analyte to wall interaction and no joule heating, σ_{inj}^2 can then be obtained by subtracting σ_{diff}^2 from the average total peak variance σ_{tot}^2 . For an injector to detector distance of 45 mm and an average retention time of 10.1 s ($\pm 0.6\%$), σ_{tot}^2 and σ_{inj}^2 are 1.3 mm^2 ($\pm 11.6\%$). With equation 1.15, the injected plug length can be estimated to be $\sim 4.0 \text{ mm}$. For a cross sectional area of $2280 \mu\text{m}^2$, the injected sample volume, V_{inj} , is then $\sim 9.1 \text{ nL}$. The maximum volume of the injected plug

in this study has an upper limit about 20 times larger than a geometrically defined plug. The corresponding upper limit on the number of injected molecules is 5470, corresponding to ≈ 570 detected molecules.

This study demonstrates the excellent concentration detection limits obtainable by confocal epifluorescence fluorescence detection for microchip based analysis systems. Concentration

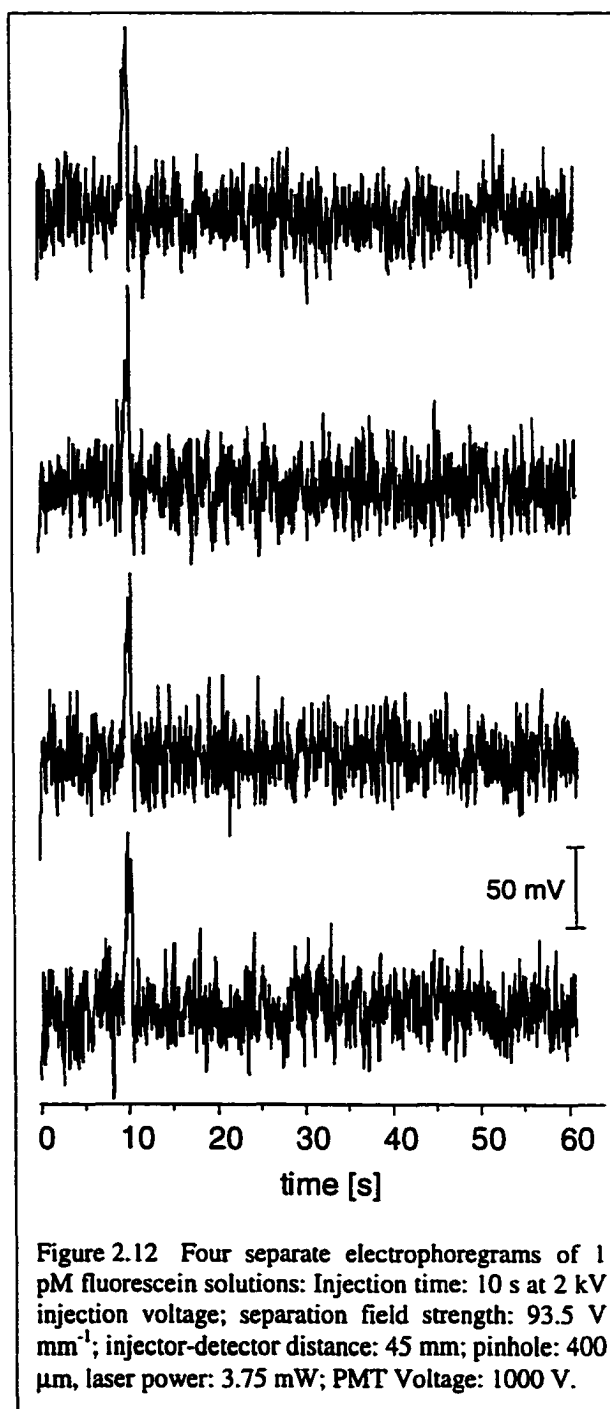


Figure 2.12 Four separate electrophoregrams of 1 pM fluorescein solutions: Injection time: 10 s at 2 kV injection voltage; separation field strength: 93.5 V mm^{-1} ; injector-detector distance: 45 mm; pinhole: $400 \mu\text{m}$; laser power: 3.75 mW; PMT Voltage: 1000 V.

detection limits in the 0.3 to 1 pM range will allow the advantages of biological assays on chip such as high speed, low reagent consumption and high throughput to be fully exploited for trace biochemical analytes. The measured sectioning powers for the pinholes indicate that for larger apertures a linear extrapolation of Wilson's model, along with the use of equation 3.1, is predictive for the optimal pinhole size. The probing efficiency of 11.4 % obtained here for 30- μ m deep channels with a 400- μ m pinhole could be increased if the channel width could be reduced. However, the etching depth determines the width of chemically etched channels in glass, since the etching process is isotropic. The measured displacement curves allow an estimate of the vertical (optical axis) positioning tolerance of the microscope as less than 5 μ m, meaning for physically scanning a multichannel device the distance between channels must be minimized to alleviate positioning tolerance demands. The finger tight, quick-fit fluid interface we have used proved to be highly convenient, reducing many problems associated with the world-to-chip interface, and should also be useful in applying chips to biochemical analyses.

2.5 Acknowledgements

I am grateful to Thompson Tang, Per Andersson, Edgar Arriaga, and Michael Morris (Department of Chemistry, University of Michigan) for helpful discussions. I would like to thank Dieter Starke, Roman Lipiecki, Stan Luxa, Erich Schachner and Hubert Hofmann, all of the University of Alberta-Machine Shop, for high quality machining of the microscope body and assembly, and the Alberta Microelectronic Corporation, AMC, for device fabrication.

2.6 References

- 1 Harrison, D. J., Manz, A., Fan, Z. H., Luedi, H., Widmer, H. M. *Anal. Chem.* 1992, *64*, 1926-1932
- 2 Fan, Z., Harrison, D.J. *Anal. Chem.* 1994, *66*, 177-184
- 3 Harrison, D.J., Fluri, K., Seiler, K., Fan, Z., Effenhauser, C.S., Manz, A. *Science* 1993, *261*, 895-897
- 4 Gozel, P., Gassmann, E., Michelsen, H.; Zare, R.N. *Anal. Chem.* 1987, *59*, 44-49
- 5 Lee, I.H., Pinto, D., Arriaga, E.A., Zhang, Z., Dovichi, N.J. *Anal. Chem.* 1998, *70*, 4546-4548
- 6 Pinto, D.M., Arriaga, E.A., Craig, D., Angelova, J., Sharma, N., Ahmadzadeh, H., Dovichi, N.J., Boulet, C.A. *Anal. Chem.* 1997, *69*, 3015-3021
- 7 Craig, D.B., Wong, J.C.Y., Dovichi, N.J. *Anal. Chem.* 1996, *68*, 697-700
- 8 Chen, D.Y., Adelhelm, K., Cheng, X.L., Dovichi, N.J. *Analyst* 1994, *119*, 349-352
- 9 Zhao, J.Y., Diedrich, P., Zhang, Y., Hindsgaul, O., Dovichi, N.J. *J. Chromatogr.* 1994, *657*, 307-313
- 10 Lu, H., Arriaga, E., Chen, D.Y., Dovichi, N.J. *J. Chromatogr. A* 1994, *680*, 497-501
- 11 Chen, D.Y., Dovichi, N.J. *J. Chromatogr.* 1994, *657*, 265-269

- 12 Zhao, J.Y., Chen, D.Y., Dovichi, N.J. *J. Chromatogr.* 1992, 608, 117-120
- 13 Wu, S., Dovichi, N.J. *Talanta* 1992, 39, 173-178
- 14 Zhang, J.Z., Chen, D.Y., Wu, S., Harke, H.R., Dovichi, N.J. *Clin. Chem.* 1991, 37, 1492-1496
- 15 Hoon Hahn, J., Soper, S. A., Nutter, H. L., Martin, J. C., Jett, J. H., Keller, R. A. *Appl. Spectrosc.*, 1991, 45, 743-746
- 16 Chen, D.Y., Swerdlow, H.P., Harke, H.R., Zhang, J.Z., Dovichi, N.J. *J. Chromatogr.* 1991, 559, 237-246
- 17 Wu, S., Dovichi, N.J. *J. Chromatogr.* 1989, 480, 141-155
- 18 Cheng, Y.F., Dovichi, N.J. *Science* 1988, 242, 562-564
- 19 Nguyen, D. C., Keller, R. A., Jett, J. H., Martin, J. C. *Anal. Chem.* 1987, 59, 2158-2161
- 20 Figeys, D., Ning, Y., Aebersold, R. *Anal. Chem.* 1997, 69, 3153-3160
- 21 Figeys, D., Aebersold, R. *Anal. Chem.* 1998, 70, 3721-3724
- 22 Figeys, D., Gygi, S. P., McKinnon, G.; Aebersold, R. *Anal. Chem.* 1998, 70, 3728-3734
- 23 Li, J., Thibault, P., Bings, N.H., Skinner, C.D., Wang, C., Colyer, C., Harrison, D.J. *Anal. Chem.* 1999, 71, 3036-3045
- 24 Bings, N. H., Wang, C., Skinner, C.D., Colyer, C.L., Thibault, P., Harrison, D.J. *Anal. Chem.* 1999, 71, 3292-3296
- 25 Zhang, B., Liu, H., Karger, B.L., Foret, F., *Anal. Chem.*, Web Release Date: June 16, 1999
- 26 Seiler, K., Harrison, D. J., Manz, A. *Anal. Chem.* 1993, 65, 1481-1488
- 27 Effenhauser, C. S., Manz, A., Widmer, H. M. *Anal. Chem.* 1993, 65, 2637-2642
- 28 Jacobson, S. C., Hergenroeder, R., Moore, A. W., Ramsey, J. M. *Anal. Chem.* 1994, 66, 4127-4132
- 29 Liang, Z. H., Chiem, N., Ocvirk, G., Tang, T., Fluri, K., Harrison, D. J. *Anal. Chem.* 1996, 68, 1040-1046
- 30 Woolley, A. T., Mathies, R. A. *Anal. Chem.* 1995, 67, 3676-3680
- 31 Huang, X.C., Quesada, M.A., Mathies, R.A. *Anal. Chem.* 1992, 64, 2149-2154
- 32 Mathies, R. A., Scherer, J.R., Quesada, M.A. *Rev.Sci.Instrum.* 1994, 65, 807-812
- 33 Hernandez, L., Escalona, J., Joshi, N., Guzman, N. *J.Chromatogr.* 1991, 559, 183-196
- 34 Beale, S. C., Sudmeier, S. J. *Anal. Chem.* 1995, 67, 3367-3371
- 35 Nie, S., Chiu, D.T., Zare, R.N., *Science* 1994, 266, 1018-1021
- 36 Haab, B. B., Mathies, R. A. *Anal. Chem.* 1995, 67, 3253-3260
- 37 Castro, A., Shera, E. B. *Appl. Opt.* 1995, 34, 3218-3222
- 38 Effenhauser, C.S., Bruin, G.J.M., Paulus, A., Ehrat, M. *Anal. Chem.* 1997, 69, 3451-3457
- 39 Fister, J.C., Jacobson, S.C., Davis, L.M., Ramsey, J.M., *Anal. Chem.* 1998, 70, 431-437
- 40 Barnes, M.D., Whitten, W.B., Ramsey, J.M. *Anal. Chem.* 1995, 67, 418A-423A
- 41 Brakenhoff, G.J., Visscher, K., van der Voort, H.T.M., in *Handbook of Biological Confocal Microscopy*, ed. Pawley, J.B., Plenum Press, New York, 1990, pp. 87-91
- 42 Jacobson, S. C., Ramsey, J. M. *Anal. Chem.* 1996, 68, 720-723

- 43 Cheng, Y.F., Dovichi, N.J. *Science* 1988, 242, 562-564
- 44 Fan, Z. H., *Ph.D Thesis, University of Alberta, Chemistry Dept. 1994, Chapter 3*
- 45 Chiem, N.C., *Ph.D. Thesis, University of Alberta, Chemistry Dept. 1997, Chapter 2*
- 46 Chiem, N. H., Harrison, D. J., *Anal.Chem.* 1997, 69, 373-378
- 47 Koutny, L. B., Schmalzing, D., Taylor, T. A., Fuchs, M. *Anal.Chem.* 1996, 68, 18-22
- 48 Chiem, N., Harrison, D. J. *Anal.Chem.* 1997, 69, 373-378
- 49 von Heeren, F., Verpoorte, E., Manz, A., Thormann, W. *Anal. Chem.* 1996, 68, 2044-2053
- 50 Hernandez, L., Marquina, R., Escalona, J., Guzman, N. A. *J. Chromatogr.* 1990, 502, 247-255
- 51 Wilson, T. in *Handbook of Biological Confocal Microscopy*, ed. Pawley, J. B., Plenum Press: New York, London 1990, pp. 113-126
- 52 Wilson, T. *J. Microscopy* 1989, 154, 143-156
- 53 Mathies, R. A., Peck, K., Stryer, L. *Anal. Chem.* 1990, 62, 1786-1791
- 54 Ingle, J.D., Wilson, R.L. *Anal. Chem.* 1976, 48, 1641-1642
- 55 Hadd, A.G., Raymond, D.E., Halliwell, J.W., Jacobson, S., Ramsey, J.M. *Anal.Chem.* 1997, 69, 3407-3412
- 56 Seiler, K., Fan, Z., Fluri, K., Harrison, D.J. *Anal. Chem.* 1994, 66, 3485-3491
- 57 Shultz-Lockyear, L.L., Colyer, C.L., Fan, Z.H., Roy, K.L., Harrison, D.J. *Electrophoresis* 1999, 20, 529-538

Chapter 3:

β -Galactosidase Assays of Single Cell Lysates on a Microchip: A Complementary Method for Enzymatic Analysis of Single Cells^{*}

3.1 Abstract

The use of glass chips, featuring a 20 μm deep fluidic network, for a continuous β -Gal assay of single cell lysates is described. The monitoring of β -gal activity in single HL-60 cells by off-chip incubation with a 200 μM fluorescein-di- β -D-galactopyranoside, FDG, for 120 minutes at 37 $^{\circ}\text{C}$, on-chip lysis with a denaturing 35 mM SDS solution and on-channel epifluorescence detection is illustrated. This report demonstrates the first-time integration of lysis and incubation of single cells onto a microfluidic chip. A non denaturing incubation mixture, containing 400 μM FDG and 0.1 % Triton[®]X-100, is used. Cells are transported one by one towards a Y shaped mixing junction by suction at a flow velocity of ~ 100 $\mu\text{m}/\text{s}$ and ~ 40 $\mu\text{m}/\text{s}$ under denaturing and non-denaturing conditions, respectively. The lytic reagents, introduced into side channels, are mixed with the cell stream at a mixing ratio of $\sim 1:1$. The time needed for lysis of 10^6 HL-60 cells with a 0.1 % Triton[®]X-100 solution is measured in a microtiterplate well to be ~ 30 -60 s. The on-chip incubation time of single cell lysates is ~ 80 -110 s. Complete and reproducible lysis of cells, monitored by video microscopy and confirmed by the absence of cell debris induced light scattering peaks in on-chip measurements, is demonstrated. Fluorescence peaks, detected for each lysate after lysis of off-chip and on-chip incubated cells ($t_{\text{inc}} \sim 80 - 110$ s), are depicted. The results of a CE analysis of an extract of 50×10^6 HL-60 cells in Triton[®]X-100, incubated with 200 μM FDG for 110 min, are given to identify fluorescein mono- β -D-galactopyranoside, FMG,

-
- ^{*} The experimental data, acquired in this study and described in this chapter, would not have been obtained without the hands-on participation of following colleagues:
Edgar A. Arriaga^{*†}: Initiation of project, capillary electrophoresis of HL-60 cell extracts (figure 3.5)
Per E. Andersson^{*†}: Initiation of project, initial on-chip experiments
Hossein Salimi-Moosavi^{*‡}: Expertise in cell handling on chip, trouble shooting, participation in acquisition of data, depicted in figure 3.3
Rod J. Szarka^{*†}: cell culture, participation in performing microtiterplate-based fluorescence assays; Figures 3.3, 3.7
Please note the acknowledgements at the end of this chapter.
^{*} University of Alberta, Department of Chemistry, Edmonton, AB, Canada T6G 2G2
[†] current address: University of Minnesota, Department of Chemistry, Minneapolis, MN 55455-431, U.S.A.
[‡] current address: Amersham Pharmacia Biotech, SE-751 84 Uppsala, Sweden.
[∞] current address: Aclara Biosciences, Mountain View, CA 94043, U.S.A.
[†] Alberta Research Council, Edmonton, AB, Canada T6N 1E4

as enzymatic product. The presented results demonstrate the feasibility of performing enzymatic assays of single cell lysates on-chip with moderate to high throughput. The advantage of enzymatic analyses of cell lysates is substantiated by performing β -Gal assays of viable cells and cell lysates, resulting in a 19 times higher fluorescence response of a 0.1 % Triton[®]X-100 lysate ($t_{inc} = 60$ min; 10^6 cells; RT). Flow cytometric analysis of viable cells is shown to require a minimum incubation time of 60 minutes for fluorescence analysis. Error sources of the analysis of viable cells, which can be circumvented by the analysis of lysates, are highlighted in this context.

3.2 Introduction

β -Galactosidase (β -Gal) assays are frequently performed in clinical chemistry and molecular biology. The β -Gal catalyzed hydrolysis of β -D-galactopyranosides is involved in lactose digestion and degradation of mucopolysaccharides [1], glycoproteins and glycolipids [2]. Several lysosomal storage diseases such as gangliosidosis [3],[4], gargoylism [5] and Morquio B syndrome [6] are the result of genetic deficiencies of β -Galactosidase and have been diagnosed by β -Gal assays of bulk homogenates of fibroblasts [7] and lymphocytes [4],[8]-[10]. In addition, characteristic alterations of β -Gal levels were found in leukemia cells [10], which could be valuable in the differentiation of various leukemias [10]. β -Gal has been widely used as a reporter enzyme in reporter gene assays to study levels of genetic expression, promoter efficiency and genetic regulatory mechanisms [11]. The β -Gal catalyzed hydrolysis of synthetic chromogenic β -D-galactopyranosides is used for indirect detection of gene or plasmid content in cell populations in this context.

The heterogeneity of cell populations makes it desirable to detect β -Gal activities in single cells in order to detect β -Gal deficiencies at an earlier stage allowing for early attempts of enzyme replacement therapy [12]. Measurements of the nuclear cell cycle function and the expression of other intracellular enzymes in single cells may then aid in mechanistic understanding of β -Gal deficiencies. Consequently a high throughput single-cell enzymatic assay with high sensitivity is required. Flow cytometry utilizing fluorogenic substrates such as fluorescein-di- β -D-galactopyranoside, FDG, [13],[14] is used routinely for high throughput fluorescence analysis of preincubated cells and provides the average as well as the distribution of β -Gal activities in a given cell population. However, there are several drawbacks of analysing viable cells for β -Gal activity: long incubation times are necessary, due to low substrate and enzyme concentrations in single β -Galactosidase deficient cells; differing permeability and surface areas of cell and

lysosomal membranes result in different substrate concentrations in distinct cytosols and lysosomes [15]; lysosomal acid hydrolases show maximum activity at acid pH levels [2], resulting in decreased quantum efficiencies of the fluorescent products and hence a loss in sensitivity. Additionally, leakage of fluorescent product(s) out of the cell and uptake of the product(s) by adjacent cells has been reported to result in systematic errors in estimation of enzymatic activity per cell [14]. Additionally, flow cytometric quantitation of β -Galactosidase activities is based on estimates of lysosomal pH's and cell sizes, thus only allowing for moderate accuracy. In order to circumvent these problems and to allow for controlled incubation conditions we introduce here a chip-based β -Gal assay of single cell lysates.

The facility of performing cell manipulations, reactions and analyses [16]-[23] in microfluidic devices has opened up the possibility of chip-based cell assays. In our group we have demonstrated the electroosmotically pumped, directional transport and SDS induced lysis of non adherent erythrocytes and yeast cells [19], a Ca- flux assay with single non-adherent cells in stopped flow mode [20] and cell-rolling based detection of anti-inflammatory drug candidates on-chip [24]. The advantages of microchip-based continuous enzymatic assays, such as reductions in analysis time and reagent consumption, were pointed out recently, by the demonstration of an assay of β -Gal activity [25]. This present study demonstrates a continuous, chip-based intracellular enzymatic assay of single cells for the first time, and thus realizes the aforementioned advantages of chip-based single cell analyses. The ability to lyse and incubate single cells in microchannels in a continuous manner, as demonstrated in this study, represents an important step towards enzymatic screening of large cell populations with high throughput.

The enzymatic analysis of single cell lysates in a microfluidic device requires the transport, lysis and incubation of single cells. The aim of this work is to describe the instrumentation and the experimental parameters that have to be considered for 1., controlled lysis of single cells, 2., subsequent incubation of single cell lysates and 3., detection of enzymatic products within the time scale of a few minutes. A cell line of promyelocytic leukemia cells (HL-60) is used as a model system to demonstrate the advantages of a chip-based β -Gal assay of leukocyte lysed on-chip. We introduce a uniquely flexible approach that we believe to be a strong complement to highly useful flow cytometry-based assays. Due to the ease and low cost of multiplexing of channel features on planar devices we see a distinct advantage in high throughput over capillary based assays. In contrast to capillaries, microfluidic devices allow for facile introduction and manipulation of single cells. Ultimately, we envision a low cost chip-based system for high throughput analyses of intracellular enzymes in single cells.

Due to the weak adhesion of HL-60 cells to the glass channel walls, all channels were dynamically coated with fetal calf serum containing phosphate buffered saline. Single HL-60 cells were driven through the microfluidic glass channels by suction. The cells were then lysed one by one and the fluorescence response of single cell lysates passing the detector was detected by a previously described confocal epifluorescence microscope [26]. Due to the resulting drastic reduction of EOF and a loss of translational control of HL-60 cells, EOF could not be used as fluid pump in this study. Further, we wished to avoid the possibility of damaging the cell membranes with applied electric fields. Therefore we utilized hydrodynamic pumping in this study.

3.3 Experimental Section

3.3.1 Reagents & Media

RPMI 1640 culture medium, gentomycin, streptomycin and Dulbecco's phosphate buffered saline (PBS) were obtained from Life Technologies (Gibco BRL, Burlington, Ontario, Canada). The fluorogenic substrate fluorescein di- β -D-galactopyranoside, FDG, calcein-AM and ethidium homodimer were obtained from Molecular Probes (Eugene, OR, USA). FDG was stored frozen as 10 mM stock solution in dimethylsulfoxide (DMSO, BDH, Toronto, ON, Canada). The stock solutions were thawed and purified (fluorescein mono- β -D-galactopyranoside, FMG, was removed) before analysis as previously described [27]. Fluorescein, FMG, Triton[®]X-100 (t-octylphenoxy polyethoxy ethanol), diethylaminoethyl cellulose and heat inactivated fetal calf serum (FCS) were purchased from Sigma (St.Louis, MO, USA). Sodium dodecylsulfate (SDS) was from Serva Feinbiochemica (Heidelberg, Germany), cetyltrimethylammonium bromide (CTAB) from Baker Chemical (Phillipsburg, NJ, USA), Igepal CA-630 (Octylphenylpolyethylene glycol) from Fluka (Buchs, CH), the reporter lysis buffer from Promega (Madison, WI, USA). All surfactant solutions, i.e. solutions of Triton[®]X-100, CTAB and Igepal CA-60 of various concentrations, were prepared in pyrogen free water. The obtained 5x reporter lysis buffer solution, supplied by Promega, was diluted in pyrogen free water. Vials and pipet tips were autoclaved before use.

3.3.2 Cell Culture

Promyelocytic leukemia cells (HL-60) were obtained from the American Type Culture Collection (ATCC) and maintained in RPMI supplemented with 5% gentomycin, 5% streptomycin and 10% fetal calf serum in a humidified atmosphere with 5 % CO₂ at 37°C. The cells were split in a 1:1

ratio every two days. Cells were counted with a hemacytometer (Fisher Scientific, Nepean, ON, Canada).

3.3.3 Devices & Equipment

3.3.3.1 Microdevices

Microchips with incorporated fluidic manifolds were manufactured by the Alberta Microelectronic Corporation (Edmonton, AB, Canada) as described previously [28]. Briefly, a previously used device layout, PCRD 2 [29] was isotropically etched into 1.7 mm thick Pyrex glass (Paragon Optical Co., Reading, PA). Access holes, 1.9 mm in diameter, were drilled mechanically into the top plates, then these were thermally bonded to the etched plates for 6 hours at 595°C. The channel layout is given in

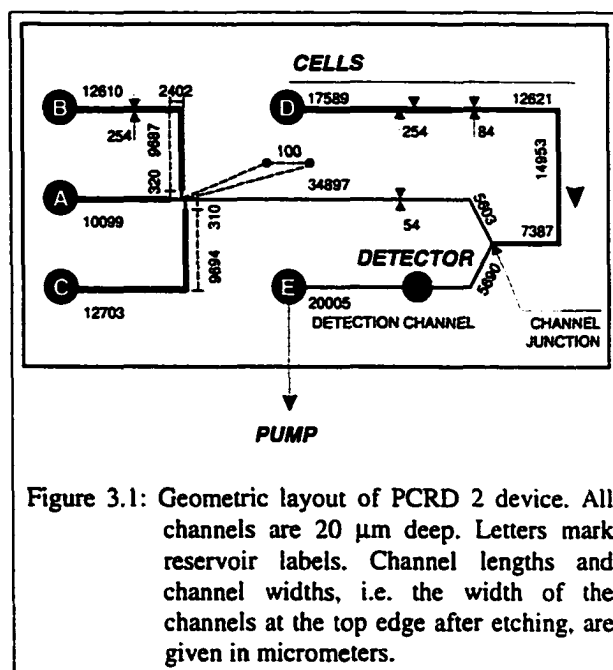


Figure 3.1: Geometric layout of PCRD 2 device. All channels are 20 μm deep. Letters mark reservoir labels. Channel lengths and channel widths, i.e. the width of the channels at the top edge after etching, are given in micrometers.

Figure 3.1. All channels were 20 μm deep. The main channel meets the side channel at a junction angle of 130 degrees. The distance from the junction to the point of detection varied for different experiments and is stated where appropriate.

3.3.3.2 Chip Instrumentation

A previously described instrumental setup [26] was modified for the chip-based assay. The setup is depicted in Figure 3.2. A previously described confocal microscope [26] was inverted in order to allow the implementation of an additional microscope for visual observation of the fluidic manifold. Briefly, excitation light from an air cooled argon ion laser is focused by a 40x 0.6 N.A. microscope objective (Carl Zeiss Jena, Germany) onto a glass device from underneath to a $\approx 12 \mu\text{m}$ spot. Fluorescence is passed through a dichroic mirror (485 DF22, Omega, Battleboro, VT, USA), reflected by a mirror and focused with a tube lens (PAC 064, Newport, Irvine, CA, USA) onto a pinhole located at the focal point of the tube lens. A 600 μm pinhole (Melles Griot, Irvine, CA) was inserted into an eyepiece tube mounted on an xy centering mount (77809, Oriol Instruments, CT, USA). A photomultiplier tube (PMT, Hamamatsu R1477; bias: 800-1000V), with a 514.5 nm bandpass filter (9 nm bandpass, Melles Griot) and a 488 nm rejection band pass

filter (Beckman Instruments, Fullerton, CA, USA), used for spectral filtering, was mounted on the microscope tube. The microchip was interfaced to flangeless fittings (P202&P200 Upchurch Scientific, Oak Harbour, WA, USA) by clamping it into a custom made plexiglass holder. A syringe pump (Harvard Apparatus, Quebec, Canada) or house vacuum with a coupled T-valve was connected to the outlet fitting with PEEK tubing (I.D. 0.005", O.D. 1/16", Upchurch Scientific) for hydrodynamic pumping of suspensions through the channels. The chip holder was mounted on a XYZ translation stage assembly (Newport 423, Irvine, CA) as described previously [26]. The analog

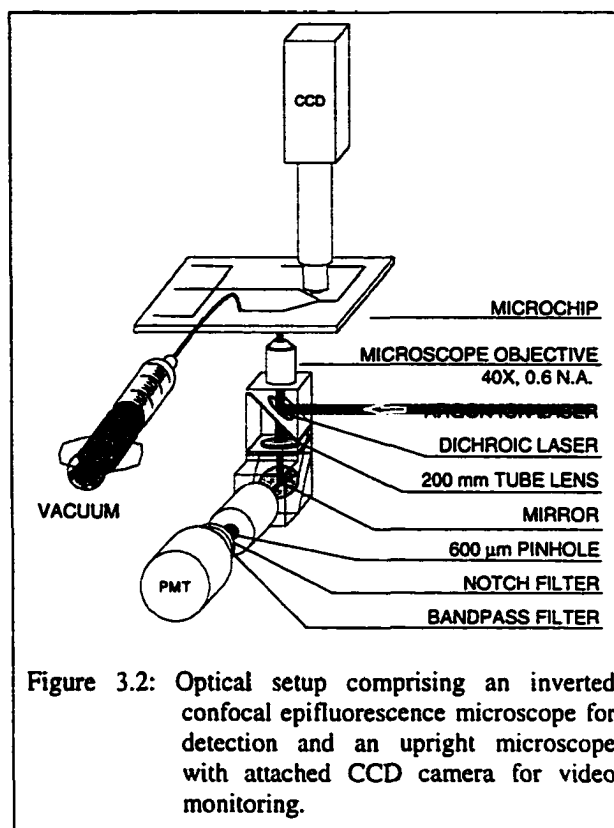


Figure 3.2: Optical setup comprising an inverted confocal epifluorescence microscope for detection and an upright microscope with attached CCD camera for video monitoring.

signal is filtered with a Butterworth 55 Hz cutoff filter (Krohn-Hite 3442). Electropherograms are recorded on a PowerMac 7100/66 with an NB-MIO16 A/D board and a program written in Labview (National Instruments, Austin, TX, USA) at a sampling rate of 200 Hz. All data is smoothed using a 7 point box smooth algorithm, included in Igor Pro Analysis (Wavemetrics, Lake Oswego, OR, USA). A microscope tube mounted on top of the channel junction allowed for observation of cell lysis and determination of flow velocity of each cell. Briefly, the assembly consisted of a 16 cm long black tube (I.D. 25 mm), a 25 x, 0.35 N.A. microscope objective (Leica, Germany), a coupling lens (D50BHC, 0.5 X, Diagnostic Instruments, Sterling Heights, MI, USA), a CCD camera (SSC-C370, Sony) and a VCR (HR-S7200, Super-VHS, JVC).

3.3.4 Procedures

3.3.4.1 Flow cytometry

Aliquots of the cell suspension were centrifuged at 1500 rpm for 15 minutes, followed by one washing step with PBS / 5% FCS. Cells were then resuspended in PBS / 5% FCS. The cell concentration was adjusted to 10^7 cells / mL and 40 μL of 2 mM FDG in PBS / 5% FCS was added to 360 μL of the suspension, followed by incubation at 37°C (5% CO₂). Cells (n ~10000 /

analysis) were analysed for fluorescence, forward and side scatter on a EPICS Profile II flow cytometer (Coulter, FA, USA). Light scatter and fluorescence signals were set in logarithmic gain. The distribution of fluorescence signals and the mean fluorescence intensity of the entire cell population were determined.

3.3.4.2 *Well Plate Assay*

β -Gal activities in viable cell suspensions and cell lysates were measured in microtiter plates (Labsystems, Helsinki, Finland) at 25°C. Fluorescence signals were acquired on a microtiter plate reader (Cytofluor 4000, Perseptive Biosystems, Framingham, MA, USA, λ_{exc} = 485 nm, λ_{em} = 530 nm). The fluorescence response in viable cells was measured in an assay mixture containing 90 μ L of cell suspension (1.0×10^6 cells / mL PBS-5% FCS) and 10 μ L of 2 mM FDG in PBS / 5% FCS. Assay mixtures of cell lysates contained 90 μ L of cell suspension and 10 μ L of 2 mM FDG detergent solutions. The initial detergent concentration was 10 times more concentrated than the final concentration in the well after mixing. Cell pellets were separated from supernatant solutions after incubation for 1-121 minutes. Separation was performed by centrifugation at 1000 rpm for 15 minutes for all assays of supernatant solutions. Background fluorescence signals of FDG, dissolved in PBS / 5% FCS and the detergent-medium mixture, respectively, were measured on the same plate. The fluorescence signals obtained were calibrated by simultaneous fluorescence measurement of 10 nM – 10 μ M FMG solutions in medium or the medium-detergent mix.

Wells were filled with 50 μ L cell suspensions of 2×10^6 cells / 50 μ L PBS and 50 μ L of 10 μ M ethidium homodimer detergent solution for all cytotoxicity assays. The minimum delay time between the addition of the detergent solution to the cell suspension and the fluorimetric measurement was 30 s. The fluorescence response of each well was then monitored in 40 s intervals. All measurements were performed in triplicate. Signal averaging and background subtraction were performed in Microsoft Excel.

3.3.4.3 *Capillary Electrophoresis*

The CE instrument with a sheath flow postcolumn LIF detector is identical to a previously published setup [27],[30]. A 25 μ m-i.d., 150 μ m-o.d., 30 cm long fused-silica capillary (Polymicro Technologies, Phoenix, AZ, USA) was used. After rinsing with 0.1 M NaOH for 15 minutes, capillaries were flushed with double distilled, deionized water for 5 minutes. A PBS / 5% FCS solution was then driven through the capillary for 15 minutes by suction. The detection

end was positioned in a sheath flow cuvette, providing hydrodynamic focusing of the capillary flow. A 488 nm argon ion laser (10 mW), was used as excitation source. Fluorescence was detected with a photomultiplier tube (R1477, Hamamatsu) after spectral filtering with a 535DF45 bandpass filter (Omega Optical). The analog signal was acquired at 10 Hz.

3.3.4.4 Chip-based Assay

3.3.4.4.1 Off-chip Incubation and On-chip Lysis

Cells were harvested, washed and incubated as described above. The device was preconditioned as follows: 100 μ L PBS and 100 μ L PBS / 5% FCS were loaded into ports A,B,C and port D, respectively. Subsequently vacuum was applied at port E for 15 minutes. Remaining PBS solution was then removed from ports A,B and C and 100 μ L of 35 mM SDS was introduced (after three rinses of the reservoirs with SDS solution) into ports A,B and C. After 15 minutes of rinsing, the flow was stopped and 50 μ L of a suspension of preincubated cells (10^6 cells / mL) was pipetted into reservoir D after removal of the PBS / 5% FCS solution. The cell flow velocity was adjusted to \sim 100 μ m/s as measured by video microscopic monitoring of cell migration.

3.3.4.4.2 On-chip Incubation and On-chip Lysis

An aliquot of 50 μ L of 10^6 cells/mL was introduced into port D after preconditioning of the device with PBS / 5% FCS and an aqueous solution of 0.1 % Triton[®]X-100, as described above for the SDS solution. The linear flow velocity was adjusted to \sim 40 μ m/s at port E.

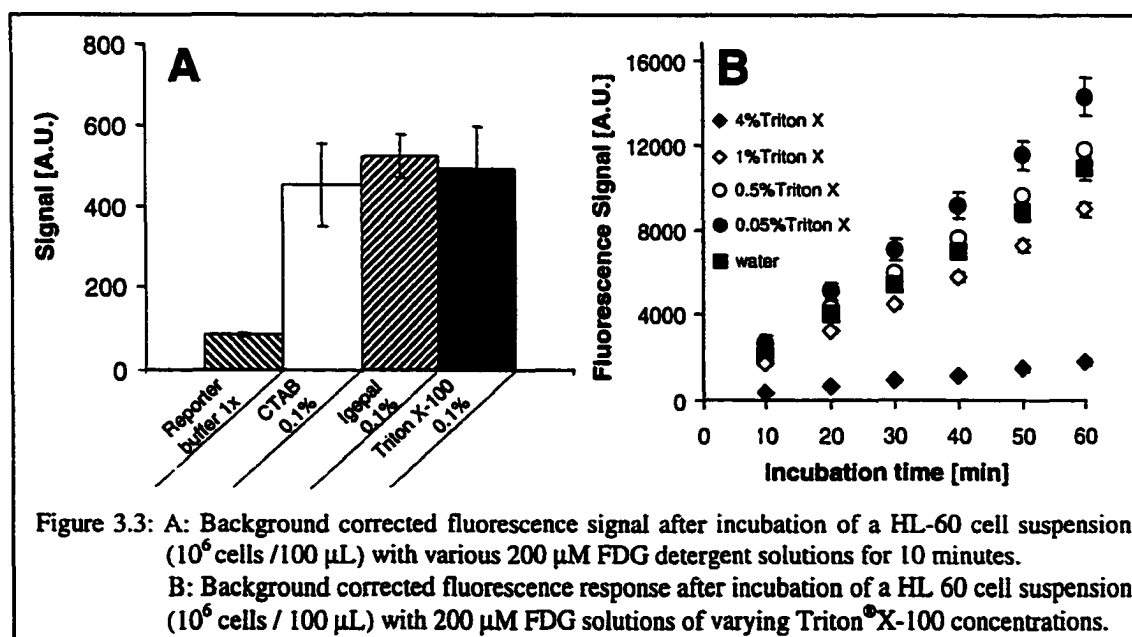
3.4 Results and Discussions

Chip based enzymatic analyses of single cell lysates require a sequence of steps. 1., Cells have to be introduced into the chip and transported at constant velocities; 2., the cells have to be lysed quickly and reproducibly; 3., the lysates have to be mixed with the substrate; 4., the lysates have to react with the substrate for a defined incubation time and 5., the single cell reaction products have to be detected. Prior to on-chip analysis we performed conventional assays of intracellular β -Gal activities in cell extracts of many cells to determine the composition of the optimum lysing solution, the optimum substrate concentration, the number of enzymatic products and the β -Gal carry over in fetal calf serum coated capillaries. The optimization procedures, employing a microtiter plate scanner, a flow cytometer and a capillary electrophoresis instrument with postcolumn detection will be described prior to demonstration of results of the chip-based single cell assays.

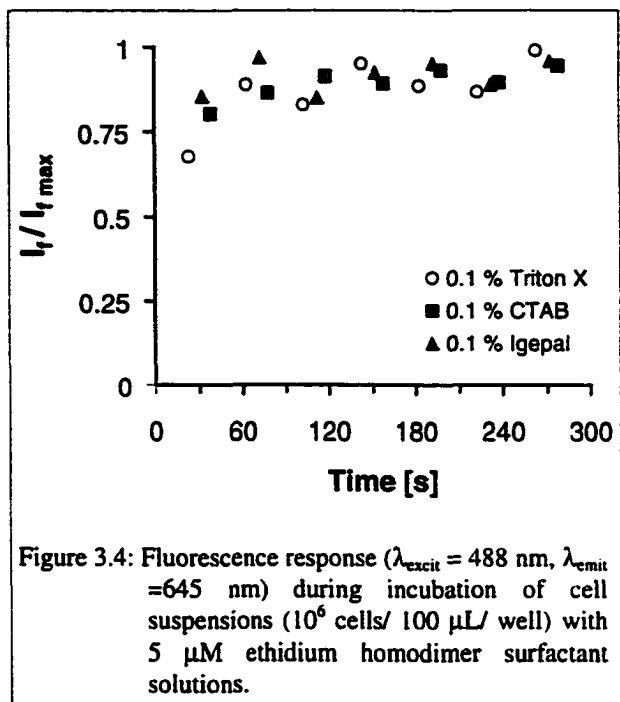
3.4.1 Optimization of The Intra Cellular β -Gal Assay of HL-60 Cells

3.4.1.1 Lysis and β -Gal Extraction

Nonionic detergents, such as Triton[®]X-100 [3],[10] and Nonidet P40 [31], as well as ionic detergents, such as sodium deoxycholate [32], taurodeoxycholate [33] and cetyltrimethylammonium bromide [32], CTAB, were reportedly used to extract β -Galactosidase out of mammalian cells. We examined the use of Triton[®]X-100 and Igepal CA-630, which is chemically indistinguishable from Nonidet P 40, as well as CTAB and a reporter lysis buffer, contained in a commercially available β -Galactosidase enzyme assay system [34], for extraction of β -Gal from HL-60 cells. Figure 3.3 shows the fluorescence response ($\lambda_{\text{excit}} = 488 \text{ nm}$, $\lambda_{\text{emit}} = 530 \text{ nm}$) after incubation of HL-60 cell suspensions (10^6 HL-60 cells/ 100 μL / well) with 200 μM FDG in various surfactant solutions for 10 minutes. As reported previously [35], HL-60 cells exhibit β -Gal activity. It can be seen that the reporter lysis buffer was unsuitable for determination of β -Gal activity in this microtitre plate format. The fluorescence signals generated by the other surfactant solutions were similar at 530 nm, as were the 200 μM FDG blank solutions. The fluorescence signals generated by the other surfactant solutions were similar at 530 nm, as were the 200 μM FDG blank solutions.



The average rate of cell lysis was first measured by performing a well-plate-based cytotoxicity assay of cell suspensions. Figure 3.4 depicts the fluorescence response ($\lambda_{\text{excit}} = 488 \text{ nm}$, $\lambda_{\text{emit}} = 645 \text{ nm}$) during incubation of cell suspensions ($10^6 \text{ cells}/100 \mu\text{L}/\text{well}$) with $5 \mu\text{M}$ ethidium homodimer surfactant solutions. The generated fluorescence response is indicative of the extent of surfactant induced cell membrane damage, since ethidium homodimer exhibits a 40-fold enhancement in fluorescence upon binding to intracellular nucleic acids. The



lysis of HL-60 cells upon addition of a Triton[®]X-100 solution ($C_{\text{Triton}^{\text{®}}\text{X-100, final}} = 0.05\% \text{ Triton}^{\text{®}}\text{X-100}$) was further monitored microscopically. The fluorescence signals show a plateau at incubation times of ≈ 60 seconds after incubation with 0.1% CTAB, Igepal CA-630 and Triton[®]X-100 solutions. The shortest exposure to surfactant we could measure was about 30 s, at which point Triton[®]X-100 solutions had reached about 70-75% of the final value, while the other two surfactants were about 75-85% of the maximum. The lysis of HL-60 cells upon mixture on-chip to give a 0.05% Triton[®]X-100 solution ($C_{\text{Triton}^{\text{®}}\text{X-100, final}} = 0.05\% \text{ Triton}^{\text{®}}\text{X-100}$) was further monitored microscopically. The minimum time to lyse a single HL-60 cell was approximately 30 s. In contrast, a similar on-chip experiment with 0.5% SDS showed less than two seconds were required for lysis, however SDS denatured the enzyme. Based on these results we selected Triton[®]X-100 as lysing agent for subsequent on-chip assays.

The fluorescence response after incubation of 1 million viable cells in $200 \mu\text{M}$ FDG solutions of varying Triton[®]X-100 concentrations is depicted in Figure 3.3 B. It has been reported that increasing concentrations of Triton[®]X-100 increase the protein recovery from a cell lysate [36]. We evaluated the extraction and enzyme assay performance as a function of time (10-60 min.) for hypotonic lysis with pure water and 0.05-4% Triton[®]X-100 in a microtiter plate format. Solutions of 0.05-0.5% Triton[®]X-100 (44.2 to $265.2 \times \text{CMC}$ [37]) showed optimum β -Gal activity, while higher Triton[®]X-100 concentrations resulted in decreased fluorescence responses. For the 0.05 % Triton[®]X-100 lytic solution, the slope and the regression coefficient, R, were

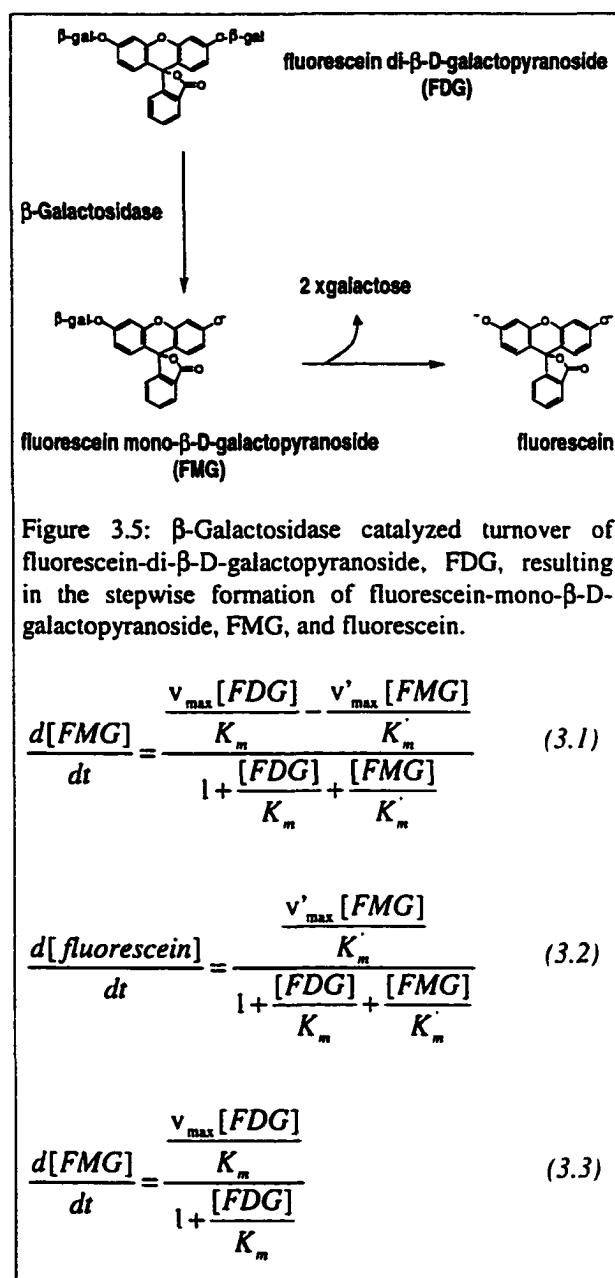
234.9 arbitrary fluorescence units (AFU)/min and 0.998, respectively. Hypotonic lysis with pure deionized water resulted in 20 % higher recovery of enzyme activity than lysis with 1 % Triton[®]X-100 solutions (147.7 AFU/min and R=0.995). This effect, which contrasts with reports of increasing recovery with increasing concentration, may be due to partial denaturation of β -Gal at higher surfactant concentration.

The epifluorescence detection setup, employed in this study for on-channel detection, was utilized previously to detect injection plugs of a few zeptomoles of fluorescein [26]. The average fluorescence response per lysed cell per minute reaction time in 0.05% Triton[®]X-100 was equivalent to the fluorescence response generated by 22 attomoles of FMG or 3 attomoles of fluorescein. Correlation of fluorescence to moles of fluorescent species was done using a calibration curve on a microtiter plate reader ($\Phi_{FMG} = 0.13 \times \Phi_{fluorescein}$ in 0.05 % Triton X, PBS/2.5% FCS solutions). We concluded that the fluorescent reaction product generated after incubation of one HL-60 cell with 200 μ M FDG for one minute, would be readily measured with the epifluorescence detector.

3.4.1.2 Reaction Rate and Reaction Products

β -Galactosidase converts the fluorogenic substrate fluorescein-di- β -galactopyrano-side, FDG, to fluorescein mono- β -D-galactoside, FMG, which is then hydrolyzed to fluorescein. The rates of formation of FMG and fluorescein can be described by eq 3.1 and 3.2 [38], where v_{max} and K_{max} are the maximum turnover rate and the Michaelis-Menten constant for the FDG hydrolysis, and v'_{max} and K'_m for the FMG hydrolysis. The different quantum efficiencies, Φ , of FMG and fluorescein ($\Phi_{FMG} = 0.13 \times \Phi_{fluorescein}$ in 0.05 % Triton X, PBS/2.5% FCS solutions, as measured on a microtiter plate fluorescence reader) necessitate the separation of these two products for quantitation of β Gal activities. The occurrence of the second hydrolysis step within a given incubation time is, however, dependent on the concentrations of FDG and FMG, v'_{max} which is dependent on enzyme concentration, K_{m_2} and K'_m . At β -Gal concentrations of <1 nM and FDG concentrations of 200 μ M (20 mM tricine buffer, pH =8), it was shown that only FMG was formed after incubation for 60 minutes [27]. This was attributed to 1., a high K'_{m_2} , 2., low enzyme concentration resulting in small v'_{max} and 3., a large excess of FDG with respect to FMG formed [27], [39]. Under the conditions employed Eq. 3.1 could be simplified to Eq. 3.3.

In order to determine the necessity of a separation step in a chip-based β -Gal assay of single HL-60 cells we incubated a Triton[®]X-100 cell extract of 50 million HL-60 cells with 200 μ M FDG for 110 min. Figure 3.6 depicts the electropherogram obtained after electrokinetic injection of the incubated mixture into a fetal calf serum coated capillary. One peak, eluting at 8.0 min, was obtained upon application of -600 V/cm across the capillary. The peak was identified with FMG by subsequent injections of FMG ($t_{\text{migration}} = 8$ min.) and fluorescein ($t_{\text{migration}} > 12$ min.) solutions. The migration time for fluorescein was variable from run to run, apparently due to $\mu_{\text{ep}} = \mu_{\text{EOF}}$, so that small changes in coating conditions caused larger changes in migration time. No fluorescein peak was detected after injection of incubated cell lysates. Hence, we concluded that no electrophoretic separation step is required after incubation of the lysate of one single HL-60 cell at incubation times < 110 minutes under the conditions employed.



β -Gal adsorbs to the walls of glass channels [25] and fused silica capillaries [27], resulting in memory effects in consecutive measurements. In order to assess the β -Gal carry over in FCS coated capillaries, we performed CE-based assays of *E-coli* β -Gal, with several subsequent injections of the substrate, FDG alone. Hydrodynamic injections of 1 nM β -Gal (20 mM tricine buffer, pH 8; $t_{\text{inj}} = 30$ s; $V_{\text{inj}} = 12.7$ kV; injected volume = 26 nL) and 400 μ M FDG (20 mM tricine buffer pH 8; injected volume = 26 nL), followed by application of -420 V/cm after 5 minutes incubation time resulted in a fluorescence peak of 44.0 mVmin peak area. Subsequent

injection, incubation and separation of a blank (buffer and 400 μM FDG) under identical conditions resulted in a peak area of 1.2 mV-min. This corresponds to 2.7 % carryover and can be compared to the 10-20% carryover observed when using bare glass channels [25]

3.4.1.3 Substrate Concentration

Detected β -Gal activities increase with increasing FDG concentrations until the enzyme is saturated with substrate. However, no improvement in the limit of detection of β -Gal was found at FDG concentrations $> K_m$ [27]. This effect is attributable to the presence of a FMG impurity in the substrate, formed by non specific hydrolysis, which leads to a background fluorescence, proportional to the substrate concentration. The results in Figure 3.7 are in good qualitative agreement with this observation. The background fluorescence resulting from nonspecific hydrolysis of FDG of increasing concentrations and the corresponding background corrected fluorescence signals after incubation of a 0.1 % Triton[®]X-100 lysate of one million HL-60 cells for five minutes are shown. Incubation with FDG concentrations above 300 μM (0.1 % Triton[®]X-100; $t_{inc}= 5$ min) clearly resulted in a decrease of background corrected fluorescence response. Consequently we used FDG concentrations < 300 μM FDG in all further on-chip β -Gal assays.

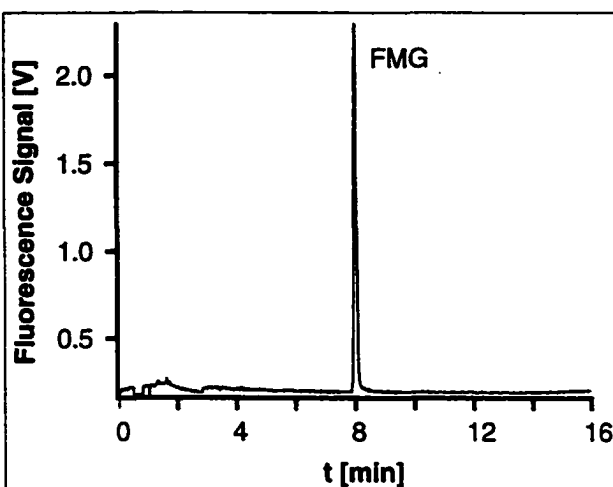


Figure 3.6: Capillary electrophoresis of a reaction mixture of a HL-60 cell suspension (50×10^7 cells / mL) with a 200 μM FDG 0.1 % Triton X-100 solution after incubation for 110 min. Running buffer: 20 mM tricine, pH 8; capillary I.D.: 50 μm , preconditioned with the running buffer containing 1 % FCS; injection: 600 V/cm, 30s; separation: 600 V/cm;

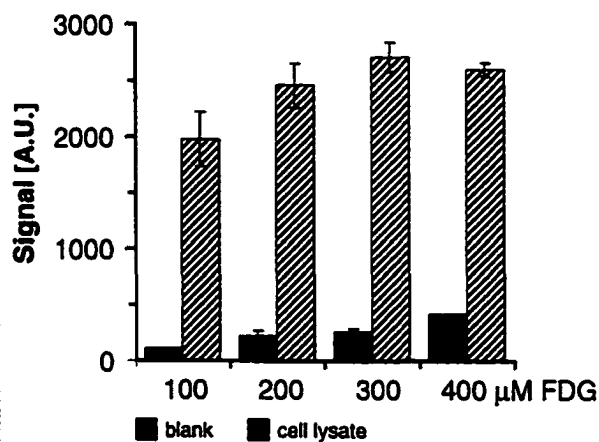
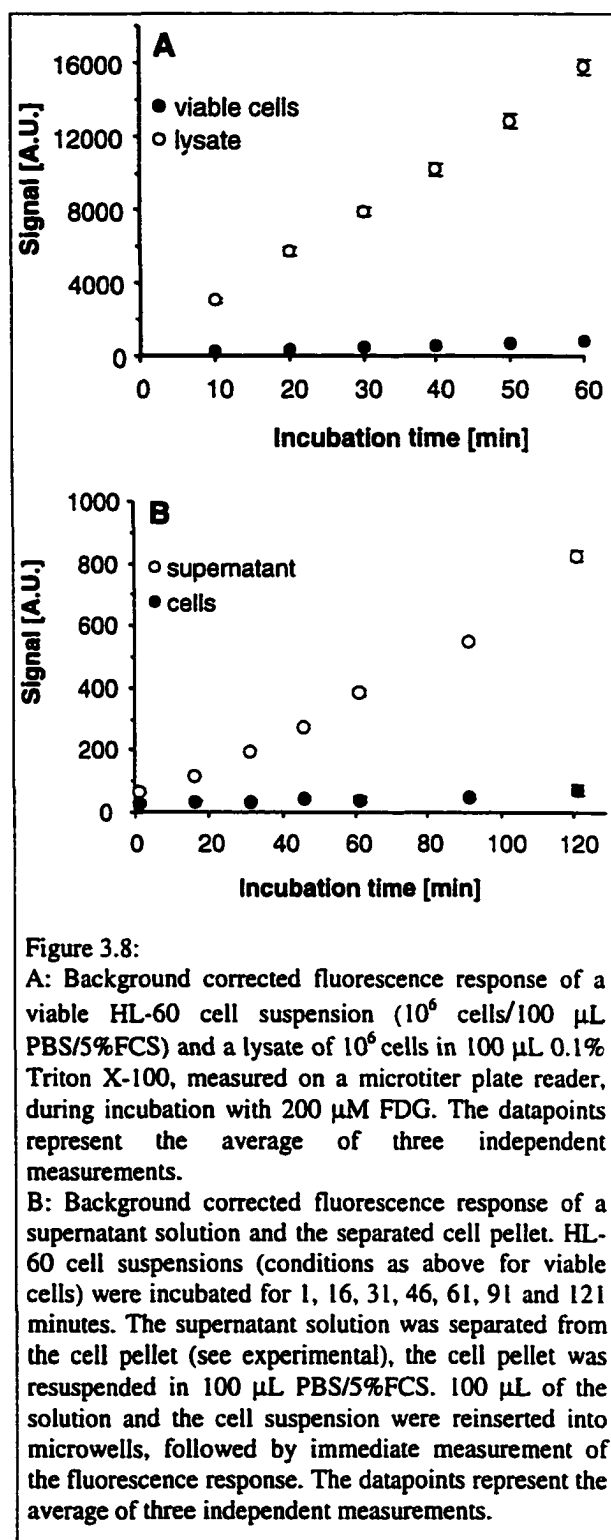


Figure 3.7: Fluorescence response dependence on FDG concentration. Incubation of a blank (PBS-5%FCS) and an HL-60 cell lysate (10^6 cells/ 100 μL 0.05% Triton[®]X-100) with FDG of varying concentration for 5 minutes at 25°C. Depicted values are averages of three independent measurements; error bars represent the standard deviation.

Incubation of viable cells with isotonic FDG solutions results in limited uptake of FDG across the cell and organelle membranes [40], so that the FDG concentration in the cytoplasm and the lysosomes is lower than the solution concentration. This effect is partly responsible for the low sensitivity of the β -Gal assay in viable cells. Figure 3.8A contrasts the background corrected fluorescence signal obtained during incubation of 1 million viable cells with the response from a Triton[®]X-100 lysate of the same number of cells. The cell lysate generated a 19 times higher background corrected fluorescence signal than the viable cell suspension when incubated with 200 μ M FDG for 60 minutes. The low sensitivity of the β -Gal assay of viable HL-60 cells results in the need for long incubation times. A cell suspension (10^7 cells / mL PBS / 5% FCS) had to be incubated for 60 minutes with 200 μ M FDG (37°C) before a significant fluorescence signal could be detected by flow cytometry, as shown in figure 3.9. An increase of the incubation time to 120 minutes led to a further increase in fluorescence signal. The low sensitivity of the β -Gal assay of viable HL-60 cells may also be attributed to the reduced FMG quantum efficiency in the acidic lysosomes, as well as product leakage out of the cell, as described previously [40],[41].



In order to examine product leakage we measured the fluorescence response of cell pellets and supernatant solutions separately after incubation of a cell suspension with FDG containing PBS solutions for 1, 16, 31, 46, 61, 91 and 121 minutes, as depicted in figure 3.8B. Supernatant solutions were separated from the cell pellet by centrifugation, and the cell pellet was resuspended in 100 μ L of a PBS/5% FCS solution. As evident from figure 3.8B, supernatant solutions exhibited 9.6 ± 1.1 and 11.7 ± 3.8 higher signals than the cell pellet after incubation with 200 μ M FDG for 61 and 121 minutes, respectively. The data trace shown for viable cells (Figure 3.8A) is therefore a cumulative signal of product in the supernatant and in the cell. Additionally, storage of the withdrawn supernatant in the microwell after removal of the cell pellet resulted in an increase of fluorescence signal over time (data not shown), pointing to remaining enzymatic activity in the supernatant. This effect is attributable to a decrease in cell viability after incubation; as measured by a hemacytometer, only 83.6% and 73.7 % of the cell population were found to be viable immediately and 60 minutes after incubation, respectively. The rates of FMG formation in the supernatant solutions were found to be two orders of magnitude lower than in the cell lysates. It is likely that product leakage [14],[40]-[42] and enzyme release from damaged cells contribute to the overall signal in the supernatant. The cell pellet signal trace was found to increase over the incubation time studied, indicating that not all of the signal increase in Figure 3.8A can be attributed to leakage from non-viable cells. This observation is in agreement with the findings from the flow cytometric analysis (vide supra), in which the supernatant is clearly removed.

The presented results clearly illustrate possible error sources, when intracellular enzymatic activity is measured in viable cells. In addition, we have also demonstrated that enzymatic assays of cell lysates can circumvent the illustrated drawbacks of *in-cella* analyses.

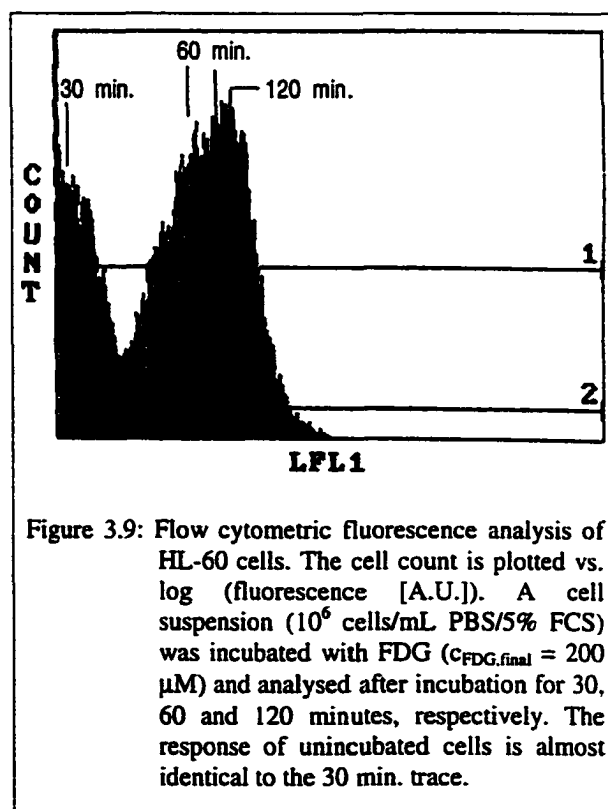


Figure 3.9: Flow cytometric fluorescence analysis of HL-60 cells. The cell count is plotted vs. log (fluorescence [A.U.]). A cell suspension (10^6 cells/mL PBS/5% FCS) was incubated with FDG ($C_{\text{FDG,final}} = 200 \mu\text{M}$) and analysed after incubation for 30, 60 and 120 minutes, respectively. The response of unincubated cells is almost identical to the 30 min. trace.

3.4.2 Cell Manipulation On-Chip

Figure 3.1 shows the schematic layout of a post-column reaction device, PCRD 2, utilized previously by Fluri et al. [29] for chemical reactions and separations. Reagents and cell suspensions were introduced into reservoirs A-C and D, respectively. For our present work with HL-60 cells, solvent flow was driven by suction applied to reservoir E, drawing solution from all four inlet reservoirs. A microscope positioned over the channel intersection allowed observation of transport and lysis of single cells, respectively. The difference in refractive indices of the PBS/5%FCS and the Triton[®]X-100 solutions allowed for visual observation of fluidic paths at the junction at high flow velocities. The pressure heads at reservoirs A-D were adjusted in such a way as to achieve a 1:1 mixing ratio. Figure 3.10 shows the sequence of transport and lysis of one single HL-60 cell. A suspension of HL-60 cells (10^6 cells / mL PBS-5% FCS), loaded into reservoir D, and a 35 mM SDS lysing solution, inserted into reservoirs A-C, were pumped towards the channel intersection. The transport of one single cell towards the junction, followed by lysis at the channel junction, is depicted in Figure 3.10. The tapering of the cell introduction channel from 84 μ m to 54 μ m at the lysing junction was found to aid in the delivery of single cells to the junction. The lysate was then transported towards the detector, 0.56 mm removed from the junction. Microscope observation showed complete lysis with SDS within 2 s.

Devices with 20 μ m deep channels were found to be optimal for reproducible lysis of single HL-60 cells (average cell diameter \sim 10 μ m). Frequent plugging of the cell introduction and waste channels occurred when shallower channels were used. Channel depths $>$ 20 μ m made it difficult to prevent simultaneous lysis of more than one cell at the liquid junction. Cell counts of 1 million HL-60 cells / mL were found to provide acceptable cell throughputs ($u = 40 - 200$ μ m/s) while preventing multiple cell transits through the waste channel. Preconditioning of the cell introduction channel with fetal calf

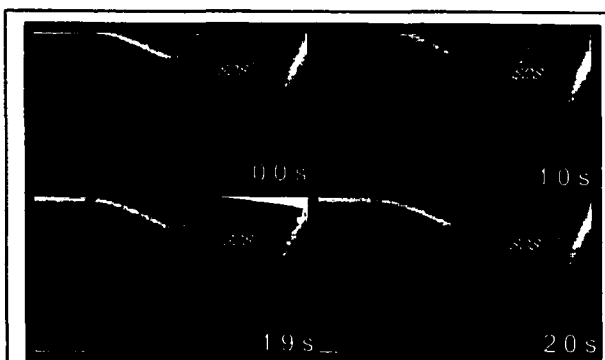
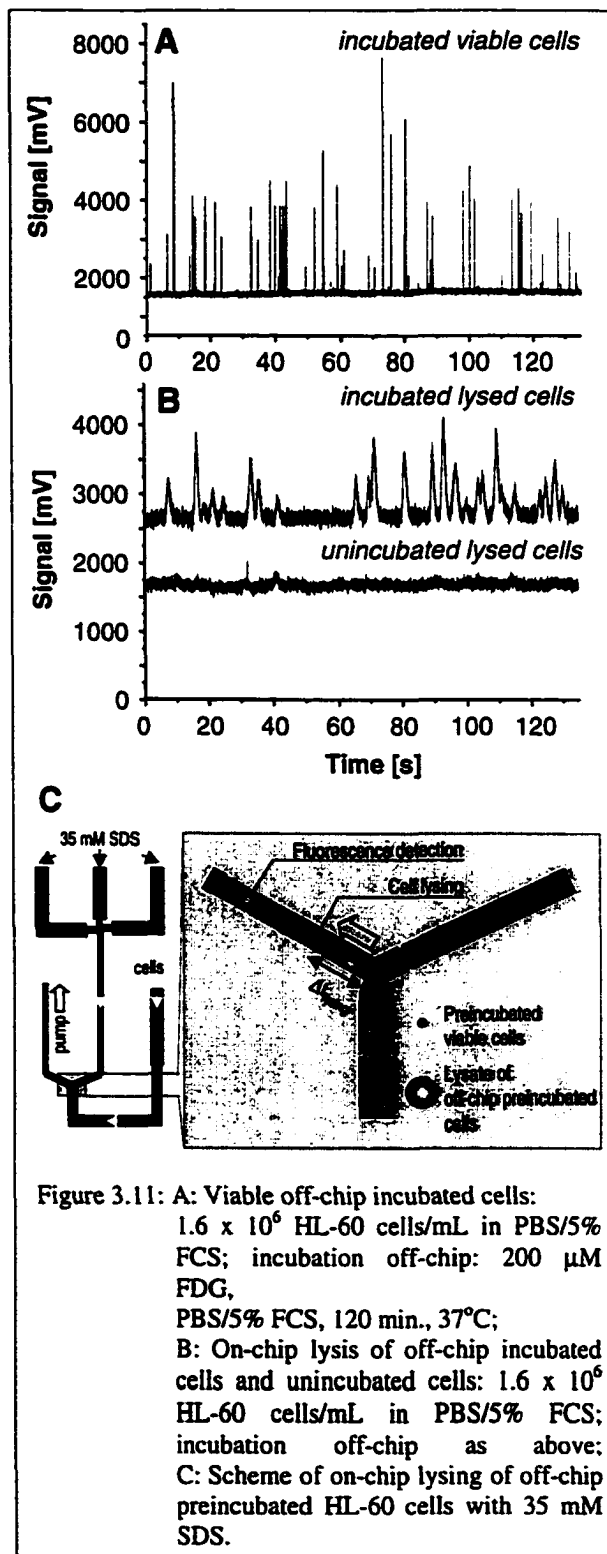


Figure 3.10: Sequence of transport and lysis of one single HL-60 cell. A suspension of HL-60 cells (10^6 cells / mL PBS-5% FCS), inserted into reservoir D, and a 35 mM SDS lysing solution, inserted into reservoirs A-C, were pumped towards the channel intersection. 0-1.0 s: transport; 1.9 s: lysis at the junction, 2.0 s: transport of lysate towards E.

serum containing PBS solutions was found to be essential in order to avoid cell adhesion to the glass walls and hence channel plugging (see experimental).

3.4.3 Lysing and Detection of β -Gal Activity of Preincubated Cells On-Chip

Figure 3.11 shows the detection of viable and lysed preincubated HL-60 cells on-chip, following an initial pre-incubation with 200 μ M FDG for 120 minutes at 37°C off-chip. These studies were performed to provide a control for later on-chip incubation experiments. First, we introduced viable unincubated cells into port D and a PBS / 5% FCS solution into ports A,B and C (see Figure 3.1). The suspension was pumped towards the epifluorescence detector. Figure 3.11A shows the light scattering peaks obtained in the absence of lysing agent. The peaks are 60 ± 10 ms wide at full width half maximum, FWHM, on average. A wide distribution of peak heights is observed due to the distribution in cell size, fluorescence intensity and the multitude of cell trajectories through the detection spot (spot size = 12 μ m, channel width = 54 μ m). Unincubated cells showed very similar traces, indicating the signal is primarily due to light scattering. Figure 3.11B illustrates the on-chip lysis of 25



cells with a 35 mM SDS solution, loaded into ports A,B and C. The single preincubated cells were lysed sequentially at the mixing point, as depicted in Figure 3.11C. The single cell lysates produced were transported to the detector, 560 μm from the junction, at a flow velocity of approximately 100 $\mu\text{m}/\text{s}$, as determined by video observation of 20 cells over a distance of 80 μm . The peaks in Figure 3.11B are attributable to fluorescence signals due to enzymatic activity of individual cells with FDG, since a negative control of unincubated cells showed no signal over background, as illustrated in Figure 3.11B. The average peak width is 1.1 ± 0.2 s (FWHM, $n=19$), resulting from a convolution of the original lysate plug length, longitudinal dispersion and the parabolic plug profile in the channel. Clearly, viable and lysed cells could be discriminated by peak width and the lysing in the presence of SDS was complete. Differences in background signals in Figure 3.11B were attributable to FMG leakage out of these preincubated cells.

Sedimentation of cells in reservoir D resulted in increasing resistances to flow of the cell introduction channel over time. Therefore it was found to be difficult to maintain constant flow velocities over a period of 15 minutes or longer. However, within the time span of one experiment, i.e. up to 5 minutes, no fluctuations in linear flow velocity and thus no background fluctuations were observed. These results demonstrate the ability to deliver cells and various reagents at well defined locations, with good spatial control of the points of lysis and detection of enzymatic activity after incubation off-chip. They also demonstrate our ability to distinguish between intact and lysed cells.

3.4.4 On-Chip Lysing, On-Chip Incubation and Detection of β -Gal Activity

On-chip incubation of single cell lysates was performed by introduction of a lytic solution of 400 μM FDG in 0.1% Triton[®]X-100 into ports A-C. A mixing ratio of 1:1 was obtained at the channel junction (see figure 3.1 or figure 3.12A) by loading different solution and suspension volumes into ports A-C and D, respectively. The difference in refractive indices of the PBS/5%FCS and the Triton[®]X-100 solutions allowed for visual observation of fluidic paths at the junction at high flow velocities. The pressure heads at reservoirs A-D were adjusted in such a way as to achieve a 1:1 mixing ratio. The lytic solution was hereby determined to occupy half of the cross sectional area of the detection channel while applying vacuum at port E. The final FDG concentration after on-chip mixing was therefore approximated to be ~ 200 μM . The linear flow velocity was set to ≈ 40 $\mu\text{m}/\text{s}$ in order to allow for sufficient lysing and incubation time during transport to the detector. The point of lysis was approximated to be 1.2-2.4 mm from the junction for a lysing time of 30-60 s (see Figure 3.12A) and a flow velocity of 40 $\mu\text{m}/\text{s}$. Hence the incubation time

after lysis, i.e. the transit time from the point of lysis to the detector (distance junction-detector = 5.5 mm), can be approximated as 80 –110 seconds. Figure 3.12B shows peaks above background for 6 single on-chip incubated cell lysates. A negative control was performed by introducing 0.1% Triton[®]X-100 into the side channel without FDG, thus lysing the cells (Figure 3.12B) with no substrate available. Clearly the observed peaks can be assigned to enzymatic turnover of FDG by β -Galactosidase contained in single cell lysates, since no signal over background was obtained for unincubated cells. In both cases, the absence of scattering peaks indicates complete cell lysis occurred. In addition, the constancy of flow during the measurement time is evident from the constant background signal (see Figure 3.12B), originating from the fairly high, flow dependent background fluorescence of the Triton[®]X-100 solution. For a sphere, which is homogeneously filled with FMG, the width of the FMG zone after lysing and incubation can be calculated from eq. 3.4,

$$x = d + \sqrt{2D_m t + \frac{abFL^2}{24D_m t}} \quad (3.4)$$

where d is the average diameter of the cell [cm], D_m is the diffusion coefficient [cm²/s], t the incubation time [s], i.e. the period from lysis to detection and L the distance between the point of lysis and detection [cm]. The geometric factor F can be calculated from the ratio b/a as described previously [43], where a and b are the half widths and depths of a rectangular channel [cm],

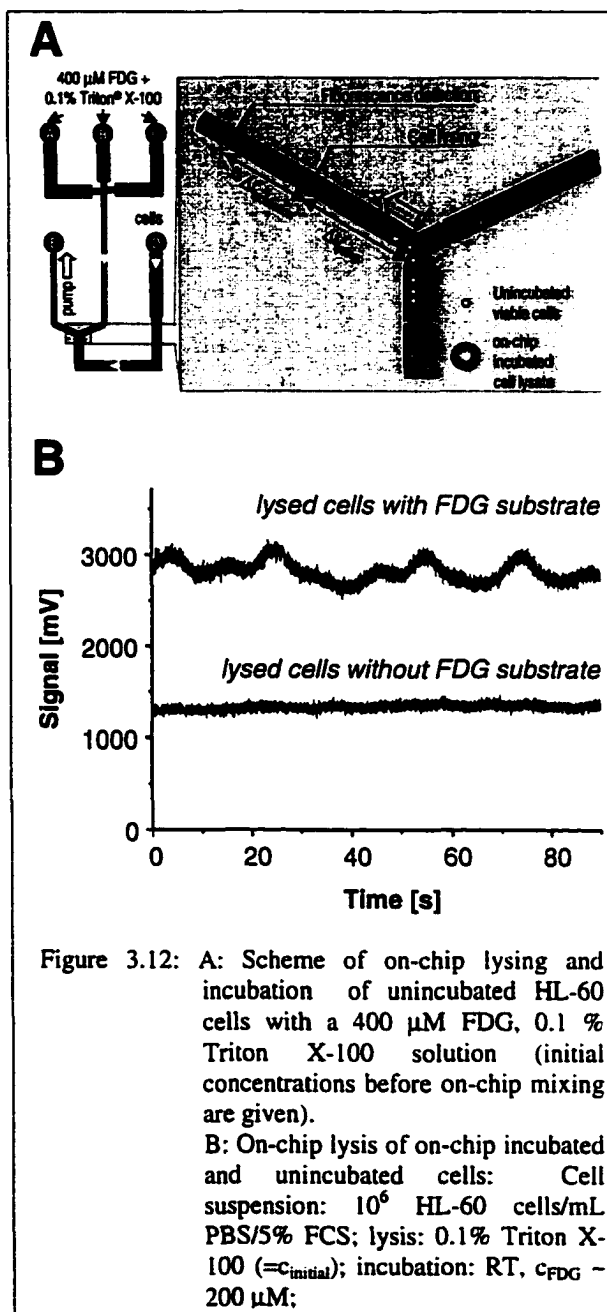


Figure 3.12: A: Scheme of on-chip lysing and incubation of unincubated HL-60 cells with a 400 μ M FDG, 0.1 % Triton X-100 solution (initial concentrations before on-chip mixing are given). B: On-chip lysis of on-chip incubated and unincubated cells: Cell suspension: 10^6 HL-60 cells/mL PBS/5% FCS; lysis: 0.1% Triton X-100 ($=c_{\text{initial}}$); incubation: RT, $c_{\text{FDG}} = 200 \mu$ M;

respectively. We used a cell diameter of 10 μm , the diffusion coefficient of fluorescein ($D_{\text{fluorescein}} = 3.3 \times 10^{-6} \text{ cm}^2/\text{s}$ [44]) for FMG, an incubation time of 80 – 110 s and a channel width of 54 μm and depth of 20 μm to estimate the zone width of 240 - 280 μm . For a linear flow velocity of 40 $\mu\text{m}/\text{s}$, a FMG plug width, w ($w = 2\sigma$), of approximately 6-7 s is obtained. This estimate seems to correlate well with the observations in Figure 3.12.

The final concentration of Triton[®] X-100 and FDG at the point of detection can be estimated by using simple diffusion equations, as described previously [45]. We assume diffusion coefficients of $3.3 \times 10^{-6} \text{ cm}^2/\text{s}$ and $5.4 \times 10^{-7} \text{ cm}^2/\text{s}$ for a small molecule, FDG, and Triton[®] X-100 [46] ($C_{\text{Triton}^{\circledR}\text{X-100}} > \text{critical micelle concentration}_{\text{Triton}^{\circledR}\text{X-100}}$, CMC), respectively. The FDG containing Triton X-100 solution is assumed to occupy half the channel width at the mixing junction. Given a 20 μm deep and 54 μm wide waste channel, we calculate the time needed to reach 98 % of the final concentration after mixing, $t(98)$, where $c_{\text{final}} = 0.5 \times c_{\text{initial}}$, of 4 and 23 s for FDG and Triton X-100, respectively. Hence there are no FDG and Triton[®] X-100 concentration gradients across the cell lysate at the point of detection.

Increase of the flow velocity or reduction of the distance from detector to junction resulted in incomplete lysis, illustrated by light scattering peaks on top of fluorescence peaks, presumably due to scattering from cell debris. Since this would lead to possible underestimation of enzymatic activity due to enzyme adsorption on or in the debris [47], complete lysis is desirable. The maximum distance from the junction to the detector is however limited by the enzymatic activity per cell, due to longitudinal dispersion after lysis. The LOD is hence determined by nonspecific hydrolysis of FDG and the background fluorescence of the lysing buffer.

The on-chip lysis and incubation of single cell lysates clearly does not result in base line resolved fluorescence peaks at the current stage, as evident from Figure 3.12. In order to alleviate the quantitation of peak area, a cell suspension of slightly decreased concentration could be employed for better separation of lysate plugs. In order to determine the β -Gal activity per single cell, the contamination of FDG with FMG, generated by nonspecific hydrolysis after purification, would have to be determined. In addition, a constant cell flow velocity would have to be established over a total analysis time of one hour and more to screen a sufficiently large cell population. The current incubation time of 80-110 s/HL-60 cell at 25°C is 33-45 times shorter than the minimum incubation time required for a flow cytometric β -Gal assay of single viable cells at 37°C (see Figure 3.9). Importantly, the analysis of single cell lysates circumvents the limitations of analysis of viable cells. Distorted measurements of intracellular enzymatic activities, due to FDG uptake variation from cell to cell, product leakage [47] and product uptake

by surrounding cells [14], may be avoided when analysing single cell lysates. Studies of inhibitor induced modulation of intracellular enzyme activity in single cells should further be facilitated by circumventing the need for inhibitor uptake into viable cells. This approach further allows for facile optimization of the pH and the ionic strength of the substrate containing lysing buffer in order to obtain maximum enzyme activity and product quantum efficiency.

The use of microfluidic devices opens up the possibility of reproducible manipulation of single non-adherent cells with moderate to high throughput. Single cells can be allowed to react with a variety of reagents at defined locations, followed by monitoring of the reaction product. The demonstrated detection of β -Gal activity in lysates of single non-adherent cells within 80 – 110 s incubation / cell illustrates the high sensitivity of this chip based approach. Modifications in the cell delivery system should allow for quantitation of intracellular enzymatic activities of large cell populations within the time frame of conventional flow cytometric assays. Consequently, we believe the presented approach is complementary to the established and highly useful flow cytometric analysis of viable cells.

3.5 Acknowledgements

I am indebted to Per Andersson and Edgar Arriaga for initiating and stimulating the discussion about chip-based β -Gal single cell assays. Without them this chapter would not have been written. I thank Edgar for teaching me how to use a single capillary electrophoresis instrument with postcolumn LIF detection, developed by Norman Dovichi and his group. This study would not have been attempted without the “ β -Gal assay expertise”, which has been made available to me by “Dovichi’s group”. The extensive CE expertise, obtainable from Edgar and acquired for years by “Dovichi’s group”, was most helpful to establish the feasibility of this chip-based assay on-chip, as evident from Figure 3.6. I am obliged to Richard Smith for giving me access to facilities at the Alberta Research Council, ARC and for useful discussions. Thanks a lot to Rod Szarka (ARC) for cell culturing instructions and for the participation in and help with most microtiterplate-based fluorescence assays (Rod participated in acquiring the data, depicted in Figures 3.3 and 3.8). Thanks a lot to Nandy Wang (ARC) for performing all flow cytometric experiments (see Figure 3.9). I am, as usual, very grateful to my friend Hossein Salimi Moosavi, who acted as trouble shooter in all aspects of this project. His experience in handling of cells in microchannels was crucial for the success of this study. I am grateful to Dave Bundle and Joana Sadowska, for giving me access to the tissue culture room and ergo their trust in the cleanliness of my experimental procedures. My great friend Nora Chan was most helpful in all questions of cell culturing, ordering of reagents, experimental questions et altera. I am grateful to Monica Palcic

for answering all my questions related to enzymology. Thanks to Thompson Tang, my good old amigo, for all the discussions. I am very grateful to Roman Lipiecki at the Machine Shop for helping me in the design and for the machining of the inverted epifluorescence microscope. We further thank the Alberta Microelectronic Center for device fabrication.

3.6 References

- 1 Brante, G. *Scand. J. Clin. Invest.* 1952, 4, 43
- 2 Wallenfels, K., Weil, R. In: *The Enzymes*, 3rd ed.; Boyer, P. D. Ed.; Academic Press: New York, London 1972, Vol. 7, pp. 617-663
- 3 Fricker, H., O'Brien, J. S., Vassella, F., Gugler, E., Muehlethaler, J. P., Spycher, M., Wiesmann, U. N., Herschkowitz, N. *J. Neurol.* 1976, 213, 273-4 Mutoh, T., Kiuchi, K., Sobue, I., Naoi, M. *Clin. Chim. Acta* 1984, 40, 223-230
- 5 Hultberg, B., Oeckermann, P. A., Dahlqvist, A. *J. Clin. Invest.* 1970, 49, 216-224
- 6 van der Horst, G. T. J., Kleijer, W. J., Hoogeveen, A. T., Huijmans, J. G. M., Blom, W., van Diggelen, O. P. *Am. J. Med. Genet.* 1983, 16, 261-275 7 Takiyama, N., Itoh, K., Shimmoto, M., Nishimoto, J., Inui, K., Sakuraba, H., Suzuki, Y. *Brain Dev.* 1997, 19, 126-130
- 8 Beutler, E., Kuhl, W., Matusomoto, M., Pangalis, G. *J. Exp. Med.* 1976, 143, 975-980
- 9 Shah, S.N., Johnson, R.C., Minn, K., Schoenfeld, F. *Mol. Chem. Neuropat.* 1995, 24, 43-52
- 10 Tanaka, T., Kobayashi, M., Saito, O., Kamada, N., Kuramoto, A., Tomofusa, U. *Clin. Chim. Acta* 1981, 117, 121-131
- 11 Beckwith, J.R. In: *Escherichia coli and Salmonella typhimurium: cellular and molecular biology*, Neidhart, F.C., Ingraham, J. L., Low, K. B., Magasanik, B., Schaechter, M., Umberger, H. E. Eds.; American Society for Microbiology, Washington, D.C., Vol.2, pp. 1344-1452
- 12 Rietra, P. J. G. M., van den Bergh, F. A. J. T. M., Tager, J.M. In: *Enzyme Therapy in Lysosomal Storage Diseases*; Tager, J. M., Hooghwinkel, G. J. M., Daems, W. Th., Eds.; *Proceedings for the Workshop on Cell Biological and Enzymological Aspects of the Therapy of Lysosomal Storage Diseases*, North-Holland Publishing Company, Leiden, The Netherlands, 1974, pp. 53-79
- 13 Rotman, B. *Biochemistry* 1961, 47, 1981-
- 14 Nolan, G. P., Fiering, S., Nicolas, J. F., Herzenberg, L. A. *Proc. Nat. Acad. Sci. USA* 1988, 85, 2602-2607
- 15 Krämer, R. In: *Advances in Biochemical Engineering Biotechnology*, Scheper, T. Ed.; Springer: Berlin 1996; Vol .54, pp. 31-74 ,
- 16 Cheng, J., Sheldon, E. L., Wu, L., Uribe, A., Gerrue, L. O., Carrino, J., Heller, M. J., O'Connell, J. P. *Nature Biotech.* 1998, 16, 541-546

- 17 Fuhr, G., Shirly, G. In: *Microsystem Technology in Chemistry and Life Sciences*; Manz, A., Becker, H.; Eds.; Springer, Berlin 1997, pp. 83-116
- 18 Kricka, L. J., Faro, I., Heyner, S., Garside, W. T., Fitzpatrick, G., McKinnon, G., Ho, J., Wilding, P. *J. Pharm. Biomed. Anal.* 1997, 5, 1443-1447
- 19 Li, P. C. H., Harrison, D. J. *Anal. Chem.* 1997, 69, 1564-1568
- 20 Andersson, P. E., Li, P. C. H., Smith, R., Szarka, R. J., Harrison, D. J. In: *Proceedings of the 9th International Conference on Solid-State Sensors and Actuators: Transducers '97*; IEEE Electron Dev. Soc., Chicago, 1997, Vol. 2, pp. 1311-1314
- 21 Altendorf, E., Iverson, E., Schutte, D., Weigl, B., Osborn, T.D., Sabeti, R., Yager, P. *SPIE Proceedings*, 1996, 2678, 267
- 22 Altendorf, E., Zebert, D., Holl, M., Yager, P. In: *Proceedings of the 9th International Conference on Solid-State Sensors and Actuators: Transducers '97*; IEEE Electron Dev. Soc., Chicago, 1997, Vol. 1, pp. 531-534
- 23 Altendorf, E., Zebert, D., Holl, M., Vannelli, A., Wu, C. Schulte, T. in: *Proc. μ -TAS Workshop '98*. Harrison, D. J., van den Berg, A., (Eds); *Kluwer Academic Publishers, Dordrecht 1998*, pp. 73-76
- 24 Salimi-Moosavi, H., Szarka, R., Andersson, P., Smith, R., Harrison, D. J. In: *Proceedings of the μ -TAS Workshop '98*, Harrison, D. J., van den Berg, A., Eds; *Kluwer Academic Publishers, Dordrecht 1998*, pp.69-72
- 25 Hadd, A. G., Raymond, D. E., Halliwell, J. W., Jacobson, S. C., Ramsey, J. M. *Anal. Chem.* 1997, 69, 3407-3412
- 26 Ocvirk, G., Tang, T., Harrison, D. J. *Analyst*, 1998, 123, 1429-1434
- 27 Craig, D., Arriaga, E. A., Banks, P., Zhang, Y., Renborg, A., Palcic, M. M., Dovichi, N. J. *Anal. Biochem.* 1995, 226, 147-153
- 28 Chiem, N., Harrison, D. J. *Anal. Chem.* 1997, 69, 373-378
- 29 Fluri, K., Fitzpatrick, G., Chiem, N., Harrison, D. J. *Anal. Chem.* 1996, 68, 4285-4290
- 30 Arriaga, E.A., Zhang, Y., Dovichi, N.J. *Anal. Chim. Acta* 1995, 299, 319-326
- 31 Eustice, D. C., Feldman, P. A., Colberg-Poley, A. M., Buckery, R. M., Neubauer, R. H. *BioTechniques*. 1991, 11, 739-40, 742-743
- 32 Majumder, G. C., Turkington, R. W. *Biochemistry* 1974, 13, 2857-2864
- 33 Mutoh, T., Kiuchi, K., Sobue, I., Naoi, M., *Clin. Chim. Acta* 1984, 140, 223-230
- 34 Schenborn, E., Goiffon, V. *Promega Notes* 1993, 41, 11
- 35 Emiliani, C, Falzetti, F, Orlacchio, A, Stirling, J.L. *Biochem. J.* 1990, 272, 211-215
- 36 Collins, M. L. P., Salton, M. R. J. *Biochim. Biophys. Acta* 1979, 553, 40-53
- 37 Fletcher, S., Barnes, N. M., *Br. J. Pharmacol.* 1997, 122, 655-662
- 38 Fiedler, F., Hinz, H. *Eur. J. Biochem.* 1994, 222, 75-81
- 39 Nir, R., Yisraeli, Y., Lamed, R., Sahar, E. *Appl. Environ. Microbiol* 1990, 56, 3861-3866

- 40 Jongkind, J.F., Verkerk, A., Sernetz, M. *Cytometry* 1986, 7, 463-466
- 41 Aparicio, C.L., Strong, L. H., Yarmush, M. L., Berthiaume, F.
Biotechniques, 1997, 23, 1056-1060
- 42 Plovins, A., Alvarez, A. M., Ibanez, M., Molina, M., Nombela, C.
Appl. Environ Microbiol 1994, 60, 4638-4641
- 43 Shultz-Lockyear, L.L., Colyer, C.L., Fan, Z.H., Roy, K.L., Harrison, D.J.
Electrophoresis 1999, 20, 529-538
- 44 Liang, Z., Chiem, N., Ocvirk, G., Tang, T., Fluri, K., Harrison, D.J.
Anal. Chem. 1996, 68, 1040-1046
- 45 Chiem, N.H., Harrison, D.J. *Clin. Chem.* 1998, 44, 591-598
- 46 Streletzky, K., Phillies, G.D.J. *Langmuir* 1995, 11, 42-47
- 47 Feliu, J. X., Cubarsi, R., Villaverde, A. *Biotechnol. Bioeng.* 1998, 58, 536-540

Chapter 4: Electrokinetic Control of Fluid Flow in Native Poly(dimethylsiloxane) Capillary Electrophoresis Devices ^{♦+}

4.1 Abstract

Capillary zone electrophoresis (CZE) devices fabricated in poly(dimethylsiloxane) (PDMS) require continuous voltage control of all intersecting channels in the fluidic network, in order to avoid catastrophic leakage at the intersections. This contrasts with the behaviour of similar flow channel designs fabricated in glass substrates. When the injection plugs are shaped by voltage control and leakage from side channels is controlled by the application of pushback voltages during separation, fluorescein samples give 64200 theoretical plates (7000 V separation voltage, $E = 1340 \text{ V/cm}$). Native PDMS devices exhibit stable retention times ($\pm 8.6 \%$ RSD) over a period of 5 days when filled with water. Contact angles were unchanged ($\pm 1.9 \%$ RSD) over a period of 16 weeks of dry storage, in contrast to the known behaviour of plasma oxidized PDMS surfaces. Electroosmotic flow (EOF) was observed in the direction of the cathode for the buffer systems studied (phosphate pH 3-10.5), in the presence or absence of hydrophobic ions such as tetrabutylammonium or dodecylsulfate. Electroosmotic mobilities of 1.49×10^{-5} and $5.84 \times 10^{-4} \text{ cm}^2/\text{Vs}$ were observed on average at pH 3 and 10.5, respectively, the variation strongly suggesting that silica fillers in the polymer dominate the zeta potential of the material. Hydrophobic compounds such as dodecylsulfate and BODIPY[®] 493/503 adsorbed strongly to the PDMS, indicating the hydrophobicity of the channel walls is clearly problematic for CZE analysis of hydrophobic analytes. A method to stack multiple channel layers in PDMS is also described.

4.2 Introduction

The widespread interest in microfluidic devices for bioanalytical purposes has resulted in efforts to facilitate the use and to reduce the cost of such devices. Glass and quartz devices have frequently been used as substrate materials for on-chip CE due to their excellent optical and

+ The experimental data, acquired in this study and described in this chapter, would not have been obtained without the hands-on participation of Mark Munroe. Mark worked on the design of ABS and PCCD masks, participated in the etching of silicon devices and in the optimization of PDMS molding procedures. Mark also acquired the data, depicted in Figures 4.10 and 4.11, under my supervision.

♦ A version of this chapter has been accepted for publication:

Ocvirk, G., Munroe, M., Tang, T., Oleschuk, R., Harrison, D. J. *Electrophoresis*, August 1999

electrical properties (see [1] for the most recent review). However, the high manufacturing costs and the frequent need for application specific surface derivatization steps have resulted in the search for a suitable alternative device material. The demands on polymer properties, channel geometries and channel surface characteristics have resulted in an extensive set of techniques for fabrication of microstructures in various polymers. The relevant techniques shall be discussed briefly.

Polymer micromachining techniques can be classified into etching and replication methods. Different etching techniques are distinguished by the methods of pattern transfer and subsequent development. Wet etching involves a photolithographic pattern transfer into a photosensitive polymer, followed by chemical development of the polymer. The epoxy bisphenol A novolac EponTM SU-8 [2] is an example for a frequently used polymer, which can be deposited onto various substrates in thick films, thus allowing for devices with high aspect ratios (see [3] as an example). The use of a second sacrificial polymer, allows for the creation of enclosed channels. The sacrificial polymer is used to fill the SU-8 network, generated in the prior machining step, followed by deposition and access hole patterning of SU-8, then by dissolution of the filler [3]-[5]. In addition to SU-8, a variety of polymers in conjunction with sacrificial fillers of different solubilities in the developing solvent have been proposed for this approach [5].

Dry etching involves direct pattern transfer into the polymer by exposure to X-rays [6], electron- [7], ion- [8] or laser beams [9]-[18]. Hereby, the fluidic pattern is defined by either scanning of the substrate across a tightly focused beam, projection of a mask onto the sheet or the exposure of masked sheets. Table 4.1 lists several polymers that have reportedly been micropatterned with beam ablation techniques.

Molding and embossing techniques offer a fundamentally different approach for mass production of polymer microstructures. A variety of materials and micromachining methods, listed in table 4.2, has been used to generate planar templates that are replicated in the subsequent embossing or molding step. Hot embossing employs a micromachined template tool, which is heated to above the phase transition temperature. The heated polymer substrate is then brought into contact, controlled pressure is applied and the tool is removed cautiously [7],[19]. High replication accuracies have been demonstrated in poly(methylmethacrylate), PMMA, and polycarbonate, PC, substrates. However, stringent requirements on the rigidity and the hardness of the tool employed have to be met. Injection molding relaxes the mechanical requirements on the master template, while imposing limitations on the choice of polymer. Table 4.3 lists several recently demonstrated examples of injection molded polymer microstructures.

Table 4.1: Polymer Micromachining by Photoablation

Polymer		Beam	Selected references
Polystyrene	PS	Excimer laser $\lambda= 193, 248$ nm	[9],[10]
Polycarbonate	PC	$\lambda= 193$ nm	[9],[14]
Polyimide	PI	$\lambda= 248$ nm	[11]-[13]
Cellulose acetate	CA	$\lambda= 193$ nm	[9]
Poly(ethyleneterephthalate)	PETP	$\lambda= 193$ nm	[9],[14]
Polyesters	-	$\lambda= 308$ nm	[15]
Polyester-polycarbonate blend	-	$\lambda= 308$ nm	[15]
Polycarbonate	PC	$\lambda= 248$ nm, 308nm,	[10],[15],[20]
Poly(methylmethacrylate)	PMMA	$\lambda= 248$ nm	[16]
Poly(tetrafluoroethylene)	PTFE	-	[17]
Polyethylene	PE	$\lambda= 193$ nm	[18]
Polypropylene	PP	$\lambda= 193$ nm	[18]
Fluoropolymers	-	Ion beam	[8]

In order to obtain enclosed channels, all replication techniques require elaborate bonding techniques, such as thermal fusion [21], ultrasonic welding or adhesive bonding [22]. The irreversible nature of the bond results in a monolithic structure, necessitating device disposal in case of channel clogging, an often unavoidable result of introducing biological samples into feature widths of 10 μm or less. However, transparent covers in some cases can be bonded to opaque or colored substrates allowing for optical detection in a wide range of non transparent polymer microstructures.

Whitesides et al. first introduced crosslinked polydimethylsiloxane (PDMS), a durable hydrophobic elastomer, as an attractive material for the creation of micropatterned objects [23]-[25]. Hereby a vinyl terminated siloxane base is crosslinked by platinum catalyzed hydrosilation with a silane terminated curing agent [26]. The patterned silicone substrates can be reversibly bonded, are optically transparent down to ~ 230 nm (see figure 4.1), have a refractive index of 1.430 [27], exhibit high electrical volume resistivity ($2 \times 10^{15} \Omega\text{cm}$ [27]), moderate heat conductivity (0.15 W/mK [28]) and low surface energy (~ 22 mN/m [29]), and can be molded off a variety of master devices at very low cost [30]-[34]. For capillary electrophoresis (CE) applications it is useful that the wettability and acidity of the PDMS surface can be tailored, by addition of various fillers and a range of well described surface modification protocols [29],[35].

Table 4.2: Templates for Embossing and Molding: Materials and Machining Methods

Template material	Machining method	Smallest shown feature size [μm]	Replication	
Various metals	Laser ablation	< 100	-	[36]
Aluminum	CNC milling	>~50	PP thermoforming	[21]
Various metals	Wire Electric Discharge Machining	> 30	-	[37]
Various metals	Direct Metal Mastering (DMM) [†]	~0.6	PC, PMMA injection molding and stamping	[38]
Various metals	UV lithography of photoresist, followed by Si-dry etching, followed by electroplating of the Si substrate	~0.6	-	[39]
Ni	UV lithography of photoresist, followed by Si-wet etching, followed by electroplating of the Si substrate	~30	PMMA injection molding	[22]
Ni	UV lithography of photoresist, followed by Si-wet etching, followed by electroplating of the Si substrate	~10	PC injection molding	[40]
Ni	UV lithography of photoresist, followed by electroplating of the developed photoresist	~0.6	PC, PMMA injection molding and stamping	[41]
Various metals	-*-	~0.6	Photopolymerization of UV curable polymers*	[42]
SiO ₂	Electron beam lithography of photoresist, followed by reactive ion etching of SiO ₂	0.025	PMMA embossing	[7]
Si	UV lithography of photoresist, followed by Si-dry etch	~5	PMMA, PC hot embossing	[19]
Cu,Ni,Au,Ag	LIGA, i.e.lithography of PMMA resists with X-rays, followed by electroplating of the resist	<0.1	-	[6]
Various metals	Deep UV lithography of polyimide resists, followed by electroplating	~40	-	[43]
Cu	UV lithography of photoresist, followed by Cu etching with a FeCl ₃ solution	50	PDMS molding	[33]
Epon SU-8	UV lithography	3	PDMS molding	[44]

[†] A Piezoelectric stylus with a diamond tip is scanned across a metal master, followed by electroplating.

* A UV sensitive polymer is sandwiched between a master and a transparent base plate, followed by UV curing of the polymer.

Effenhauer et al. [30] used untreated PDMS devices to perform capillary electrophoresis in hydroxypropylcellulose filled channels, but no separations were reported in free solution. The study demonstrated that the low work of adhesion between a PDMS device and a PDMS slab in water (~ 75 mN/m [29]) is sufficient to prevent leakage liquid leakage between the device and the cover slab. More recently, Duffy et al. [34] examined the use of plasma oxidized PDMS devices for CE, asserting surface oxidation of the hydrophobic PDMS to be a requirement for cathodic EOF, and also the filling of PDMS channels with aqueous solutions.

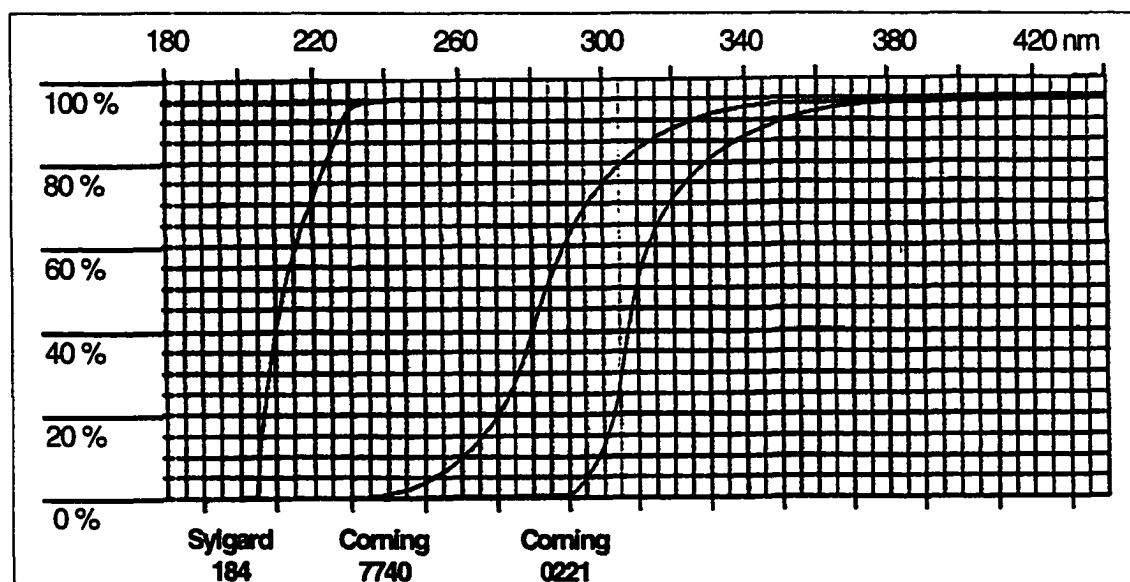


Figure 4.1: Measured transmittance [%] of a 1 mm thick Sylgard 184 slab for wavelengths in the UV/VIS. The transmittance of 1mm thick Corning 7740 (Pyrex) and Corning 0211 glass[†] is plotted for comparison.

[†] Corning Glassware Specifications Guide, Corning, NY, USA

Table 4.3: Injection Molded Microfluidic Devices

Substrate material	Template master	Smallest Feature size [μm]	Selected References
PMMA	Si etch + consecutive Electroforming of Ni-master	~ 30	[22]
PMMA	N.A.	N.A.	[45]
PMMA	Wire	41.7 ± 17.5	[46]
N.A.	Laser ablation of polymer + consecutive electroforming	N.A.	[47]

Capillary zone electrophoresis in open, native capillary PDMS devices has not been performed previously. In this report we outline the differences in potential control programs

needed to obtain high efficiency separations in glass versus PDMS devices. We also report data exhibiting strong cathodic EOF in silica filled PDMS devices of the same Sylgard 184 formulation used by others [30],[34]. In addition, the origin of the electroosmotic flow was examined by measuring the effect of pH changes and the addition of hydrophobic flow modifiers to the running buffer. We also tested the effect of curing time on wettability and surface charge by measuring contact angles and electroosmotic mobilities of devices of increasing age. The long term stability of untreated PDMS was found to strongly contrast with oxidized PDMS, which exhibits dynamic surface properties due to hydrophobic recovery after oxidation [48,49].

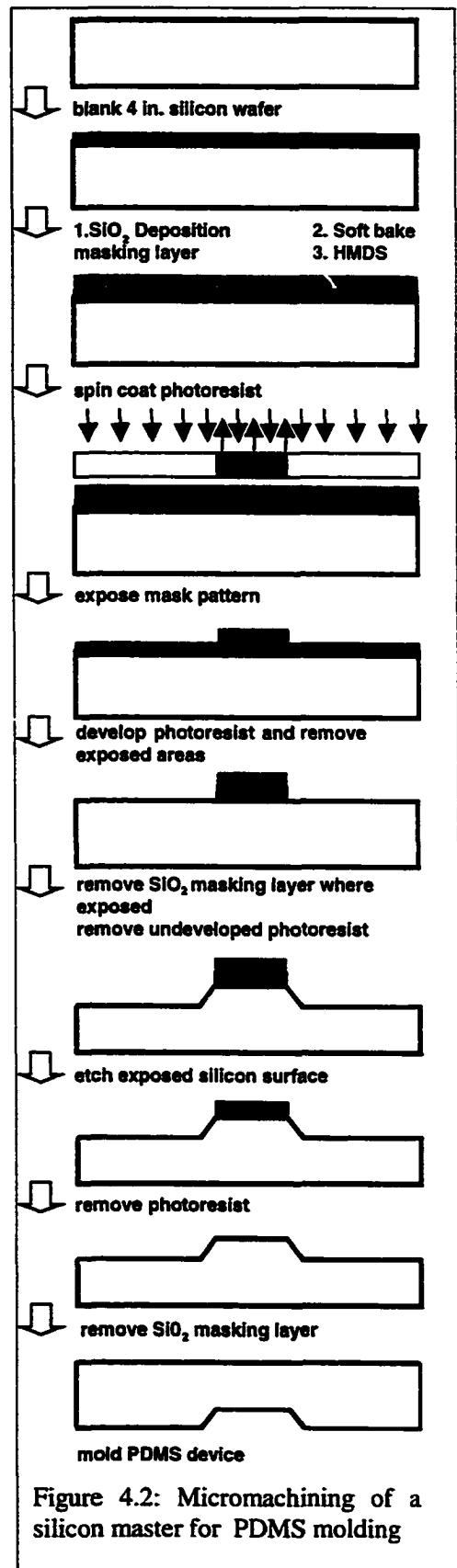
Several reports have shown possibilities of employing a modular concept for the integration of sample preparation, mixing, reactions, separation and detection into one device stack, as originally envisioned in the μ -TAS concept [11],[51]-[53]. Various bonding techniques have been employed to connect single devices to form a three dimensional flow circuit [54]-[56]. However, in those designs the more cost intensive devices such as pumps and detectors must be disposed of along with the exclusively fluidic components. In this report we suggest the use of PDMS devices for the fabrication of a stacked system composed of disposable PDMS fluidic elements, which can be reversibly sealed to the permanent components. We demonstrate here the first step towards multiple stacking, i.e. the stacking of two PDMS devices with zero dead volume. This approach may be extended to the facile stacking of several fluidic networks contained in thin PDMS sheets at very low cost.

4.3 Experimental Section

4.3.1 Master Fabrication

Polished <100> oriented p-type silicon wafers (Evergreen Semiconductor Materials, San Jose, CA, USA) were used as masters, forming a positive relief mold for PDMS devices. The fabrication process is depicted in figure 4.2. Wafers, 4" in diameter, were oxidized at 1100°C for \approx 7 hours resulting in an oxide layer of 8000-9000 Å, measured with a Nanospec film thickness measurement system (Nanometrics, Sunnyvale, CA, USA). The oxidized wafers were treated with hexamethyldisilazane (HMDS) to promote the adhesion of the photoresist (Waycoat HPR 504, Olin Hunt) followed by soft baking. A Karl Süss mask aligner (Karl Süss KG GmbH, Garching, Germany) was used for photolithography. Photomasks were designed using L-Edit (Tanner Research, Pasadena, CA, USA) and generated by Adtek photomask (Montreal, Canada). After photoresist development (Microposit 354, Shipley, Marlboro, MA, USA) and hard baking, the SiO₂ layer was etched with an aqueous 10:1 buffered oxide etch solution (40 % HF / 49 %

$\text{NH}_4\text{F} = 10:1$, Olin-Hunt) at an etch rate of $\sim 100 \text{ \AA} / \text{min}$. After removal of photoresist with acetone, and thorough aqueous rinsing for acetone removal, the wafer was mounted horizontally in a teflon etch holder. The etch bath was optimized for minimization of etch back of photolithographically patterned corners, i.e. etching of the $\langle 311 \rangle$ and $\langle 411 \rangle$ planes, for high smoothness of channel walls and for minimum etch rates of the SiO_2 masking layer. An etch solution of 40 % KOH / 10% isopropanol, an etch temperature of $\sim 76^\circ\text{C}$ and a stir rate of 240 rpm were found as optimum etch conditions. Features of 10-20 μm top width and 10 – 25 μm depth were generated at an etch rate of $\sim 0.4 \mu\text{m}/\text{min}$, resulting in low surface roughness, as evident from figure 4.3. Lower etch temperatures resulted in higher surface roughness of channel walls. A surface profilometer (Alphastep 200, Tencor Instruments, KLA-Tencor Corp., San Jose, CA) was used to establish the etch rate and the final channel depths and top widths. The etched wafer was cut to size using a Model 1100 wafer saw (Microautomation, Fremont, CA).



4.3.2 Device Molding

An aluminum base plate (13 x 20 cm) and an aluminum frame (1.9 cm wide and 2.2 mm thick) screwed onto the base plate, were used as a mold. The size of the base was chosen to be significantly larger than the template in order to alleviate device peel off and to provide planarity of the molded slab. The base was perforated in the template contact area to provide solvent access to facilitate removal of the master after molding. The assembly was coated with silicone release fluid (Silchem, ON, Canada, DF 55-50) before molding. A silicon master, 62 x 35 mm in size, was then cleaned with isopropanol and water, blown dry with pre-filtered nitrogen and placed on the molding plate. All operations were performed in a Class 1000 clean flow hood. PDMS base and curing agent (Sylgard[®] 184, Dow Corning, Midland, MI, USA) were thoroughly mixed in a 10:1 ratio and poured onto the silicon master. The PDMS was first allowed to rest at room temperature for one hour to permit the removal of air bubbles. The device was then cured for three hours at 75 °C. After cooling, the device was peeled off the master, cut to size and cleaned with pre-filtered methanol and deionized water. High replication accuracies were obtained routinely as shown by the SEM of a layout detail in figure 4.3. A cover slab was molded in the same fashion using a glass microscope slide as a master. Holes, 3 mm in diameter, were punched into the PDMS cover, allowing for external access to the fluid manifold in the device. The device and the cover were cleaned rigorously with filtered methanol and water and then dried with filtered nitrogen prior to assembly.

4.3.3 Materials & Reagents

A 1 mM stock solution of fluorescein di-sodium salt (Sigma) was prepared in a 1.9 mM borate (Baker, Phillipsburg, NJ)/ 6.3 mM Tris (tris(hydroxymethylamino)methane, Sigma) pH 9 buffer. Further solutions were prepared by serial

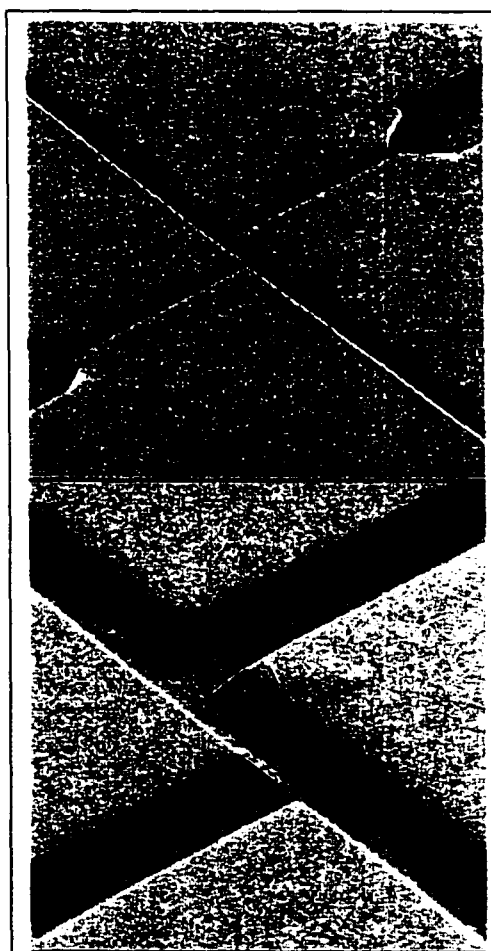
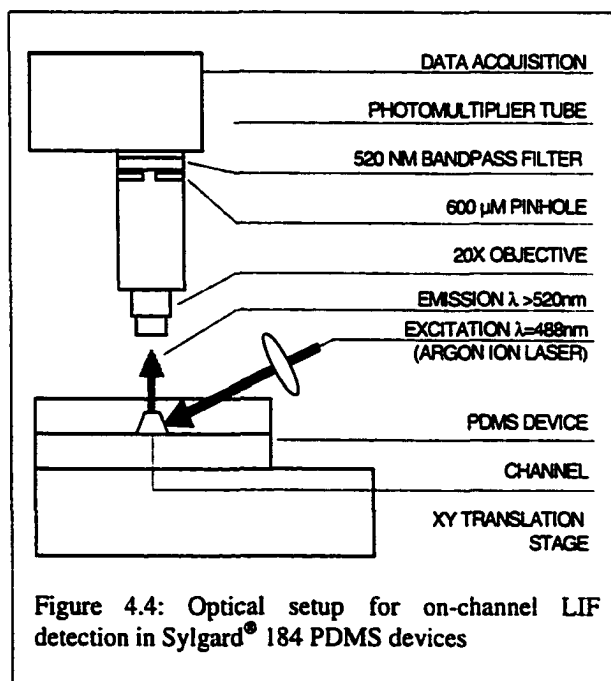


Figure 4.3: SEM images of a double T injection detail, molded into PDMS; device layout ABS-10

dilution of the 1 mM fluorescein stock solution with the same running buffer. Phosphate buffers (1 mM phosphate, 10 mM KCl) were used as background electrolytes for all EOF studies. The pH values (pH 3–9) were established by mixing appropriate proportions of 1 mM solutions of orthophosphoric acid (Mallinckrodt Laboratory Chemicals, Phillipsburg, NJ, USA), disodiumhydrogen orthophosphate (BDG, Toronto, ON, Canada), sodium dihydrogen orthophosphate (BDH) and tri-sodium orthophosphate (BDH), and measuring the pH. All buffers were prepared in double distilled and deionized water. Sodium dodecylsulphate was from Serva Biochemicals (Heidelberg, FRG), tetrabutylammonium chloride from ICN Biomedicals (Costa Mesa, CA, USA) and BODIPY[®] 493/503 (4,4-difluoro-1,3,5,7,8-pentamethyl-4-bora-3a,4a-diaza-s-indacene) from Molecular Probes (Eugene, OR, USA). Reagent grade methanol (Fisher Scientific) was used for all device cleaning procedures.

4.3.4 Instrumental Setup

The optical setup is identical to previously described assemblies [57] and is depicted in figure 4.4. The only modifications are the use of an achromatic lens for focussing of excitation light (achromat, Newport PAC064, $f=200$ mm, Newport, Irvine, CA, USA) and a 20 x/ 0.28 N.A. aspheric lens (New Focus, Santa Clara, CA, USA) for collection of fluorescence emission. A 600 μm pinhole (Melles Griot, Irvine, CA, USA) was inserted at the image plane. The high voltage control system for the chips was modified from previous wiring schemes. Figure 4.5



shows the wiring of 3 high voltage power supplies and 4 relays. The series of events is described in figure 4.5: High voltage (HV) supplies connected to the sample reservoirs and the buffer waste were from Gamma High Voltage Research (RMC15/0.12P, Ormond Beach, FL, USA) and Spellman (CZE1000R, Spellman, Plainview, NY, USA), respectively. The analog signal was filtered with a Butterworth 15 Hz cutoff filter (Krohn-Hite 3442), giving a 150 ms rise time. Electropherograms were recorded on a PowerMac 7100/66 with an NB-MIO16 A/D board and a program written in Labview (National Instruments, Austin, TX, USA) at a sampling rate of 50

Hz. All data was smoothed using a 7 point box smooth algorithm, included in the Igor Pro analysis software (Wavemetrics, Lake Oswego, OR, USA).

4.3.5 Device Conditioning

Degassed methanol was introduced into the reservoirs and flushed through the manifold by subsequent application of vacuum at all ports. Later, methanol was removed from the reservoirs, replaced with degassed water, then vacuum was reapplied. Reservoirs were rinsed three more times with water before the introduction of running buffer. Prior to the first injection the device was flushed for 15 minutes with the running buffer at a field strength of 1000-1200 V/cm.

4.3.6 EOF Measurement

In order to obtain the EOF dependence on pH we used the previously published [58] current monitoring method. Equal aliquots of phosphate buffers (1 mM, pH 3 - 10.5, 10 mM KCl), with additives such as tetrabutylammonium chloride present when the subject of study, were introduced into all 4 device reservoirs of a ABS 18 device (see figure 4.6). Channels were then conditioned with the buffer by application of -2 kV from B and C to D for 5 minutes and subsequently from A to D for a total time of 15 minutes. A diluted

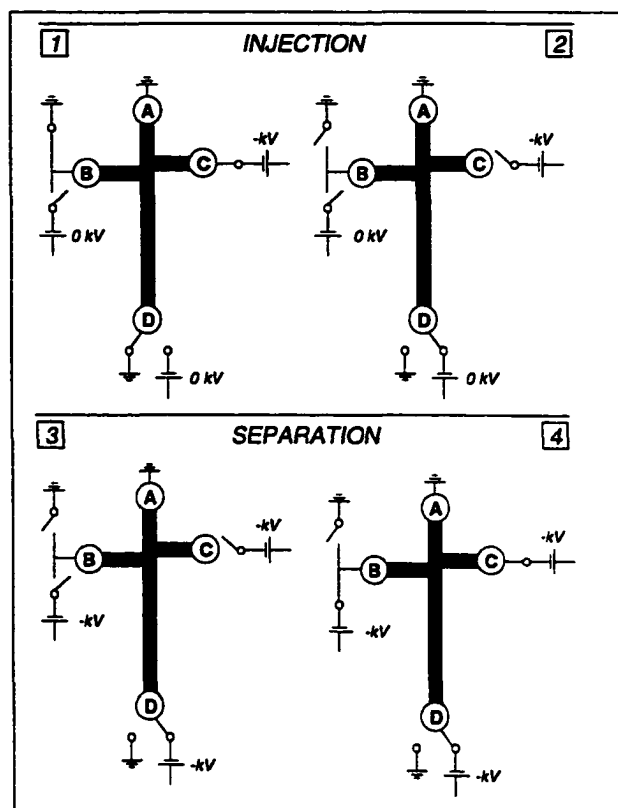


Figure 4.5: Voltage control sequence for sample injection and separation on PDMS devices; Reservoirs A: running buffer; B: sample, C: sample waste, D: buffer waste; HV_c: injection power supply, HV_d: separation power supply, HV_b: power supply at B. Step 1: Set injection voltage at HV_c, A, B, D grounded; step 2: Switch relay c to disconnect HV_c, switch relay d to connect HV_d to D; step 3: Set separation voltage at HV_d, set pushback voltages at HV_b and HV_c, disconnect B from ground; step 4: Switch relays b and c to connect HV_b and HV_c with B and C, respectively.

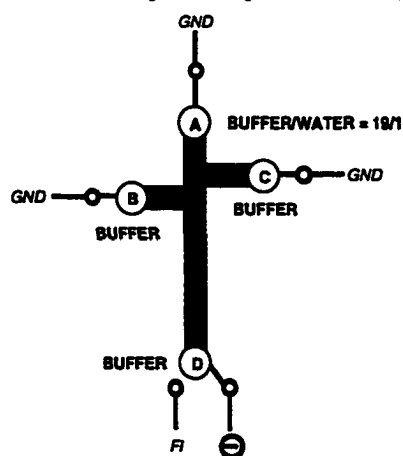


Figure 4.6: EOF measurement by current monitoring

buffer (buffer : water = 19:1) was then introduced into A, A and D were connected to ground and -2kV respectively, while B and C remained floating. The time required to fill the separation channel (AD) with diluted buffer, i.e the time to reach a new current plateau, was recorded. Average electroosmotic mobilities were obtained from three consecutive measurements on the same device.

4.3.7 Contact Angle Measurement

Contact angles were measured on sessile water droplets, deposited onto the PDMS slab with a 50 μL microsyringe (Hamilton, Reno, NV, USA), which was mounted perpendicularly above the PDMS surface. The measurement was performed with a manual contact angle goniometer (Model 100-00-(115/220), Ramé-Hart, Mountain Lakes, NJ, USA). A sharply defined image of a sessile drop was observed as a silhouette, followed by construction of a tangent to the silhouette and manual readout of the contact angle.

4.4 Results and Discussion

Several groups [59]-[61] have reported cathodic EOF in PDMS coated fused silica capillaries, while Duffy et al [34] have assumed PDMS would not exhibit native EOF. The several possible sources of surface charge include; 1., adsorption of a potential determining ion, PDI, onto the surface [62], 2., charge present in the PDMS due to the synthetic steps (such as polymerization catalyst) or to fillers; 3., charge introduced to the surface by acid-base chemistry of surface functionality such as silanol groups. To aid in differentiating these various surface charge sources we examined the EOF as a function of pH, and as a function of the concentration of PDI with various adsorptive strengths.

The devices utilized in this study are depicted in figure 4.7. The ABS-10, ABS-18 and PCCD 25 devices used channel depths of 10, 18 and 25 μm , respectively. All channel dimensions are given in table 4.4. The “double-T” injectors are 120 and 140 μm long on the PCCD 25 and ABS devices, respectively.

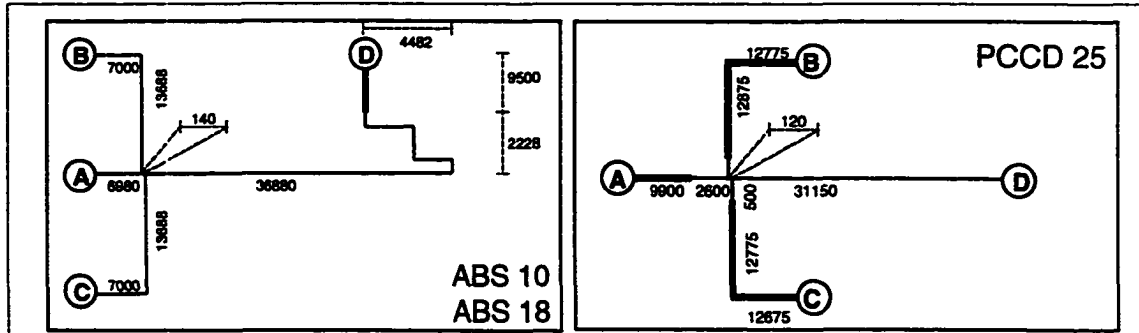


Figure 4.7: Geometric layouts of devices ABS 10, ABS 18 and PCCD 25, molded into PDMS. Channel depths are 10, 18 and 25 μm , respectively. Letters mark reservoir labels. Channel lengths are given in micrometers. Resistances (R_x) and resistances to flow ($\Delta p_x/\eta F$) of all channels are given in table 4.4.

Table 4.4: Device Dimensions and Impedances

	ABS 10	PCCD 25	PCCD 25 coupled
Channel depth [μm]	10	25	25
Top channel width [μm]: narrow/wide	34/215	60/235	60/235
Bottom channel width [μm]: narrow/wide	20/200	25/200	25/200
$\Delta p_A/F$ [μL^{-1}] (a)	3.0	0.4	0.4
$\Delta p_B/F$ [μL^{-1}] (a)	8.9	0.4	0.4
$\Delta p_C/F$ [μL^{-1}] (a)	8.9	0.4	0.4
$\Delta p_D/F$ [μL^{-1}] (a)	20.1	4.0	8.0
R_A/ρ [μm^{-1}] (b)	25.8	4.2	4.2
R_B/ρ [μm^{-1}] (b)	76.4	4.7	4.7
R_C/ρ [μm^{-1}] (b)	76.4	4.6	4.6
R_D/ρ [μm^{-1}] (b)	172.9	29.3	58.6

(a) Resistances to flow are expressed as pressure drops, Δp [Pa], per unit dynamic viscosity, η [Pas], and unit volumetric flow rate, F [μL]; Δp was calculated under the approximation of rectangular channels as described before [77]; the overall channel width was set equal to the channel width at the top edge; channel depths were measured by profilometry;

(b) electrical resistances, R [Ω], are normalized to resistivity [$\Omega\mu\text{m}$] and are estimated from the channel length to cross section ratio.

4.4.1 EOF in PDMS Devices

The current monitoring method [58] was used for EOF measurement, as described in section 4.3.6. Performing the experiment with a reversed potential did not result in a current change,

indicating cathodic EOF over the range of buffer systems studied (*vide infra*). No siphoning was observed from A to D, and hence the electroosmotic mobility, μ'_{EOF} , could be obtained by eq.4.1

$$\mu'_{EOF} = \frac{L}{tE} \quad (4.1)$$

where L is the effective length, i.e. the length normalized to the smallest channel cross sectional area [63], from reservoir A to D, t the time to reach the current plateau and E the applied field strength. The measured electroosmotic mobility μ'_{EOF} is statistically indistinguishable from the electroosmotic mobility of the undiluted buffer, μ_{EOF} , as demonstrated by Huang et al. in their original experiments [58]. The observation of cathodic EOF in Sylgard 184 PDMS channels for all buffer systems studied is consistent with most previous reports and indicates there is a negative charge on the walls under all conditions we explored.

We evaluated the interaction of a range of anions and cations of different hydrophobicities with the Sylgard 184 PDMS wall. If adsorption of electrolyte ions such as chloride and phosphate onto the wall is the predominant contributor to EOF, then addition of anions with higher PDMS affinity than the background electrolyte (BGE) should result in an increase in EOF. We found that the addition of fluorescein anions at pH 9 did not result in a significant increase of μ_{EOF} between 10^{-9} and 10^{-6} M. The addition of 10^{-9} to 10^{-4} M tetrabutylammonium chloride (TBACl) to the BGE at either pH 3 or pH 9 also did not result in any significant EOF changes, as shown in Table 4.5. At 1 mM TBA⁺ there was a decrease in EOF. Tests with KCl at 10 versus 11 mM in the BGE showed there was no effect on EOF due to this approximately 10% change in ionic strength. This control demonstrates that the changes due to 1 mM TBACl, which are consistent with adsorption of this cation, are not an artifact of the small ionic strength change.

The strongly hydrophobic anion of sodium dodecyl sulphate (SDS) increased EOF substantially when added to the BGE at high enough concentration. Figure 4.8 shows the changes in μ_{EOF} with SDS concentration. This response is correlated to the adsorption isotherm of SDS (*vide infra*). The EOF increased by a factor of 1.4 or 22.6 when adding 10^{-3} M SDS to solutions at pH 9 or 3, respectively. The data in Table 4.5 and Figure 4.8 are consistent with the higher adsorption coefficient of SDS⁻ vs TBA⁺. Contrasting the behavior of the two ions confirms that it requires a strongly adsorbing ion in order to affect the zeta potential of PDMS. Further, such ions must be present at significant concentration to cause an effect.

This response is correlated to the adsorption isotherm of SDS, in that the μ_{EOF} depends linearly on the ζ potential, and the surface charge density is proportional to the amount of SDS adsorbed. The relationship between ζ potential and charge density is complex, but increases monotonically. The ζ potential may be approximated by the Gouy Chapman equation, which

states an inverse hyperbolic sin dependence of potential on surface charge. For potentials less than about 25 mV this dependence is approximately linear, but at maximum adsorption this potential will be exceeded.

Our data show that a strongly adsorbing ion would influence the surface potential of Sylgard® 184 PDMS surfaces at low concentrations. Consequently, it seems unlikely that many buffer ions, which tend to be weakly adsorbing, could act as a PDI and control the surface potential. However, the fact SDS changes the EOF of PDMS, but not glass [59],[64], indicates the tendency of hydrophobic compounds to adsorb on PDMS. The similarity of μ_{EOF} measured at 1 mM SDS at both pH 3 and 9 is in agreement with observations in polypropylene capillaries with SDS present [65], indicating adsorption of SDS regardless of the surface charge on the polymer.

Very strongly adsorbing neutral molecules are known to extract into PDMS. Establishing the values of the equilibrium constant, K_{PDMS} , for extraction into Sylgard 184 from the BGE is beyond the scope of this study. It is known that for weakly hydrophobic compounds the water/octanol partition coefficients found in the solvent phase microextraction literature [66],[67] can be predictive of PDMS extraction of a compound. As an example, experiments with the neutral, relatively hydrophobic, BODIPY® 493/503 dye showed that it could not be analyzed by CE in a PDMS device. This neutral EOF marker extracted into the PDMS substrate and did not migrate in an applied field.

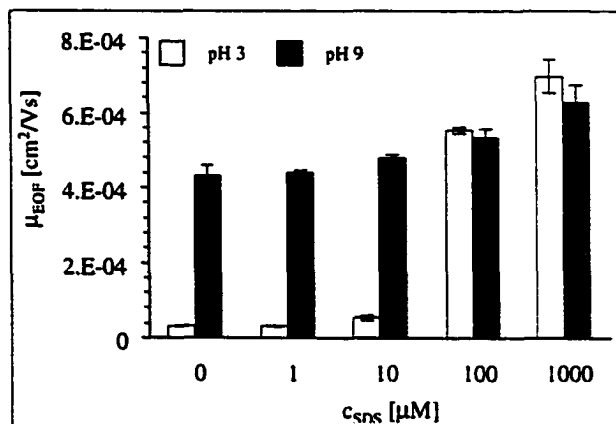
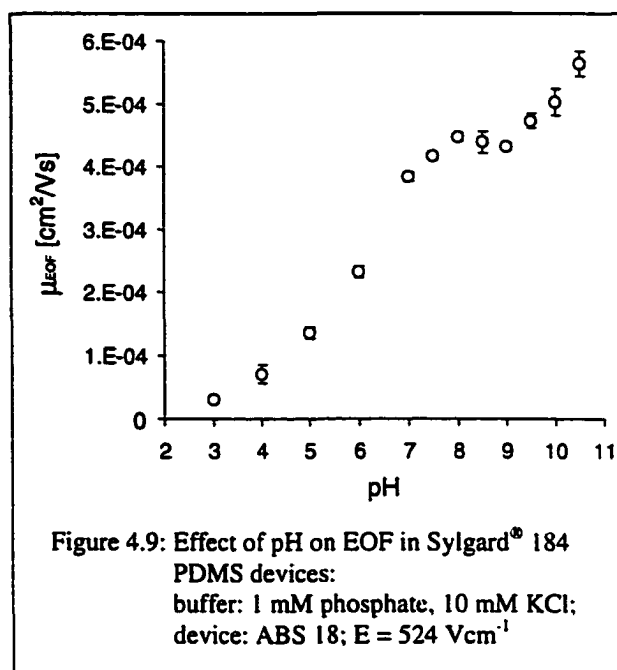


Figure 4.8: Effect of SDS addition to the running buffer on the electroosmotic mobility in Sylgard® 184 PDMS devices at pH 3 and 9 buffer: 1 mM phosphate, 10 mM KCl; device: ABS 18

Table 4.5. Effect of Tetrabutylammonium ion (TBA^+) on Electroosmotic Mobility

[TBACl] moles/L	μ_{EOF} pH 3 $\times 10^4 cm^2/s$	μ_{EOF} pH 9 $\times 10^4 cm^2/s$
10^{-9}	0.86 ± 0.09	4.32 ± 0.07
10^{-7}		4.01 ± 0.06
10^{-6}	0.81 ± 0.06	4.39 ± 0.01
10^{-5}	0.83 ± 0.04	4.03 ± 0.07
10^{-4}	0.833 ± 0.005	4.04 ± 0.01
10^{-3}	0.58 ± 0.03	$3.28 \pm .008$

Besides absorption and adsorption phenomena onto the PDMS matrix, hydrolysis of siloxane bonds to form silanol functionalities can result in an EOF change and higher water wettability [68]. To test for this possibility we performed ATR-IR analyses of PDMS slabs after soaking in BGE of pH 4, 7 and 10 for 24 hours. We could not detect any bands in the 3400 cm^{-1} region, characteristic of fundamental O-H stretching vibrations. Further, the EOF did not increase significantly after storage overnight in the employed pH 3 and pH 9 buffers.



The dependence of μ_{EOF} on pH is given in figure 4.9. Measurements were performed in the direction of decreasing pH values. Data points represent the average of 3 measurements; error bars depict the standard deviation. The zeta potential and μ_{EOF} from pH 3 to 10.5 is negative, showing a sigmoidal shape from pH 3-8 with an inflection point at $\sim\text{pH } 6.5$. Electroosmotic mobilities increase further at $\text{pH} > 9$, which might be attributed to specific hydroxide ion adsorption, as described earlier for glass surfaces [69]-[71]. The strong pH dependence of EOF points strongly to acidic sites on the PDMS walls. Due to the non-adsorbent character of the BGE ions and the evidence shown above, the contribution of adsorbed buffer ions to the wall potential seems to be negligible under neutral and alkaline conditions. The first inflection point of the titration curve can be interpreted to correspond to the pK_a of acidic groups in the PDMS support. The stunning similarity of the curve in fig. 4.9 and the widely known pH dependence of EOF in fused silica capillaries [72] can be attributed to the amount of silica filler introduced by the manufacturer into the Sylgard 184 formulation [73]-[75].

In order to assess the durability of PDMS, we examined the wettability of 10 identically cured substrates stored dry at $25\text{ }^\circ\text{C}$ for a period of 2 hours to four months. The water PDMS contact angle measured immediately after curing at 75°C for 3 h was $104.5 \pm 2.0^\circ$ ($n=10$). The average contact angles measured over four months did not differ statistically from this value within the 95 % confidence interval. This demonstrates the remarkable stability of the cured elastomer over the time investigated. To demonstrate the electroosmotic constancy of PDMS, the

EOF was determined at pH 9 over five consecutive days. The average electroosmotic mobility, μ_{EOFav} , within one day was $4.1 \pm 0.1 \times 10^{-4} \text{ cm}^2/\text{Vs}$ ($\pm 2.5 \%$, $n=5$), μ_{EOFav} over five days was $4.1 \pm 0.3 \times 10^{-4} \text{ cm}^2/\text{Vs}$ ($\pm 8.6 \%$, $n=20$) on one particular device. The average device to device reproducibility ($n=3$) of μ_{EOF} was better than 8 %. The EOF is up to 23% lower than mobilities measured in glass devices (Corning 0211, Corning, NY, USA) under identical conditions (data not shown). We also want to emphasize that native PDMS devices were reused over a span of one week without significant losses in separation efficiency for fluorescein. A shelf life for cured substrates of many weeks seems feasible. This contrasts with the known instability of plasma oxidized PDMS surfaces [48],[49].

The hydrophobic PDMS microchannels can easily be filled with degassed aqueous solutions in absence of any leakage between the top and bottom slabs. Pre-loading with methanol was generally used, in order to prime the chips for introduction of aqueous solutions. Problems with bubble formation after proper conditioning of the device (see experimental section) occurred extremely rarely. When present, the air bubbles could be removed by simultaneous application of a vacuum and pressure at the entrance and exit ports of the channel.

4.4.2 CE Performance

In order to obtain reproducible electrophoretic separations with sufficient separation efficiency, well defined sample plugs are required. Clearly, voltage control of all device ports in order to fully shape the plugs during injection, followed by application of pushback voltages at the sample reservoirs, minimizes the injector band broadening contribution in glass devices [57],[76],[77]. However, well defined sample plugs can be formed in glass devices without active potential control of all channels simultaneously [77]-[80]. This study demonstrates that there is a need for complete voltage control in untreated PDMS devices during both sample injection and separation, in order to avoid catastrophic sample leakage into the separation channel. In contrast to glass based double-T injectors, we found it was necessary to control the potential on all reservoirs during all stages of sample injection. Attempts to float reservoirs B and C during separation resulted in drastic overloading due to leakage into the separation channel. Consequently, the plug shaping as described in the Experimental section was used in all subsequent studies. Figure 4.10A shows an electropherogram obtained within the PCCD 25 device, with plug shaping used during injection, but with the side channels B and C left floating during the separation step. The resulting leakage of fluorescein from the sample ports B and C into the separation channel prevented reproducible plug formation. Figure 4.10B was obtained by applying pushback voltages of -550 V at ports B and C, with -5 kV at port D. This procedure was found to provide sufficient

backflow into the side channels to eliminate any leakage, yielding 15,400 theoretical plates, N , for a peak migration time of 3.9 seconds.

We attempted to improve the separation performance on PCCD 25 by 1., optimization of the pushback voltages, V_{pb} , for a given separation voltage, V_{sep} , and 2., by optimization of the applied separation voltage. Applying -550 V at ports B and C with a -5 kV separation voltage resulted in a calculated potential at the junction of -580 V, and an effective field strength, E_{eff} , of 1420 Vcm^{-1} across the separation channel. Obviously, this calculation suggests there would still be a flow out of the side channels and into the separation channel. However, we have found the optimal leakage control potential is usually within $\pm 50 \text{ V}$ of the calculated value [63]. Consistent with this observation, no leakage was seen with -600 V applied to ports B and C, but the decreased E_{eff} in the separation channel lead to slower separations and thus lower plate numbers [63]. With -500 V or a more positive potential applied to ports B and C (-5 kV on D) the peak was significantly broader, due to leakage out of

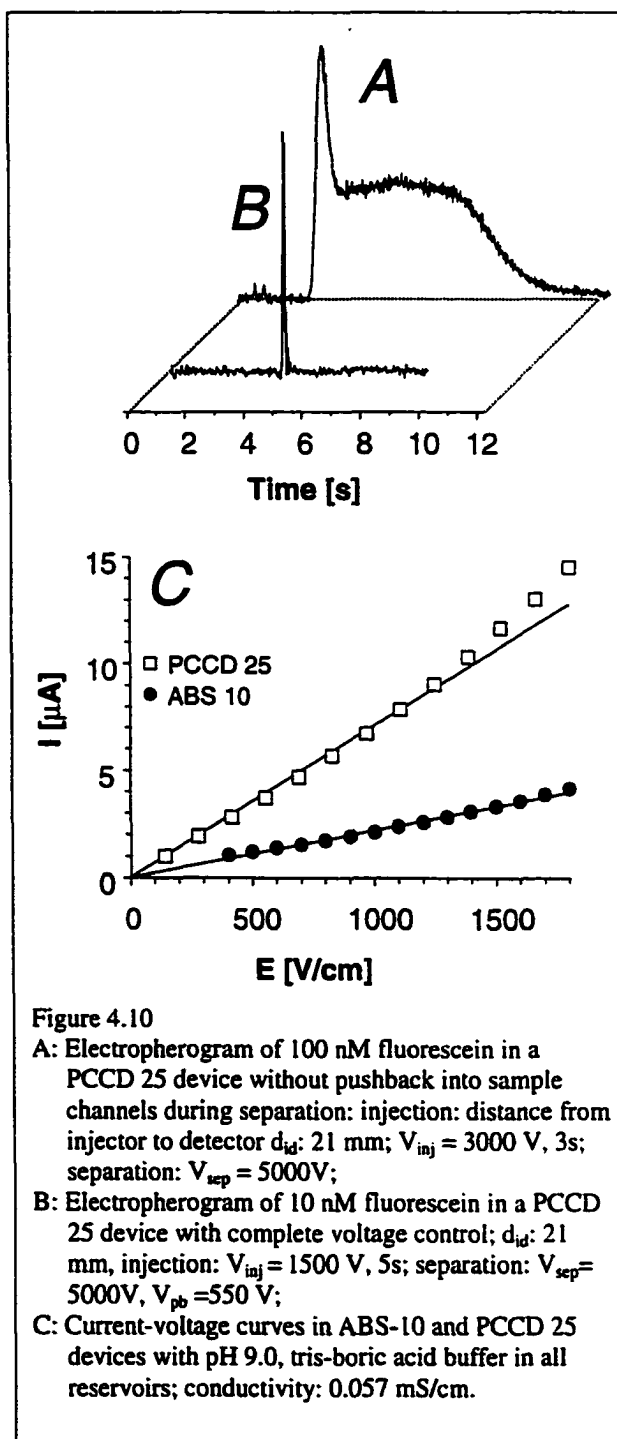


Figure 4.10
 A: Electropherogram of 100 nM fluorescein in a PCCD 25 device without pushback into sample channels during separation: injection: distance from injector to detector d_{id} : 21 mm; $V_{inj} = 3000 \text{ V}$, 3s; separation: $V_{sep} = 5000 \text{ V}$;
 B: Electropherogram of 10 nM fluorescein in a PCCD 25 device with complete voltage control; d_{id} : 21 mm, injection: $V_{inj} = 1500 \text{ V}$, 5s; separation: $V_{sep} = 5000 \text{ V}$, $V_{pb} = -550 \text{ V}$;
 C: Current-voltage curves in ABS-10 and PCCD 25 devices with pH 9.0, tris-boric acid buffer in all reservoirs; conductivity: 0.057 mS/cm .

the side channels. Application of $E_{eff} > 1420 \text{ Vcm}^{-1}$, ($V_{sep} < -5 \text{ kV}$ with optimized V_{pb}) resulted in decreased separation efficiencies, attributable to excessive heat input ($> 1.4 \text{ W/m}$) and thermally induced band broadening. Lowering the effective field strength ($< 1420 \text{ Vcm}^{-1}$) in conjunction with optimized pushback potentials also yielded lower theoretical plate numbers. Both observations are in good agreement with the Ohm's Law response depicted in Figure 4.10C,

showing a non-linear current-voltage correlation at $E_{\text{eff}} < 1300\text{-}1400 \text{ Vcm}^{-1}$. We concluded that the modest separation performance of the PCCD 25 device could not be improved by electrical means.

A significantly different device layout, ABS 10, with $10 \mu\text{m}$ deep channels molded into PDMS showed superior performance. Figure 4.11 shows 5 consecutive injections of fluorescein for 15 s, followed by application of $E_{\text{eff}} = 1340 \text{ Vcm}^{-1}$ across the separation channel. Excellent injection volume (RSD = 1.5 %, $n=5$) and migration time reproducibility (RSD = 0.9 %, $n=5$), as well as $64200 (\pm 3.7\%, n=5)$ theoretical

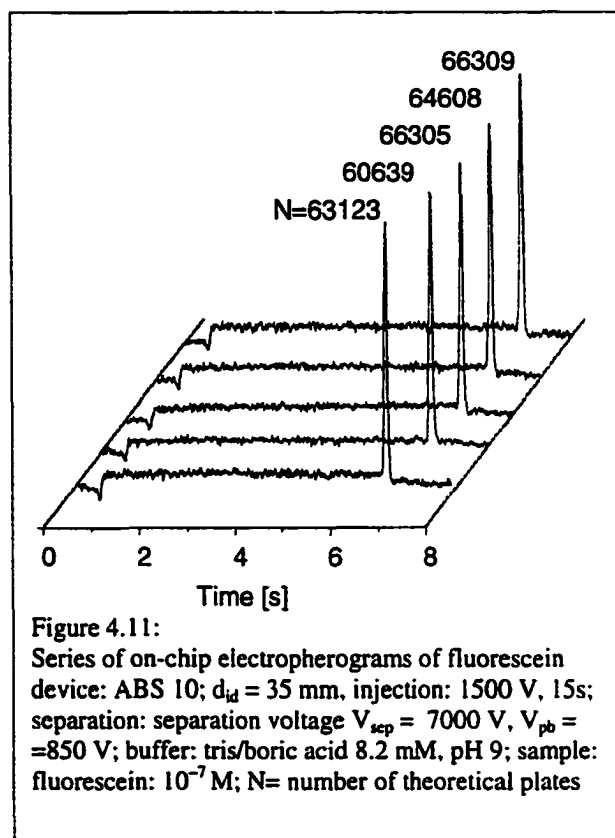


Figure 4.11: Series of on-chip electropherograms of fluorescein device: ABS 10; $d_{\text{id}} = 35 \mu\text{m}$, injection: 1500 V, 15s; separation: separation voltage $V_{\text{sep}} = 7000 \text{ V}$, $V_{\text{pb}} = -850 \text{ V}$; buffer: tris/boric acid 8.2 mM, pH 9; sample: fluorescein: 10^{-7} M ; N = number of theoretical plates

plates were realized. However, voltage control of all ports during loading and separation was required for adequate performance, as observed with the PCCD 25 device. The geometric differences between the two layouts, shown in table 4.1, apparently lead to significantly different fluidic characteristics. The resistance to flow of all channels in ABS 10 is significantly higher than in the PCCD 25 device, due to shallower and narrower channels. Consequently, the device should be less sensitive to leakage effects and thus have better defined sample plugs [77],[81]. The higher electrical impedance of the channels in ABS-10 also meant that higher fields could be applied to improve efficiency without inducing Joule heating.

4.4.3 Device Stacking:

We explored the possibility of using the self adhesive properties for the construction of three dimensional microfluidic structures. Two identical PCCD 25 devices were superimposed as depicted in figure 4.12A. Alignment marks molded into the devices facilitated the alignment and contact of the devices by hand. Figure 4.12B shows a magnified view of the Z shaped interface created, as seen from above, resulting in an overlap of $60 \mu\text{m}$ length, $50 \mu\text{m}$ depth and $\sim 180 \text{ pL}$ junction volume. The shape of the junction is attributable to the superposition of the anisotropically etched features generated in the Si mold by the mask lines. We then explored the

potential of using the extended separation channel for electrophoretic injections. Fluorescein plugs were formed in layer a and transported electroosmotically across the junction to layer b. Figure 4.13 depicts two electropherograms obtained when detecting 50 μm before and after the channel overlap. When detecting 50 μm before the channel overlap, 12725 theoretical plates were obtained. Detection of a fluorescein plug 50 μm after the overlap resulted in 12750 theoretical plates.

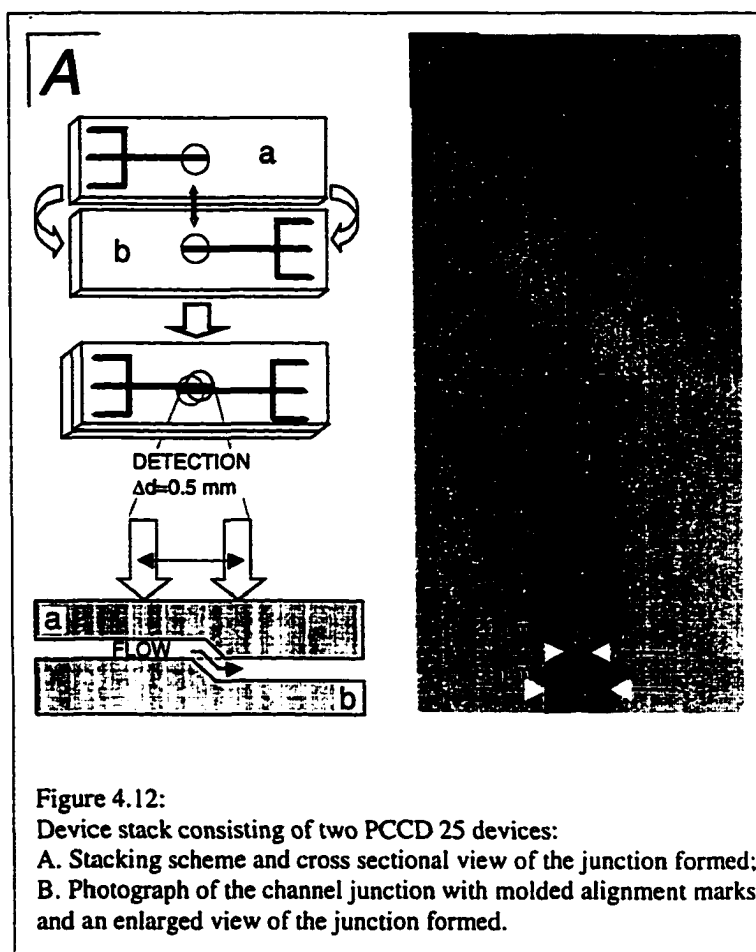


Figure 4.12:
Device stack consisting of two PCCD 25 devices:
A. Stacking scheme and cross sectional view of the junction formed;
B. Photograph of the channel junction with molded alignment marks and an enlarged view of the junction formed.

4.5 Conclusion

This report establishes that unmodified Sylgard[®] 184 PDMS is a suitable substrate for microfluidic, open tubular CZE devices. The results show that PDMS devices require continuous voltage control of all intersecting channels in the fluidic network, in order to avoid catastrophic leakage at the intersections. This contrasts with the behaviour of similar flow channel designs fabricated in glass substrates [77]-[80]. The reasons behind this difference remain unknown, despite our study of the sources of EOF in PDMS devices. PDMS microchannels, filled with electrolytes, exhibit negative zeta potentials in the pH 3-10.5 range. The resulting EOF is highly pH dependent, changing by a factor of 29.4 over the pH range studied. The lack of effect of moderately hydrophobic ions on the EOF, and the nature of the pH dependence of EOF, provide strong evidence that the silica fillers introduced by the polymer manufacturer are the source of the surface charge. The high reproducibility and stability of EOF demonstrated during several weeks of either storage or use represents a significant advantage over the recently suggested use of surface oxidized PDMS [34]. However, the hydrophobicity of the channel walls is clearly problematic for CZE analysis of hydrophobic analytes, which tend to have a high PDMS affinity.

On the other hand, the tendency of hydrophobic materials to adsorb may mean that open tubular chromatography could be effectively performed within these devices. The tendency of SDS to adsorb on a negatively charged PDMS surface, in contrast to its behavior on glass, indicates the importance of hydrophobic interactions in governing adsorption on PDMS. This observation suggests that the adsorption of more weakly adsorbing analytes might be overcome by the addition of strong surfactants to the background electrolyte. Additionally, the ability of SDS to mask the pH effect on the EOF could prove beneficial in reducing the influence of pH on the electrokinetic control of fluid flow within the device. The device to device coupling scheme presented offers a simple solution for the interconnections with zero dead volume.

4.6 Acknowledgements

Thanks a lot to Mark Munroe, summer student and technician in our group, for his enthusiasm and his persistence. Without Mark's participation in PDMS molding, fluidic control on PDMS devices and PDMS device characterization, this chapter would not have been written in this form. I am further indebted to Thompson Tang and Richard Oleschuk for valuable discussions. I am grateful to Ken Westra (AMC) for etching most of the silicon devices. Thanks a lot to George Braybrook (Department of Geology) for obtaining the excellent SEM images, depicted in Figure 4.3. The measurement of PDMS absorbance characteristics by the departmental spectral services laboratory is highly appreciated. I would further like to thank Zhenghe Xu and his team (Department of Chemical Engineering) for giving me access to and instructing me in the use of their goniometer, used in all contact angle measurements in this study.

4.7 References

- 1 Effenhauser, C.S., in: Manz, A., Becker, H. (Eds.); *Microsystem Technology in Chemistry and Life Science*, Springer, Berlin 1998, pp. 51-82
- 2 EponTM Resin SU-8 Shell Chemical
http://www2.shellchemical.com/CMMWEB\GLOBCHEM.NSF/LinkPage/EPON_Specialties
- 3 Renaud, P., van Lintel, H., Heuschkel, M., Guerin, L. in: Harrison, D.J., Van den Berg, A. (Eds.); *Proceedings of the μ TAS '98 Workshop*, Kluwer Academic Pub., Dordrecht 1998, pp. 17-22
- 4 Webster, J.R., Burns, M.A., Burke, D.T., Mastrangelo, C.H. In *MicroTAS 98* pp.249-252
- 5 Mastrangelo, C. H., Man, P. F., Webster, J. R. WO 9807069, 1998

- 6 Ehrfeld, W., Muenchmeyer, D. *Nucl. Instrum. Methods A* 1991, 303, 523-532
- 7 Chou, S.Y., Krauss, P.R., Renstrom, P.J. *Science* 1996, 272, 85-87
- 8 Lee, L.P., Berger, S.A., Pruitt, L., Liepmann, D. in: Harrison, D.J., Van den Berg, A. (Eds.), *Proc. μ TAS '98 Workshop*, Kluwer Academic Pub., Dordrecht 1998, pp. 245-248
- 9 Roberts, M.A., Rossier, J.S., Bercier, P., Girault, H. *Anal. Chem.* 1997, 69, 2035-2042
- 10 Lazare, S., Granier, V., *J. Appl. Phys.* 1988, 63, 2110-2115
- 11 Mensinger, H., Richter, T., Hessel, V., Doepper, J., Ehrfeld, W., in: Van den Berg, A., Bergveld, P. (Eds.), *Micro Total Analysis Systems*, Kluwer Academic Pub., Dordrecht 1995, pp. 237-242
- 12 Matson, D.W., Martin, P.M., Bennett, W.D., Kurath, D.E., Lin, Y., Hammerstron, D.J. in: Harrison, D.J., Van den Berg, A. (Eds.), *Micro Total Analysis Systems '98*, Kluwer Academic Pub., Dordrecht 1998, pp. 371-374
- 13 Lin, Y., Xu, Y., Wen, J., Matson, D., Smith, R.D. in: Harrison, D.J., Van den Berg, A. (Eds.), *Micro Total Analysis Systems '98*, Kluwer Academic Pub., Dordrecht 1994, pp. 343-346
- 14 Srinivasan, R., Mayne-Banton, V. *Appl. Phys. Lett.* 1982, 41, 576-579
- 15 Stebani, J., Wokaun, A., Lippert, T., Kunz, T. EPO 770924, 1997
- 16 Preuss, S., Langowski, H. C., Damm, T., Stuke, M., *Appl. Phys. A* 1992, 54, 360-362
- 17 Kuper, S., Stuke, M. *Appl. Phys. Lett.* 1989, 54, 4
- 18 Srinivasan, R., Sutcliffe, E., Braren, B. *Laser Chem.* 1988, 9, 147-154
- 19 Becker, H., Dietz, W., Dannberg, P., *μ TAS '98*, pp. 253-256
- 20 Xiang, F., Lin, Y., Wen, J., Matson, D.W., Smith, R.D., *Anal. Chem.* 1999, 71, 1485-1490
- 21 Kolobow, T., Ito, Y., *U.S. patent* 4,551,251, 1985
- 22 McCormick, R.M., Nelson, R.J., Goretty Alonso-Amigo, M., Benvegna, D. J. , Hooper, H.H.. *Anal. Chem.* 1997, 69, 2626 -2630
- 23 Kumar, A., Whitesides, G.M., *Appl. Phys. Lett.* 1993, 63, 2002-2004
- 24 Wilbur, J.L., Kumar, A., Kim, E., Whitesides, G.M., *Adv. Mater.* 1994, 7, 600-604
- 25 Kumar, A., Biebuyck, H.A., Whitesides, G.M., *Langmuir* 1994, 10, 1498-1511
- 26 Hardman, B., Torkelson, A., in: Mark, F.H., Bikales, N.M., Overberger, C.G., Menges, G. (Eds.); *Encyclopedia of polymer science and engineering*, Wiley, New York 1989, Vol.15, pp. 254-255;
- 27 Sylgard 184 product specification, Dow Corning Corp., Midland, MI, USA;
- 28 "The World's Source for Plastic Materials Information"
<http://www.freemds.com/datasheet.asp?varAAA=11140&A=8>, IDES Inc., Laramie, WY, USA
- 29 Chaudhury, M.K., Whitesides, G.M., *Langmuir* 1991, 7, 1013-1025
- 30 Effenhauser, C.S., Bruin, G.J.M., Paulus, A., Ehrat, M. *Anal. Chem.* 1997, 69, 3451-3457
- 31 Folch, A., Ayon, A., Hurtado, O., Schmidt, M.A., Toner, M. *Trans. ASME J. Biomech. Eng.*, 1999, 121, 28-34

- 32 Delamarche, E., Schmid, H., Michel, B., Biebuyck, H., *Adv. Mater.* 1997, 9, 741-746
- 33 Baldock S.J., Bektas, N., Fielden, P.R., Goddard, N.J., Pickering, L.W., Prest, J.E., Snook, R.D., Treves Brown, B.J., Vaireanu, D.I., in: Harrison, D.J., Van den Berg, A. (Eds.), *Proc. μ TAS '98 Workshop*, Kluwer Academic Pub., Dordrecht 1998, pp. 359-362
- 34 Duffy, D.C., McDonald, J.C., Schueller, O.J.A., Whitesides, G.M. *Anal. Chem.* 1998, 70, 4974-4984
- 35 Chaudhury, M.K., Whitesides, G.M. *Science* 1992, 255, 1230-1232
- 36 Gillner, A., Hellrung, D. *Proc. Microengineering '98*, Stuttgart 1998
<http://www.ilt.fhg.de/d/publikationen/volltext/gillner9809/index.htm>
- 37 Lorenz, H., Despont, M., Vetiger, P., Renaud, P., *Microsyst. Technol.* 1998, 4, 143-146
- 38 Pohlmann, Ken C., *The Compact Disc Handbook*, A-R Editions, Inc., Madison, 1992, pp. 12
- 39 Elders, J., Jansen, H.V., Elwenspoek, M., *Proc. MEMS '95*, Amsterdam 1995, pp. 238
- 40 Larsson, O., Öhman, O., Billmadn, Å, Lundbladh, L., Lindell, C., Palmskog, G., *Transducers '97, Proceedings of the 9th International Conference on Solid-State Sensors and Actuators, IEEE Electron Dev. Soc., Chicago 1997*, pp. 1415-1418
- 41 Emmelius, M., Pawlowski, G., Vollmann, H.W., *Angew. Chem. Int. Ed. Engl.* 1989, 28, 1445-1471
- 42 Compaan, K., Kramer, P., *Philips Tech. Rev.* 1973, 33, 178
- 43 Frazier, A.B., Allen, M.G., *J. MEMS*, 1993, 2, 87-94
- 44 Hosokawa, K., Fujii, T., Endo, I., *μ TAS '98*, pp. 307-310
- 45 Soane, D. S.; Soane, Z. M. *U.S. Patent* 5,126,022, 1992
- 46 Martynova, L., Locascio, L.E., Gaitan, M., Kramer, G.K., Christensen, R.G., MacCrehan, W.A., *Anal. Chem.* 1997, 69; 4783-4789
- 47 Kaltenbach, P., Swedberg; S. A., Witt, K.E., Bek; F. Mittelstadt; L. S. *U.S. Patent* 5,882,571, 1999
- 48 Morra, M., Occhiello, E., Marola, R., Garbassi, F., Humphrey, P., Johnson, D.
J. Colloid Interface Sci. 1985, 137, 11-24
- 49 Hillborg, H., Gedde, U.W., *Polymer* 1998, 39, 1991-1998
- 50 Fettingner, J.C., Manz, A., Lüdi, H., Widmer, H.M., *Sensors & Actuators B* 1993, 17, 19-25
- 51 Verpoorte, E.M.J., VanderSchoot, B.H., Jeanneret, S., Manz, A., Widmer, H.M., DeRooij, N.F., *J. Micromech. Microeng.* 1994, 4, 246-256
- 52 Dempsey, E., Diamond, D., Smyth, M.R., Urban, G., Jobst, G., Moser, I., Verpoorte, E.M.J., Manz, A., Widmer, H.M., Rabenstein, K., Freaney, R., *Anal. Chim. Acta* 1997, 346, 341-349
- 53 Van den Berg, A., Lammerink, T.S.J., in: *Microsystem Technology in Chemistry and Life Science*, Manz, A., Becker, H. (Eds.); Springer, Berlin 1997, pp. 44-45
- 54 Shoji, S., Esashi, M., in: *Proc. μ TAS '94*, Van den Berg, A., Bergveld, P. (Eds.); Kluwer Academic Pub., Dordrecht 1994, pp. 165-178

- 55 Jaeggi, D., Gray, B.L., Mourlas, N.J., van Drieënhuizen, B.P., Williams, K.R., Maluf, N.I., Kovacs, G.T.A. *Proc. Solid State Sensor and Actuator Workshop '98*, Hilton Head, SC, 1998, pp.112-115
- 56 Gonzalez, C., Collins, S.D., Smith, R.L. *Technical Digest, Transducers 97, 9th Intl. Conf. Solid-State Sensors Actuat.*, Chicago 1997, pp. 527-530
- 57 Fan, Z., Harrison, D.J. *Anal. Chem.* 1994, 66, 177-184
- 58 Huang, X., Gordon, M.J., Zare, R.N., *Anal. Chem.* 1988, 60, 1837-1838
- 59 Wu, Q., Claessens, H.A., Cramers, C.A., *Chromatographia* 1992, 33, 303-308
- 60 Terabe, S., Utsumi, H., Otsuka, K., Ando, T., Inomata, T., Kuze, S., Hanaoka, Y., *J. High Resolut. Chromatogr.* 1986, 9, 666-670
- 61 Lux, J.A., Yin, H.F., Schomburg, G., *J.High Resolut. Chromatogr.*1990, 13, 145-147
- 62 Morris, C.J.O.R., Morris, P. *Separation Methods in Biochemistry*, Pittman Publishing, London, 1976, pp. 718-724
- 63 Seiler, K., Fan, Z. H., Fluri, K., Harrison, D. J., *Anal. Chem.* 1994, 66, 3485-3491
- 64 Chen, M., Cassidy, R.M. *J. Chromatogr.* 1992, 602, 227-234
- 65 Fridström, A., Markides, K.E., Lee, M.L. *Chromatographia* 1995, 41, 295-300
- 66 Arthur, C.L., Kilam, L.M., Motlagh, S., Lim, M., Potter, D.W., Pawliszyn, J. *Environ. Sci. Technol.* 1992, 26, 979-983
- 67 Buchholz, K.D., Pawliszyn, J. *Anal. Chem.* 1994, 66, 160-167
- 68 Chou, H.P., Spence, C., Scherer, A., Quake, S. *Proc. Natl. Acad. Sci. USA* 1999, 96, 11-13
- 69 Benton, D.P., Elton, G.A.H. *Trans. Faraday. Soc.* 1953, 49, 1213-1224
- 70 Parks, G.A. *Chem.Rev.* 1965, 65, 177-198
- 71 Tadros, T.F., Lyklema, J. *J. Electroanal.Chem.* 1968, 17, 267-275
- 72 Lukacs, K.D., Jorgenson, J.W. *J.High Resolut. Chromatogr.* 1985, 8, 407-411
- 73 Sylgard 184 product info after request, Dow Corning Corp., Midland, MI, USA
- 74 Smith, D.M., Drake, G.A., London, J.E., Thomas, R.G. *Los Alamos National Laboratory report* 1978, LA-7369-MS
- 75 Burns; G. T., Reiter; M. R. *U.S. patent* 5,661,210, 1997
- 76 Jacobson, S.C., Hergenroder, R., Koutny, L.B., Warmack, R.J., Ramsey, J.M., *Anal. Chem.* 1994, 66, 1107-1113
- 77 Shultz-Lockyear, L.L., Colyer, C.L., Fan, Z.H., Roy, K.L., Harrison, D.J. *Electrophoresis* 1999, 20, 529-538
- 78 Effenhauser, C.S., Manz, A., Widmer, H.M. *Anal. Chem.* 1993, 65, 2637-2642
- 79 Chiem, N., Harrison, D.J. *Anal. Chem.* 1997, 69, 373-378
- 80 Chiem, N., Harrison, D.J. *Clin.Chem.* 1998, 44, 591-598

- 81 Qiu, X.C., Hu, L., Masliyah, J.H., Harrison, D.J. *Transducers '97, Proceedings of the 9th International Conference on Solid-State Sensors and Actuators*, IEEE Electron Dev. Soc., Chicago 1997, pp. 923-926

Chapter 5: Conclusions and Suggestions for Future Experiments

This chapter serves to summarize the results from the previous chapters and to suggest further experiments and directions of the work presented. A wide range of instrumental and applicational developments has been presented in this thesis in the scope of μ TAS. Therefore it seems most appropriate to discuss the results in the order of the chapters.

The development of a confocal epifluorescence microscope for on-channel detection has led to the realization of fluorescein detection limits, LOD's, in the high fM range for continuous flow analysis and in the low pM range for capillary electrophoresis (see Chapter 2). This detection performance is adequate for most bioanalytical assays of interest. Further enhancements of signal to noise ratios in the sub pM range have to be based on further reductions of background signals and increased collection and probing efficiencies for increased sample specific fluorescence responses. Further background reductions necessarily involve the use of microscope objectives with increased numerical apertures, smaller spatial apertures and hence improved sectioning power. Consequently the probe volume will be reduced and the mass detection limit will be improved. In most routine analyses, low concentration detection limits seem of greater relevance than the actual mass detection limits achieved. Therefore we suggest to increase the probing efficiency, i.e. the number of injected molecules detected, for further improvement of concentration detection limits. Such an improvement could be realized in several ways. First an adjustment of the channel width to the probing laser spot diameter is suggested. In the present study this would imply a 12 μ m constriction in the separation channel. On the other hand, the channel depth could be increased in order to increase the number of molecules detected. Finally, illumination orthogonal to the detection microscope would allow for excitation of the whole channel cross section, while optical sectioning is provided by the detection microscope. The last approach would involve the optical coupling of excitation light into the detection segment of the separation channel. The definition of the cone of excitation light would then be crucial for superior detection performance. Due to the difficulty of inserting and positioning optical fibers into planar glass devices, optical waveguides, integrated onto the device, seem to be the preferable solution for this approach.

The first-time demonstration of an enzymatic assay of single cell lysates on a microchip shows that chip-based analyses of single cells hold great promise as a powerful cell analysis tool. In order to quantitate the enzymatic activity of single cells and to provide high throughput in this approach, a more sophisticated fluid delivery system has to be employed. Currently, the

sedimentation of cells in the cell reservoirs results in a reduction of cell throughput and flow velocity over time. Several different approaches for cell delivery onto the chip have been presented (see references in chapter 3). Most approaches resemble the systems employed in commercial flow cytometers. Hereby, a pressurized vessel, which contains the cell suspension, is connected to the fluidic analysis system. Another more challenging approach involves the culturing of cells in shallow cell channels prior to hydrodynamic transport of cells into an analysis channel on the same device. Attempts to realize this approach are in progress in several laboratories (see for example [1]). The addition of an electrophoretic separation step after lysis and reaction of single cells on-chip would be a very desirable feature of any single cell assay. The challenges to implement this step lie in the precise and timed fluidic control of cells, lysis and running buffers. New device layouts would be required for the realization of this concept.

The inexpensive, facile and rapid definition of microfluidic manifolds in PDMS substrates provides a strong incentive for the use of these devices. The constancy of EOF and the possibility of electrokinetic fluid handling in PDMS microchannels, demonstrated in chapter 4, are additional attractive features for the routine use of this substrate. Additionally, this study demonstrates that originally reported wetting problems of PDMS microchannels do not represent a significant experimental problem, if proper conditioning procedures are followed. The hydrophobicity of the material, however, imposes significant restrictions on the range of samples analyzed and buffer compositions used. PDMS has been used extensively as stationary phase for solid phase microextraction, SPME. We encountered extraction problems into the device when attempting to use BODIPY[®] 493/503, a highly lipophilic probe, as EOF marker. PDMS/analyte partition coefficients can be obtained from the SPME literature for various compounds. Further estimates can be made from water-octanol partition coefficients published for a wide range of compounds. The bulk properties of PDMS further exclude the use of many organic solvents, which may be used as additives in electrophoretic running buffers. PDMS is known to swell significantly upon exposure to hydrophobic solvents. When a PDMS device is filled with an aqueous solution, no leakage between the two slabs is observed due to the sufficient work of adhesion between the slabs. Upon addition of various organic solvents, however, leakage between the slabs may occur. The use of formulations, which result in hydrophilic functionalities on the PDMS surface, may eliminate the aforementioned limitations. Indeed, an arsenal of different PDMS bases and curing agents are available commercially, which should allow one to find ways to tailor the PDMS surface properties. Finally, it shall be mentioned that the analyte-PDMS interaction may be used for open tubular chromatographic separations in PDMS channels, where EOF could be used for fluid pumping. The need for channel features in the 1-2 μm range,

required for this application, could easily be realized due to the available template micropatterning techniques and the high replication fidelity of PDMS molding. Summarizing, we have elucidated the potential of native PDMS substrates for CZE analyses. Samples of moderate hydrophobicity and thus PDMS/sample partition coefficient can be analysed with high separation efficiency in native PDMS substrates. The range of analytes can be extended when untreated PDMS microchannels are filled with separation matrices, such as hydroxypropylcellulose, HPC. In a recent study [2], peptides and DNA fragments were separated by capillary electrophoresis in HPC filled native PDMS channels. Due to this wide range of possible analytes, the low manufacturing costs and the favorable self-adhesive properties, PDMS remains a very attractive substrate for CE-chips.

The expertise gained in the development of the epifluorescence detection scheme and of a chip-to-capillary connector, described in this thesis, have been utilized in the construction of a miniaturized and portable "Lab-on-a Chip" unit, designed for the detection of biological warfare agents [3]. The chip-based single cell assay has sharpened our insight into cell manipulation on-chip and led to the first-time pumping of fluids on-chip with syringe pumps in our group. More importantly, the present approach is the first reported enzyme analysis of single cells on a chip, thus demonstrating the research community the ever increasing range of applications of μ TAS. The presented system could certainly become part of a drug discovery in which drugs were made in pg amounts on-chip and the affect on cell protein expression be analysed one cell at a time. The use of PDMS as device material for microchips, introduced into this group within the scope of this thesis, has contributed to world wide efforts to realize microfluidic devices of higher complexity. The characterization of native PDMS substrates for CZE and the demonstration of reproducible electrokinetic fluid handling in these devices encourage the further use of this readily available and inexpensive substrate for the fabrication of μ TAS.

- 1 DeBusschere, B.D., Borkholder, D.A., Kovacs, G.T.A. in: *Proc. μ TAS Workshop '98*, Harrison, D.J., Van den Berg, A. (Eds.); Kluwer Academic Pub., Dordrecht 1998, pp. 443-446
- 2 Effenhauser, C.S., Bruin, G.J.M., Paulus, A., Ehrat, M. *Anal. Chem.* 1997, 69, 3451-3457
- 3 Lee, W.E., Jemere, A.B., Attiya, S., Chiem, N.H., Paulson, M., Ahrend, J., Burchett, G., Bader, D.E., Ning, Y., Harrison, D.J. submitted to *J. Cap. Electrophoresis, June 1999*